

Studies on electrochemical surface modification
for molten-salt blanket system in fusion reactor

Takashi Watanabe

DOCTOR OF
PHILOSOPHY

Department of Fusion Science
School of Physical Sciences

The Graduate University for Advanced Studies

2011(School Year)

Dedication

I dedicate my dissertation work to my family, many friends and exceptional person.

I specially feel of this graduation to my loving parents Tsutomu and Michiko Watanabe. Thank you for all the unconditional love, guidance, support and effort to the wellbeing of your child. I express great appreciation to my uncle Yuji Sakamoto. Words cannot express my gratitude to you. My brothers, Susumu and Akira Watanabe have never left my side and are very special.

I got many young friends in NIFS, Dr. Kinuya Saito, Dr. Akiyoshi Murakami, Dr. Kyohei Natsume, Dr. Dongxun Zhang, Mr. Pengfei Zheng, Mr. Yoshimitsu Asahi and Mr. Takeshi Miyazawa. I learned a lot with you every day. There are no days in my life which were felt more joy than the days passed with you. I never forget those days. I believe that you, young generations, will just realize the first fusion reactor. I want to see the day with you.

Finally, Ms. Shinobu Yuki has supported me for 3 years. You have made me what I am today in NIFS.

May this dedication be a small contribution toward the honors you deserve.

Acknowledgments

After obtaining a doctoral degree about 10 years ago, I have been working for a national institute. There, I have developed lithium batteries and sensor devices. In fact, I wanted to work for development for fusion science and engineering. I had looked for an opportunity for entering to nuclear fusion field before coming to NIFS. However, I could not get it. Then, to find the way to fusion science and engineering, I decided to take a doctoral course in Sokendai and then met Prof. Akio Sagara at NIFS. He opened the way to the fusion science and engineering for me. In other words, thanks to him, I realized my long cherished dream. He showed me current status in fusion reactor development and also led me for the direction of the way ahead. He told me that blanket system will be the most important key technology to realize real fusion reactors. Without his helps and supports, this dissertation would not been completed. My deepest and greatest appreciation goes to Prof. Akio Sagara.

I wish to thank Prof. Takuya Nagasaka, Prof. Akira Nishimura, Prof. Yasuji Kozaki, Prof. Yoshihiko Hirooka from NIFS, Prof. Akihiro Suzuki

from the University of Tokyo and Dr. Tomoko Ohshima from TYK Co. Ltd. for performing the experiment and sharing fruitful discussions. I thank Mr. Keiichiro Yasuji from Yasuji Inc. for designing the electrochemical reactor. I learned basic electrochemistry from Prof. Tetsuichi Kudo and Prof. Mitsuhiro Hibino from the University of Tokyo, and I discussed Dr. Hiroyuki Tsujimura from IMSEP Co. Ltd. and Prof. Yasuhiko Ito from Doshisya University about electrochemistry of molten salt. I greatly thank them. Dr. Yuki Edao and Prof. Satoshi Fukada helped me for measurements for hydrogen permeability. I have to give them my thanks a lot. And I learned a lot from the lecture by Prof. Hiroshi Yamada, Prof. Kazuo Kawahata, Prof. Yasuhiko Takeiri, Prof. Osamu Kaneko, Prof. Shinsaku Imagawa, Prof. Kiyomasa Watanabe, Prof. Toshiyuki Mito, Prof. Takashi Mazuzaki, Prof. Hideo Sugama, Prof. Ritoku Horiuchi, Prof. Hideaki Miura, Prof. Suguru Masuzaki.

Prof. Shoichi Okamura, Prof. Takeo Muroga, Prof. Motoyasu Sato, Prof. Nagato Yanagi, Ms. Mayumi Ito and Mr. Kohtaro Uesugi helped me before coming to NIFS, and they were supporting me about various things after starting my research in NIFS. And Ms. Mieko Ukai, Ms. Yuko Kakamu, Ms. Kaoru Banzai, Mr. Tomohito Taki, Ms. Misuzu Yamaguchi, Ms. Tomoko Matsusaki, Ms. Ai Matsubara, Ms. Ai Inoue, Ms. Kyoko Shimazaki, and Ms. Yoko Yamaguhi, I am very grateful to them. I have obtained precious experiences for the 3 years in NIFS and Sokendai. I am obliged to them for the trouble they have taken for me.

Many programs and seminars were organized and held in

SOKENDAI. The staffs from SOKENDAI were also supporting me. Especially, with the aid of the special program for big project research, I could attend an international conference, SOFT 2010 in Portugal, visit ITER construction site in France, and I have achieved large amount of my dissertation work. I express my thanks to Ms. Atsuko Fujisawa and all the stall staffs from SOKENDAI.

Finally, I express my very greatest appreciation to Prof. Masatoshi Kondo and Prof. Teruya Tanaka. Regarding experimental and technical support for this dissertation work, I own it all to them. And I also express my special appreciation to Director-General Prof. Akio Komori and all the NIFS staffs for giving me an opportunity to learn Fusion Science.

March 23, 2012

Takashi Watanabe

渡邊 崇

Studies on electrochemical surface modification for molten salt blanket system in fusion reactor

Takashi Watanabe

Abstract

This doctoral dissertation presents studies for materials for devices in molten fluoride salt blanket system in fusion reactor. When steel materials are employed as a structural material, its corrosion with the fluoride salt is a critical issue. To prevent it, many kinds of ceramics and coating processes have been discussed for compatibility with fluoride salts. However, there are many problems such large area coating over 1000m², toughness related with peeling and crack, wastes after the coating process and healing of damage parts. In this dissertation, a surface modification method through an electrochemical process using molten fluoride salt itself was proposed to form robust functionally graded material layers at the structural material surface and to overcome these problems.

First, several kinds of oxides and nitrides were thermodynamically considered for compatibility with fluoride molten salts. The thermodynamic consideration predicted that oxides dissolve into molten fluoride salt and that nitride have compatibility with molten fluoride salt. And prior to development of the surface modification process, compatibilities of oxides and nitrides in FLiNaK at 600°C were examined in immersion test over 1000 hours using bulk test specimens such Er₂O₃, Y₂O₃, Al₂O₃ and AlN. The results also demonstrated that nitride, AlN, indicated excellent compatibility with molten fluoride salt, FLiNaK. Secondly, coating processes were considered. To form robust graded compositional nitride layers using compositional elements from the structural material, an electrochemical

process was proposed. In the process, the surface of structural material is electrochemically treated in molten fluoride salt including Li_3N as a nitrogen source. Thirdly, because the experiments using molten fluoride salt have to be conducted in dry environment at high temperature over 500°C , an original experimental setup, which consists of a stainless steel reactor, a nickel crucible, thermocouples, heaters and electrodes, was designed and assembled for the experiments. It was installed in a dry Ar gas filled glove box. Aluminum rods were used as counter and reference electrodes. The specimen of 316 stainless steel (ss316) was bound tightly by a nickel wire at an end of nickel rod and it worked as working electrode. The potential standard was determined by the following equilibrium redox reaction of aluminum lithium alloy: $\text{Al} + \text{Li}^+ + \text{e}^- = \text{LiAl}$. The reaction can cause two half-reactions: oxidation at anodic reaction (loss of electron) and reduction at cathodic reaction (gain of electron). Temperature was controlled by a PID controller connected via cables to the heater. The electrodes were insulated by alumina tubes from the stainless steel reactor vessel. These electrode assemblies were connected via cables to a potentiostat and a function generator. Data was recorded by a data logger connected with the potentiostat. Fourthly, cyclic voltammograms were measured using the experimental setup. From the results, the nitriding condition was decided. Fifthly, ss316 surface was treated in a binary eutectic mixture of LiF-KF (FLiK) including Li_3N in a potentiostatic condition. The treatment was conducted at 1.0V with respect to lithium redox potential as the standard potential, ie, 1.0V vs. Li/Li^+ . For the treatment for 100 and 240 minutes, nitrogen was introduced into a depth of 35 and $65\mu\text{m}$ from the surface, respectively. When $d[\mu\text{m}]$ is defined as the depth of nitrogen introduced layer and $t[\text{min}]$ is defined as the treatment time, it was found that d is approximately proportional to t , ie, $d[\mu\text{m}] \cong 0.3 \times t[\text{min}]$. These specimens were analyzed using analytical methods such X-ray diffraction (XRD), electron probe micro analyzer (EPMA), electron energy dispersive X-ray spectrometry (EDX), X-ray photoelectron spectroscopy (XPS), and scanning

electromicroscopy (SEM). It was revealed that chromium nitride CrN formed selectively. The composition ratios of the nitride layer and the bulk layer were evaluated as Cr17.5wt% - Fe70.8wt% - Ni11.3wt% - Mo0.4wt% and Cr17.0wt% - Fe71.9wt% - Ni9.9 wt % - Mo1.2wt%, respectively. It was also suggested that face-center cubic (fcc) structure transformed to body-centered tetragonal (bct) structure. These results would mean that while the metal composition ratio was mostly held, the phase transformation was caused. Formation of solid solution α -Fe_{n(n>8)}N was also suggested. Although oxygen impurities were also expected to be introduced to the nitride layer, in fact, oxygen was not introduced into the layer. This means that nitrogen was mainly introduced in the layer through the treatment. Finally, considering the experimental conditions such as temperature, nitrogen concentration and specimen composition, nitride formation was theoretically analyzed based on combination of thermodynamics and electrochemistry. CrN, Cr₂N, Fe₂N and Fe₄N were considered from composition of ss316. Potential-nitride formation diagram and potential-nitrogen ion concentration diagram were made. From discussions on formation of these nitrides based on these conditions, it was theoretically derived that CrN is most stable. This theoretical consideration was well in agreement with the experimental result. In conclusion, these results demonstrate availability of this nitriding method and will allow a guideline for optimization of this nitriding process in molten fluoride salt.

This doctoral dissertation consists of five chapters and one appendix. Chapter 1 presents back ground and proposal of this work, ie, issues and problems on a molten salt blanket system in a fusion reactor. Chapter 2 presents thermodynamical discussion of compatibilities of several ceramics (metal oxides and nitrides). Compatibilities for those ceramics were evaluated based on thermodynamical theory. The prediction indicated that nitrides are compatible with molten fluoride salts. Chapter 3 presents the experimental descriptions and results. Introduction of nitrogen into SS316 specimen surface and formation of nitride layer were described. Chapter 4

presents theoretical explanation based on thermodynamics and electrochemistry. Formation of nitrides about iron and chromium is discussed. Chapter 5 presents conclusions. Appendix presents the results of immersion test using 4 bulk specimens of Er_2O_3 , Y_2O_3 , Al_2O_3 , AlN at 600°C over 1000 hours.

In recent years, nitrides have been focused on as fluorescent materials and magnetic materials. Especially, nitrogen solid solution of iron, $\alpha\text{-Fe}_n\text{N}$ ($n>8$), is expected as a alternative material without Nd, rare-earth element. Nitriding technique established in this work will be able to be applied not only to blanket system in fusion reactor, but also to many kinds of industrial applications.

Études sur modification électrochimique de surface pour système de couverture à sel fondu de réacteur de fusion nucléaire

Takashi Watanabe

Résumé

Cette dissertation doctorale présente des études pour les matériaux pour les appareils dans système de la couverture du sel de fluorure fondu dans le réacteur de fusion nucléaire. Lorsque les aciers sont employées comme un matériau structural, sa corrosion avec le sel du fluorure est une question critique. Pour l'éviter, beaucoup des céramiques et des processus de revêtement a été discuté concernant la compatibilité avec les sels du fluorure. Cependant, il y a beaucoup de problèmes comme le revêtement de grande surface plus que 1,000 m², la dureté contre pelage et le fissure, les gaspillages après le processus de revêtement de la couche et la guérison des parties du dégât. Dans cette dissertation, une méthode de la modification de la surface à travers un processus électrochimique qui utilise du sel du fluorure fondu lui-même a été proposée de former des couches robustes de matériels fonctionnels à la surface de matériel de construction et vaincre ces problèmes.

En premier, plusieurs oxydes et nitrures étaient thermodynamiquement considérés sur la compatibilité avec les sels de fluorure fondus. Et avant développement du processus de la modification de la surface, compatibilités d'oxydes et de nitrures avec FLiNaK à 600°C ont été examinées par l'essai de l'immersion sur 1000 heures qui utilisent des spécimens de Er₂O₃, Y₂O₃, Al₂O₃ et AlN. Les résultats ont aussi démontré que une niture, AlN, a indiqué son excellente compatibilité

avec sel du fluorure fondu, FLiNaK. Deuxièmement, le procédé de revêtement a été considéré. Pour former une couche robuste échelonnée en composition comprenant nitrure issue des éléments de la composition dans le matériau structurelle, un processus électrochimique a été proposé. Dans le processus, la surface du matériau structurelle est électrochimiquement traité dans le sel de fluorure fondu comprenant Li_3N comme source d'azote. Troisièmement, parce que les expériences utilisant le sel du fluorure fondu doivent être mené dans environnement sec à haute température plus de 500°C , un dispositif expérimental original qui est composé de un réacteur en acier inoxydable, un creuset en nickel, des thermocouples, un chauffage et des électrodes, a été conçu et il a assemblé pour les expériences. Il a été installé dans la boîte à gant rempli d'un gaz sec de Ar. Les baguettes aluminiumes ont été utilisées comme contre-électrode et électrode de référence. Le spécimen en 316 acier inoxydable (ss316) a été lié hermétiquement par un nickel fil à une fin de la baguette en nickel et il a fonctionné comme électrode de travail. Le standard de potentiel a été déterminé par la réaction du redox de l'équilibre suivante d'alliage de lithium aluminium: $\text{Al} + \text{Li}^+ + \text{e}^- = \text{LiAl}$. La réaction peut causer deux demi-réactions: un oxydation anodique (perte d'électron) et une réduction cathodique (gain d'électron). La température était contrôlée par un contrôleur PID relié par câbles à le chauffage. Les électrodes ont été isolés par les tubes en alumine du réacteur en acier inoxydable. Ces assemblages de l'électrodes ont été reliés par câbles à un potentiostat et un générateur de fonctions. Un enregistreur relié au potentiostat a enregistré les données. Quatrièmement, les voltammograms cycliques ont été mesurés par le montage expérimental. D'après les résultats, la condition pour la nitruration a été décidée. Cinquièmement, la surface du ss316 a été traitée dans un mélange binaire eutectique LiF-KF (FLiK) comprenant Li_3N dans une condition potentiostatique. Le traitement a été mené à 1.0V en ce qui concerne potentiel d'oxydoréduction de potentiel de lithium comme la potentiel standard, i.e., 1.0V contre Li / Li^+ . Pour le traitement pour 100 et

240 minutes, l'azote a été introduit dans une profondeur de 35 et 65 μm de la surface, respectivement. Lorsque d [μm] est défini comme la profondeur de la couche dans laquelle l'azote est introduit et t [min] est défini comme le temps du traitement, il s'est avéré que d était approximativement proportionnel à t , i.e., d [μm] $\cong 0.3 \times t$ [min]. Ces spécimens a été analysé utilisant des méthodes d'analyse suivantes: la diffraction des rayons X (XRD), le micro-analyseur à sonde à électrons (EPMA), la spectroscopie des rayons X par dispersion d'énergie (EDX), la spectroscopie photoélectronique à rayons X (XPS), et la microscopie électronique à balayage (SEM). Il s'est avéré que le nitrure du chrome CrN formait sélectivement. Les ratios de la composition dans la couche de nitrure et celle en vrac ont été évaluées comme Cr17.5wt% - Fe70.8wt% - Ni11.3wt% - Mo0.4wt% et Cr17.0wt% - Fe71.9wt% - Ni9.9wt% - Mo1.2wt%, respectivement. Il a aussi été suggéré ce visage-centre que une structure cubique au centre (fcc) avait transformé à une structure tétragonale à face centrée (fct). Ces résultats signifieraient que, pendant que le ratio de la composition du métal était principalement tenu, la transformation de la phase cristalline a été causée. La génération d' $\alpha\text{-Fe}_n\text{N}$ ($n > 8$) comme solution solide a aussi été suggéré. Bien que des impudicités d'oxyde aient aussi été attendues être introduit à la couche du nitruru, en fait, l'oxyde n'a pas été introduit dans la couche. Cela signifie que l'azote était principalement introduit dans la couche à travers le traitement. Finalement, la génération de nitrure a été analysée théoriquement basé sur la combinaison de thermodynamique et électrochimie en considération de les conditions expérimentales telles que la température, la concentration de l'azote et la composition du spécimen. Les nitrures, CrN, Cr₂N, Fe₂N et Fe₄N, ont été considérés de la composition de ss316. Le diagramme de potentiel-formation de nitrure et le diagramme de potentiel-concentration de ion azote a été préparé. Sur les discussions sur formation de les nitrures dans les conditions, il a été théoriquement conclu que CrN est très stable. Cette considération théorique a bien été d'accord

avec les résultats expérimentaux. Dans la conclusion, ces résultats démontrent la disponibilité de cette méthode de la nitruration et fourniront une directive pour l'optimisation de ce nitriding traité dans le sel du fluorure fondu.

Cette dissertation doctorale consiste en les cinq chapitres et l'appendice. Le chapitre 1 présente le contexte et la proposition de ce travail, ie, les questions et les problèmes sur le système de la couverture du sel fondu dans le réacteur de la fusion nucléaire. Le chapitre 2 présente discussion thermodynamique des compatibilités de plusieurs céramiques (oxydes et nitrures du métal). Les compatibilités pour ces céramiques ont été évaluées basé sur la théorie thermodynamique. La prédiction a indiqué que les nitrures sont compatibles avec les sels du fluorure fondus. Le chapitre 3 présente les descriptions expérimentales et les résultats. L'introduction d'azote dans la surface du spécimen en 316 acier inoxydable (ss316) et la formation de la couche de nitrure a été décrite. Le chapitre 4 présente l'explication théorique basée sur la thermodynamique et l'électrochimie. La formation de nitrures de fer et chrome est discuté. Le chapitre 5 présente des conclusions. L'appendice présente les résultats de l'essai d'immersion utilisant les 4 spécimens massives d' Er_2O_3 , Y_2O_3 , Al_2O_3 , AlN à 600°C pour 1000 heures.

Les nitrures se sont concentrés comme matériaux fluorescents et matériaux magnétiques au cours de ces dernières années. Surtout, la solution solide de nitrure de fer, $\alpha\text{-Fe}_n\text{N}$ ($n > 8$), est attendu comme matériel de remplacement sans Nd, un élément de rare-monde. La technique de nitruration établie dans les études sera non seulement applicable au système de la couverture dans le réacteur de la fusion, mais aussi à beaucoup de genres d'applications industrielles.

Studies on electrochemical surface modification for molten salt blanket system in fusion reactor

Takashi Watanabe

Acknowledgements	i
Abstract / Résumé	v
Contents	xiii
Figure list	xvii
Table list	xix
Chapter 1 Introduction	1
1. Current state on energy issue	1
1.1 Brief summary in history in energy issue	1
1.2 Prospective on energy issue	5
1.3 Fusion reactor as an energy generator	8
2. Roles and requirements of blanket system for fusion power reactor	16
2.1 Overview	16
2.2 Economics and fuel supply	17
2.3 Blanket power generation system	21
3. Molten salt blanket system	27
3.1 FLiBe	27
3.2 FLiNaK	29
3.3 Compatibility	32
3.4 Heat transfer	35
3.5 Tritium inventory	35
4. Purpose of the present work	40
References	44

Chapter 2 Thermodynamic prediction	51
1. Introduction	51
2. Compatibility with lithium fluoride	52
3. Results of thermodynamics evaluation	54
References	56
Chapter 3 Electrochemical nitriding	59
1. Introduction	59
2. Experimental	62
3. Results and Discussion	69
3.1 Electrochemical behavior	69
3.2 Surface structure	71
3.3 Cross-section	73
3.4 XPS analysis	79
3.5 XRD analysis	85
References	88
Chapter 4 Thermodynamic consideration	91
1. Thermodynamic consideration	91
2. Equilibrium electrochemical synthesis	92
3. Conclusions	108
References	109
Chapter 5 Conclusions	111

Appendix Corrosion characteristic of AlN, Y₂O₃, Er₂O₃ and

Al ₂ O ₃ in FLiNaK for molten salt blanket system	115
1. Introduction	115
2. Experimental	117
2.1 Specimen preparation	117
2.2 Test condition	118
3. Results	120
3.1 Surface observation	120
3.2 Weight change of specimens	127
3.3 Chemical analysis	128
4. Discussion	129
4.1 Thermodynamic stability	129
4.2 Solubility of oxide and nitride in FLiNaK	130
4.3 Corrosion resistance of AlN in FLiNaK	132
4.4 Corrosion of Al ₂ O ₃ , Er ₂ O ₃ and Y ₂ O ₃ in FLiNaK	133
5. Conclusion	135
References	136
Publication list	139

Figure list

Chapter 1

- Figure 1. 1. Trends in rate of energy utilization in the world from 1850 to 2100. 7
- Figure 1. 2. Phase diagrams of FLiBe and FLiNaK. 31
- Figure 1. 3. Relationship among materials at heat exchanger in molten salt blanket system. 33
- Figure 1. 4. HF behavior in molten FLiBe with dipping beryllium. 34
- Figure 1. 5. Schematism of blanket system. 37
- Figure 1. 6. Surface modification of structural material by electrochemical nitriding in fluoride molten salt. 44

Chapter 2

- Figure 2. 1. Ellingham diagram of nitrides and oxides. 55

Chapter 3

- Figure 3. 1. Experiment setup for electrochemical measurement and treatment. 63
- Figure 3. 2. Time-temperature curves for the electrochemical treatment. 67
- Figure 3. 3. Cyclic voltammogram of for 316 SS electrode in fluoride eutectic salt FLiK. 70
- Figure 3. 4. SEM images. 72
- Figure 3. 5. Compositional analysis of cross-section of the specimen treated in FLiK including 2mol% of Li_3N for 100min by EPMA. 76
- Figure 3. 6 Compositional analysis of cross-section of the specimen treated in FLiK by EPMA and metal weight ratio evaluated by EDX. 78
- Figure 3. 7. Compositional depth variation obtained by XPS. 80

Figure 3. 8. XPS spectra of the specimen before and after electrochemical treatment for 100min in FLiK containing Li_3N .	82
Figure 3. 9. Separation of chromium 2p peaks in XPS.	84
Figure 3. 10. X-ray diffraction patterns.	87
Figure 3. 11. Phase change from fcc structure to bct structure in nitrogen introduction.	88
 Chapter 4	
Figure 4. 1. Deposition potential of nitrides in Fe-Cr-N ³⁻ system on the nitriding of 316 SS.	95
Figure 4. 2. Equilibrium electrochemical synthesis (EES) diagram on nitriding of 316SS.	97
Figure 4. 3. Potential-pN ³⁻ diagram of chromium nitride and iron nitride in fluoride eutectic salt.	103
 Chapter 5	
 Appendix	
Figure A.1 Capsule for immersion test. It consists of SS316 tube and Swagelok.	119
Figure A.2 Photos of specimens before and after immersion test.	120
Figure A.3. Surface images of specimen by SEM and surface element analysis by XPS.	122
Figure A.4. Impurity concentrations in Flinak before and after immersion test.	129
Figure A. 5. Corrosion in AlN-Flinak-316L steel system.	133
Figure A. 6 Corrosion in Al_2O_3 -Flinak-316L steel system.	134

Table list

Chapter 1

Table 1. 1 Generation systems for blankets around 500 °C and efficiency.	23
Table 1. 2. Physical properties of FLiBe and FLiNaK.	31
Table 1. 3. Structural material and dimensions for FFHR2 blanket system.	38
Table 1. 4. Tritium inventory evaluation of FLiBe for FFHR.	38

Chapter 2

Chapter 3

Table 3.1 Composition of 316 stainless steel specimen and treated specimen.	65
---	----

Chapter 4

Table 4. 1. Deposition potential of nitrides on 316 stainless steel specimen	96
Table 4. 2. Thermodynamic data at 873K	102
Table 4. 3. Standard potential E° / V referred to the Li ⁺ /Li couple.	102
Table 4. 4. Change in standard Gibbs free energy at 873K.	105

Chapter 5

Appendix

Table A. 1 Composition of specimens (at%).	118
Table A. 2 Weight Change for immersion test (unit: g/m ²).	127
Table A. 3. Impurity composition in Flinak before and after immersion test.	128

Table A. 4. Gibbs energy for reaction of ceramics material in Flinak at 600°C.

130

Chapter 1 Introduction

1. Current state on energy issue

1.1 Brief summary in history in energy issue

Our life depends on fossil fuel at the present day. It has been used after at the birth of the industrial revolution in the 18th century. Coal has been using for generating energy. Heat generated by burning it raises steam from water. It was applied for source of power like a steam engine. The steam engine using coal was the first great wave of industrialization based on a truly disruptive technology. Coal remained the dominant fuel until right after the end of World War II (WWII).

After WWII, Industrialization, urbanization and motorization have shaped the modern energy economy which we know in this day. Trend of energy economy is associated with increasing quantities of

energy consumption, efficiency of energy use in production and consumption, diversification of sources of energy, and demand for clean and convenient energy at the point of use. The next major transition in energy economy trend came with electricity and the internal combustion engine. Heat from burning fossil fuel began to generate electric power through steam engine. Steam turbine extracts thermal energy from pressurized steam and drive electric power generator. Steam power plant is still leading and prime power sources.

While coal is solid fuel, petroleum oil is liquid fuel. Because of easy handling of oil, coal gave the place as a power source to oil with change of times for transport. Coal remains the principal fuel in power generation. Although coal is gradually being replaced by natural gas and recently by renewable, fissile fuel remains main power source at the present moment. In our country, Japan, electric power of 1 billion kWh is consumed for public power supply industry. Considering combination of energy sources, 65% was occupied by fossil fuel which consists of coal, liquid natural gas and oil. And 70 million automobiles are running consuming gasoline or diesel oil as fuel. These automobiles consume oil

of 57 million kilo liters a year in 2004[1].

In addition to being energy resource, oil plays another important role as a resource to produce many kinds of chemicals. Plastics and chemical textiles prepared from oil especially became widely used as a most accessible material in our daily life. Almost all kinds of industrial products are made of them. Oil is indispensable for our modern life with metal and semiconductor material. We depend on oil on almost all aspect in our life.

However, there are also disadvantages for using oil. Emission of carbon dioxide, CO_2 , to atmosphere became to be forced on as an environment related issue from the end of 20th century. It can be said that CO_2 not only causes acid rain but also work as a green house gas. According to the 4th report from Intergovernmental Panel on Climate Change (IPCC), they pointed out that emission of CO_2 by consumption of fissile fuel to atmosphere after the industrial revolution involves global warming for several decays. Besides the environmental issue, minable amount of sessile fuel came to a significant and serious issue. Amount of minable fossil fuel is limited. At the end of 2010, amount of minable oil

is 1383.2 billion tons, that of minable natural gas 187.1 trillion cubic meters and that of minable coal 86.1 billion tons[2].

As an alternative energy resource, atomic energy was developed in the middle of 20 century. Uranium has been used as an energy resource for over half a century. Although it began to be developed with military usage during WWII, minable amount of uranium is estimated as 5.4 million tons at the end of 2009[3]. If nuclear fuel cycle comes to completion using fast breeding reactor (FBR), more energy might be extracted drastically. However, in fact large amount of spent fuel is stored in spent fuel pool next to each reactor. And reprocessing for removing impurities from the spent fuel will produce large amount of plutonium with high level radioactive waste. If using uranium at current consumption rate, it will exacerbate problems on nuclear fuel storage. When operation of nuclear reactors and storage of nuclear fuel is managed, catastrophic disaster, earthquake and tsunami, should be also considered. And bringing out nuclear material to black market related terrorism should be prevented. And all kind of apparatus for nuclear engineering should be also protected from terrorist attacks. The

overhead cost for management of nuclear fuel is increasing due to these situations. Development of atomic energy has a close relation to nuclear arms development. Besides technical issues, the development as an energy engineering often causes political issues in the international community.

1.2 Prospective on energy issue

Population and economic growth are the two most driving force behind the demand for energy. Since 1900 world population has more than quadrupled, real income has grown by a factor of 25, and energy consumption by a factor 22.5. In other words, countries which affiliated into Organization for European Economic Cooperation (OEEC) and Organization for Economic Co-operation and Development (OECD) have led the global economic growth. Over the last 20 years, world population has increased by 1.6 billion people, and it will rise by 1.4 billion over the next 20 years. While income growth is trending up, population growth is trending down. However, in the next 20 years global integration will more progress. And low and medium income economies in non OECD

countries will grow rapidly. The world's real income has risen by 87% over the past 20 years. This implies to rise by 100% over the next 20 years. At the global level, the most fundamental relationship in energy economics remains robust, i.e, more people will get more income. This means the production and consumption of energy will rise.

It is often discussed using R/P ratio which is defined as dividing proved reserves by production. Considering R/P ratio of fossil fuels, R/P ratio of minable coal is estimated as 118 years, oil as 46.2 years and gas as 58.6 years at the end of 2010, respectively. Movable crude reserves about these fossil fuels have been revaluated every year. It steadily increases with progress of extractive technology and exploration of new coal field and oil field. However, because explosive economic progress in non OECD countries including China or India will cause upsurge of consumption of fossil fuel, minable year on fossil fuel does not seem to extend drastically. Figure 1. 1 demonstrates trends in rate of energy utilization in the world from 1850 to 2100. This suggests that what kind of energy was used depends on industrial establishment. Besides date, there would be local difference. Coal is also used c and is not outdated

energy. And natural gas will be a main energy source. Considering nuclear energy, not for military use, it will be used also for consumer use. From view point of energy security, combination of several kind of energy is eligible to disperse risk in energy issue. Our country, Japan, has imported oil as a main energy source. Increase of energy options means to be more secure in energy issue.

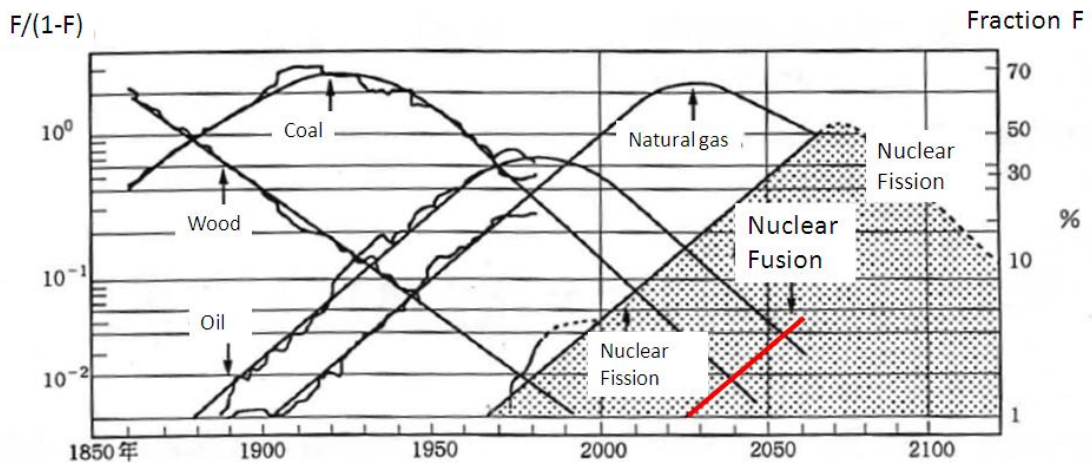


Figure 1. Trends in rate of energy utilization in the world from 1850 to 2100 [4]. F = fraction of market penetrated. Prediction on fusion energy was added to the original figure by K. Furukawa[5].

To overcome energy issue, many kinds of energy development are carried out. Fusion engineering is one of them. Energy is generated by fusion reaction due to fusion between light atoms like hydrogen. For example, reaction between deuterium and tritium generates ^4He with

energy of 3.52MeV and neutron with energy of 14.1MeV. Deuterium accounts for approximately 0.0156% (or on a mass basis: 0.0312%) of all naturally occurring hydrogen in Earth's oceans. Although naturally occurring tritium is extremely rare on earth, it is produced in nuclear reactors by neutron activation of lithium. Ocean water includes lithium of 0.1-0.2 mg/litter. These mean that infinite natural energy resource exists in oceans. Research and development on fusion reactor began in the middle of the 20th century. Although more than half a century have already passed since the commencement of research and development, it will need to take longer development period to realize a commercial reactor.

1.3 Fusion reactor as an energy generator

1.3.1 Brief summary of history in research and development on Fusion reactor

Research and development for fusion reaction as an energy device started in the middle of the 20 century. Sir George Paget Thomson and Moses Blackman in UK obtained the first patent related to a fusion reactor in 1946 and started experiments with pinch concept.

Around the same time, Ronald Richter proposed the Huemul Project in Argentina. Although his group announced positive results in 1951, unfortunately, these results were false. The UK pinch programs were greatly expanded and progressed to the ZETA and Sceptre devices. In the US, pinch experiments like those started in the UK started at the Los Alamos National Laboratory. Similar devices were also built in the USSR. At Princeton University, Lyman Spitzer developed a new approach in 1950, which is known as stellarator in this day. And Lawrence Livermore National Laboratory entered the field with their own variation, the magnetic mirror. These three groups have remained the primary developers of fusion research in the US to this day. In time since these early experiments, two new approaches developed that have since come to dominate fusion research. The first one was the tokamak approach developed in USSR, which combined features of the stellarator and pinch to produce a device that dramatically outperformed either. In our country, Japan, K. Uo also proposed Helical Heliotron field for plasma confinement in 1958[6]. The majority of magnetic fusion research to this day has followed the tokamak approach. In the late

1960s the concept of "mechanical" fusion using lasers was developed in the US, and Lawrence Livermore switched their attention from mirrors to lasers. Although more than fifty years have already passed since the first fusion reaction, applications for energy device are still being developed. It took less than ten years for fission to go from military applications to civilian fission energy production. This is very different in the fusion energy field and accounts for that, unlike the original prospect, control of fusion reaction with technology in the middle of the 20th century has been found to be very difficult over time.

At the end of the 20th century, technical development of superconductivity material allowed us to make coil generating strong magnetic field and is realizing the thermonuclear fusion reactor. And in France, International thermonuclear Experimental Reactor (ITER) is being constructed today in the 21st century. The project is funded and run by seven member entities - the European Union (EU), India, Japan, the People's Republic of China, Russia, South Korea and the United States. ITER is attempting to carry out commencement of operation from 2018 and will be the first fusion reactor which generates electric

power.

1.3.2 Requirements on thermal fusion reactor as an energy device

Considering reactor to generate electricity by some fusion reactions in a practical reactor, obtaining large amount of heat energy by the fusion reactions, easy control of the fusion reactions and establishment of continuous fuel supply into the reactor are required for long operation period. The reactions between two deuterium (D-D reactions) and those between deuterium and tritium (D-T reaction) satisfy the mentioned conditions. Deuterium is a naturally occurring isotope of hydrogen and is universally available from water. Considering these reactions, from the view point of fuel supply, the D-D reactions are easier than D-T reaction. Although more difficult to facilitate than the deuterium-tritium reaction, the fusion can be achieved through the reaction of deuterium with itself. This reaction has two branches that occur with nearly equal probability:



The first branch produces tritium. Although a D-D reactor will

not be completely tritium-free, it does not require an input of tritium and/or lithium. Most of the tritium produced will be burned before leaving the reactor, which reduces the tritium handling required, but also means that more neutrons are produced and that some of these are very energetic. The neutron from the second branch has an energy of only 2.45 MeV, whereas the neutron from the D-T reaction has an energy of 14.1 MeV, resulting in a wider range of isotope production and material damage. Assuming complete tritium burn-up, the reduction in the fraction of fusion energy carried by neutrons is only about 18%. The primary advantage of the D-D reactor is that tritium breeding is not required. This means that the D-D reactor is released from restriction of lithium resources and that neutron spectrum is somewhat softer.

However, due to the critical plasma condition for the D-D reactions, the plasma should be heated over 1000 million K. It is impossible to maintain the heated plasma at the high temperature by existing plasma control technique. From view point of material engineering, there is no thermal resistant material against the heated plasma. Accordingly, because the D-T reaction can cause lower

temperature at one order than D-D reaction, development of fusion reactor due to the D-T reaction is attempted to realize it this day.

The D-T reaction is as follows:



In this reaction, energy of 14.1 MeV is generated. The large mass ratio of the hydrogen isotopes makes the separation rather easy compared to the difficult uranium enrichment process. Tritium however occurs naturally in only negligible amounts due to its radioactive half-life of 12.32 years. Consequently, the deuterium-tritium fuel reaction requires the breeding of tritium from lithium using one of the following reactions:



and



The reactant neutron is supplied by the D-T fusion reaction shown above, the one that also produces the useful energy. The reaction with ${}^6\text{Li}$ is exothermic, providing a small energy gain for the reactor. The reaction with ${}^7\text{Li}$ is endothermic but does not consume the neutron. At least some ${}^7\text{Li}$ reactions are required to replace the neutrons lost by reactions with other elements.

To produce tritium, several systems are proposed. One is Fusion–Fission hybrid system. For example, a combination of molten salt fission reactor and fusion reactor is proposed. In LiF-BeF₂ molten salt Including UF₄ and/or ThF₄, lithium also carries out the nuclear fission reaction simultaneously with the nuclear fission reaction of uranium and/or Lithium also carries out a nuclear fission reaction simultaneously with the nuclear fission reaction of uranium. It is possible to produce tritium with generating electricity by nuclear fission plant simultaneously. From view point of economy, power generating cost seems to be low. In commercial power generation, light water reactor is in practical use in our country. Tritium is also obtainable from heavy water reactor like a CANDU reactor (short for CANada Deuterium Uranium reactor) without any certain target for reaction of tritium production. Development and construction of molten salt reactor or heavy water reactor for the system are in the order of ascending priorities. And almost all country using fission reactor will replace it to fusion reactor. They do not have the plan about fusion-fission hybrid system. In country, tritium production by neutron irradiation to ⁶Li-Al

alloy target is considered. Tritium produced in the target is collected[7].

Another one of tritium production system is nuclear spallation. When protons accelerated to several hundred MeV to several GeV using accelerator are collided to heavy atoms, tritium was produced [8,9]. Tritium is produced in the exclusive plant only for tritium production from lithium. The tritium is transported to independent fusion reactor. And it was burned with deuterium there. Comparing fusion reactor with blanket system for tritium breeding, the fusion reactor can be downsized. The last one introduced in this section is blanket system. Containers filled with lithium or lithium compound, blanket, are installed surrounding reactor core. Lithium is irradiated with neutron generated from the fusion reaction in the reactor core to produce tritium. Fuel cycle is completed in the fusion reactor itself. Because apparatuses for storage and transport of tritium are not needed, a compact system with fuel cycle can be assembled. This system is independent of fission reactor and acceptable in several countries which do not want to construct fission reactor. Because the reactor is upsized to install blanket around the reactor core and tritium permeation barrier is

needed, construction cost will increase. Reservation of initial tritium for ignition is also an important issue. The main research and development in the fusion engineering field aim at development of reactor equipped with the blanket system. This work is also for development of equipments in blanket system.

2. Roles and requirements of blanket system for fusion power reactor

2.1 Overview

Fusion energy possesses advantages in safety and energy security. It also provides slightly load to environment. Due to these reasons, it is expected as a prospective backbone energy source. To leverage it as a backbone energy source, it should be supplied in some kind of usable energy form. Blanket plays an important role to transfer from fusion energy to usable energy form for application. In this chapter, roles and requirements of power reactor to be practical use of fusion energy are shown from view points of economics, fuel supply, power generation system, maintenance, radioactive waste, and interaction between wall and plasma[10].

2.2 Economics and fuel supply

Practical application of fusion energy requires technology for transformation from fusion energy to usable energy form. In the same time, it should be stably supplied to consumers at reasonable and economic price.

2.2.1 Economics about blanket and fusion energy

Blanket in power reactor plant affects on economics of fusion energy. The affection is derived from many kinds of factor. First of all, cost for manufacturing and mandatory-replacement parts is considered. To reduce it, reasonable blanket was favorable. Due to design compact and high performance blanket with simple structure expensive material such Li-6 condensation, Be and vanadium alloy should be reduced.

Second, thermoelectric conversion rate should be gained. It directly affects on electric output. To obtain high efficiency, blankets using helium cooling or lithium cooling are attractive. However, in this system using intermediate heat exchanger and steam generator in thermal transfer system besides blanket itself, coolant material would

affect on construction and maintenance cost.

Third, operation rate should be gained by elongation of life time and simplification of replacement. Considering material which we can use, high energetic neutron load wall material requires frequent replacement of plasma counterwall such as first wall. Deterioration of breeding rate by burning breeding material also require its replacement. Those replacements will reduce utilization rate of the power reactor plant. Because of these reasons, reliable blanket with long life time should be designed. In same time, replace procedures which are done within short term should be developed.

Finally, neutron multiplication factor should be considered. Almost of fusion energy output is transferred to blanket by neutron. Then, neutron multiplication factor affects on its thermal output. It means that it affects on electric power cost. For example, using Be, although the construction rate would be increased, energy multiplication factor would be increased. This means that economics is consequently improved.

2.2.2 Tritium procurement and breeding

Tritium breeding is a function which conventional power systems have never possessed. Because abundant deuterium (D) and tritium (T) are used in fusion energy as fuel, the fuel is not unevenly distributed. This means that it is more advantageous in energy security than other energy. Fusion power reactor generates energy by burning D and T. Although it depends on system design, beryllium (Be) also is consumed as neutron multiplier. 1GW class power plant would consume about 105kg/y of D and 370kg/y of T, respectively. Be would be also consumed about 200kg/y. Stable supply is indispensable to complete the fusion power plant. According to stock assessment, D and T will be supplied continuously and stably. However, since Be supply has a quantitative restriction, Be recovery from spent blanket and efficient recycle of Be are required. The system which does not need Be neutron multiplier should be developed in future.

Although T is one of fuel for D-T reaction, in fact, it is defined an intermediate product for the whole system. The blanket in power plant needs enough capability for tritium self sufficiency. For the purpose, net

tritium breeding ratio (TBR) should be over 1.07 [11, 12]. However, from the viewpoint of status in development of structural material, uncertain in nuclear data and technology for maintenance, it is formidable task to develop the blanket at present. There is no clear prospect about blanket development.

It will be obtained through development of experimental production such a test blanket module (TBM) for ITER.

Starting fusion power plant needs a large amount of initial load fuel [13]. Supply of T might have decisive influence for introduction of fusion energy to energy market as a commercial power plant. Since T has no demand in general industry, T should be produced just for fusion reactor. To achieve prosperous introduction of fusion power reactor to energy market, the initial reactors might produce initial load T for the next reactors. If T reservation spends long time, the introductory pace for fusion power plant will decelerate.

Starting without initial load T has been also discussed. The introductory pace does not limited by T breeding. This scenario needs TBR over 1.07. The limitation of the introductory pace will be mitigated

a little.

2.3 Blanket power generation system

2.3.1 Current status in system design

Electric power generation system for blanket system in fusion power reactor will be designed based on that for conventional nuclear power plant. Fission reactor corresponds to blanket. Fusion power plant will take over facilities such waste disposal and treatment facility, turbine plant facility and electric generating facility from fission power plant. Specific facilities which do not exist in conventional fission power plants should be developed. For example, following facilities and equipments are listed: first wall, breeding blanket, diverter, vacuum vessel, vacuum system, superconductive magnet coil, cooling system, cooling system, high frequency heating device (NBI and RF), tritium recovery system and tritium storage system. Among them, first wall, breeding blanket and tritium storage system needs technological developments. The facilities and equipments for ITER have been already developed in ITER EDA and will be applied to the fusion power reactors

in next generation. At the present stage, the structure of the blanket itself is being developed in universities and institutes associated with nuclear engineering. Several design concepts for blanket have been proposed using different kinds of structural material, coolant, and breeding. On the other hand, if problems for material can be overcome, reheat cycle system, which has been progressed in development for light water nuclear reactor, could be used for fusion reactor. Thermal power generation by supercritical water or heated vapor could be applied to fusion power plant. Considering cooling order (primary cooling system or secondary cooling system), coolant material and temperature for operation should be selected. Table 1. 1 demonstrates comparison among typical generation systems using critical pressure water and He gas cooling blanket. In case of blanket using liquid metal or molten salt including lithium, operation could be possible at higher temperature over 500°C. Steam turbine similar to that for fast breeding reactor (FBR) can be considerable.

Table 1. 1. Generation systems for blankets around 500 °C and efficiency.

	Super critical pressure water (Direct cycle)	Super critical pressure water (Indirect cycle)	He gas (Indirect cycle)
Fusion power output	2300MW	2300MW	2300MW
Blanket Cooling heat energy	2400MW	2400MW	-
Pressure	25MPa	13MPa	10MPa
Inlet/Outlet temp.	280/500°C	290/510°C	250/500°C
Flow rate	1250.2kg/s	1258.5kg/s	1865.1kg/s
Electric power generation system			
Main steam pressure	25MPa	13MPa	15mPa
Turbine inlet temp.	500°C	480°C	470°C
Flow rate	1250kg/s	1037kg/s	908kg/g
Total electricity	1203MWe	1090MWe	1028MWe
Power generation efficiency	41.4%	37.5%	35.3%

2.3.2 Requirements for electric power reactor

Assuming fusion power plant as an electric power generator, it should adapt to electric grid consisting of several kinds of power sources.

Then, following factors should be considered: economics based on electric power demand in future, competitive strength against other electric power source and adjustability for load following operation.

2.3.3 Maintenance

There are typical concepts in maintenance: hard time (HT), on condition (OC) and condition monitoring (CM). HT: from viewpoint of planning maintenance, disassembly, inspection, replacement and fix are done for each part at regular intervals. OC: only function inspection without disassembly is done for a facility. If it passes the inspection, it is used until the next inspection. CM: monitoring function of a facility at all times, when any trouble is found at a facility, it is checked and fixed. In initial fusion power plant, HT maintenance will be done. After accumulation of experience and knowledge, OC maintenance and CM maintenance will be done. However, it is predicted that radioactive dust and tritium will exist extensively inside fusion power plant. This affects on operating efficiency, simplification and shortening on maintenance. From viewpoint of economics also, considering operating efficiency,

simplification and shortening on maintenance, the plant should be designed.

Diverter and first wall blanket will be exposed to particle load and heat load. Because these facilities are used under the harshest condition, maintenance and replacement are needed at regular intervals [14,15]. Overcoming cumbersome related with maintenance, concepts such liquid free surface diverter and gas diverter are also proposed [16].

In general, maintenance scenario depends on reactor type and its operation scenario. For example, utilization rate over 80% for first wall in case of DEMO reactor can be achieved by replacement of blanket module including first wall every 3 years based on HT maintenance [17]. To extend maintenance interval, SiC/SiC hybrid material and vanadium alloy have been developed as robust materials against neutron damage. However, if facilities were made by those materials, it seems to be difficult to use those facilities over 30 years like a pressure vessel in fission power plant.

Considering superconducting magnet, due to its high construction cost and difficulty on replacement, it will be used for reactor lifetime in

common operation scenario. However, it will need maintenance. Segmentization and replacement of superconducting magnet are discussed [18, 19].

2.3.4 Waste

In replacement of facilities for maintenance or deconstruction of reactor, radioactive structural material and adherent tritium can cause a problem as nuclear waste. Breeding material including lithium and neutron multiplying material including beryllium should be recycled from viewpoint of effective utilization of resource. After decontamination and volume reduction, considering quantity and kind of nuclear specie, the waste will be disposed. This is a process similar to that in conventional nuclear engineering.

In case of waste from fusion reactor, radioactive waste will cause by maintenance and replacement of facilities which face to plasma or be contaminated by tritium. First wall, blanket, diverter and equipments with those correspond to those. When radiation level of the waste is evaluated, those will be low level radiation waste. Those will not need

deep geological disposal. Amount of the waste depends on material selection. It is different from high level radiation disposal from nuclear fuel in conventional fission nuclear engineering. The waste from fusion power plant is low level radiation waste including gamma or beta waste. For fusion power plant, low active ferritic steel was developed. However, because it includes tungsten which can transform to beta or gamma radioactive nuclear species, amount of low level radiation waste will increase by utilization of the low active ferritic steel. In case of using low radioactive material like a SiC/SiC hybrid material, amount of the waste can be reduced. In any case, waste disposal should be evaluated based on economics from feature of wastes.

3. Molten salt blanket system

3.1 FLiBe

Molten salt was considered in development of fast breeding reactor and liquid fuel reactor in the 1940. One of the molten salts for the system used in the system is FLiBe (eutectic mixture of LiF and BeF₂). Many data was collected from the development of the system. Table 1. 2

demonstrates physical property of FLiBe [20]. Figure 1.2 demonstrates phase diagram of FLiBe. In Oak Ridge National Laboratory (ORNL) in the 1950, molten salt reactor (MSR) was operated for 5 years [21]. Based on the success in MSR, concept of helium cooling molten salt blanket was proposed at Princeton University in the 1970 [22]. Its features follow. (1)Low tritium solubility: it is lower at the 8th order than that of metal lithium. It is easy to recovery tritium it means that tritium inventory can be reduced to gram order in whole flow loop like a blanket system. (2)Leak security by low chemical activity: because it does not react water or air, the system including molten salt is protected against fire in leakage from flow loop. (3)High temperature operation at low vapor pressure: Because of low vapor pressure (4mPa at 500 °C), operation at atmospheric pressure can be constructed. (4)low electric conductivity: because of low electric conductivity (1 ohm.cm), MHD pressure loss can be avoided. (5) specific heat (1 cal/cc.degree): because it is at the same level as that of water, self cooling system can be constructed. Although system using molten salt has high safety, several disadvantages are pointed out. Assessment by US department of energy

(DOE) [23] required database about compatibility with structural material, high heat transfer as a Prandtl number liquid and tritium permeability in system operation at high temperature. In national institute for fusion science (NIFS) in Japan, blanket system for FFHR design (large helical device type reactor) has been developed since 1993 [24]. With this as a turning point, FLiBe was reconsidered in APEX in US [25]. JUPITER-II by Japan and US also started in 2001. These activities are completing the database required by above DOE assessment [26]. Achievements from these activities follow: (1) Redox by beryllium against corrosive HF in fluoride salt, (2) promotion of heat transfer at low flow rate and (3) development of large scale numerical simulation code.

3.2 FLiNaK

FLiNaK is also eutectic fluoride salt (LiF-NaF-KF). Because it does not include beryllium, it is often used in experiments for molten fluoride salt. FLiNaK salt was also researched during the late 1950s by ORNL as potential candidate for a coolant in MSR because of its low melting point, its high heat capacity, and its chemical stability at high temperatures.

Resultingly, FLiBe was employed as the solvent salt for MSR due to a more desirable nuclear cross section. FLiNaK still gathers interest as an intermediate coolant for a high-temperature MSR where it could transfer heat without being in the presence of the fuel [27].

In the immerse test carried out prior to development of electrochemical nitriding for this dissertation, FLiNaK was used as described in appendix. Table 1.2 also demonstrates its physical properties and Figure 1.2 demonstrates the phase diagram of FLiNaK. In the electrochemical nitriding described in this dissertation work, FLiK which is eutectic salt (LiF-KF) was used. These melting points are indicated in the diagram.

Table 1.2 Physical properties of FLiBe and FLiNaK

Salt	Temperature	Density	Viscosity	Kinetic coefficient of viscosity	Specific heat at constant pressure	Thermal conductivity	Thermal diffusivity	Electric resistivity	Prandtl number
	T (K(°C))	ρ (kg/m ³)	η (mPa.s)	ν (mm ² /s)	c_p (kJ/(m.K))	λ (W/(m.K))	a (mm ² /s)	ρ_e (kg/m ³)	Pr
FLiBe (LiF·BeF ₂ :66-34mol%) Melting point $T_m = 731K(458°C)$	750(477)	2014			2.39	1.00	0.21	7.13×10^5	
	800(527)	1993	7.50	3.76	2.39	1.00	0.21	5.88×10^5	17.90
	900(627)	1951	2.70	1.38	2.38	1.00	0.22	4.34×10^5	6.43
	1000(727)	1909	1.97	1.03	2.38	1.00	0.22	3.42×10^5	4.69
	1100(827)	1867	1.88	1.88	1.01	1.00	0.23	2.86×10^5	4.46
FLiNaK (LiF·NaF·KF: 46.5-11.5-42.0mol%) Melting point $T_m = 731K(454°C)$	750(477)	2182			1.88	1.20	0.29	9.17×10^5	
	800(527)	2146			1.88	1.20	0.30	8.33×10^5	
	900(627)	2073	4.10	2.00	1.88	1.20	0.31	7.09×10^5	6.40
	1000(727)	2000	2.60	1.30	1.88	1.20	0.32	6.17×10^5	4.10
	1100(827)	1927	1.80	1.80	0.93	1.20	0.33	5.43×10^5	2.80

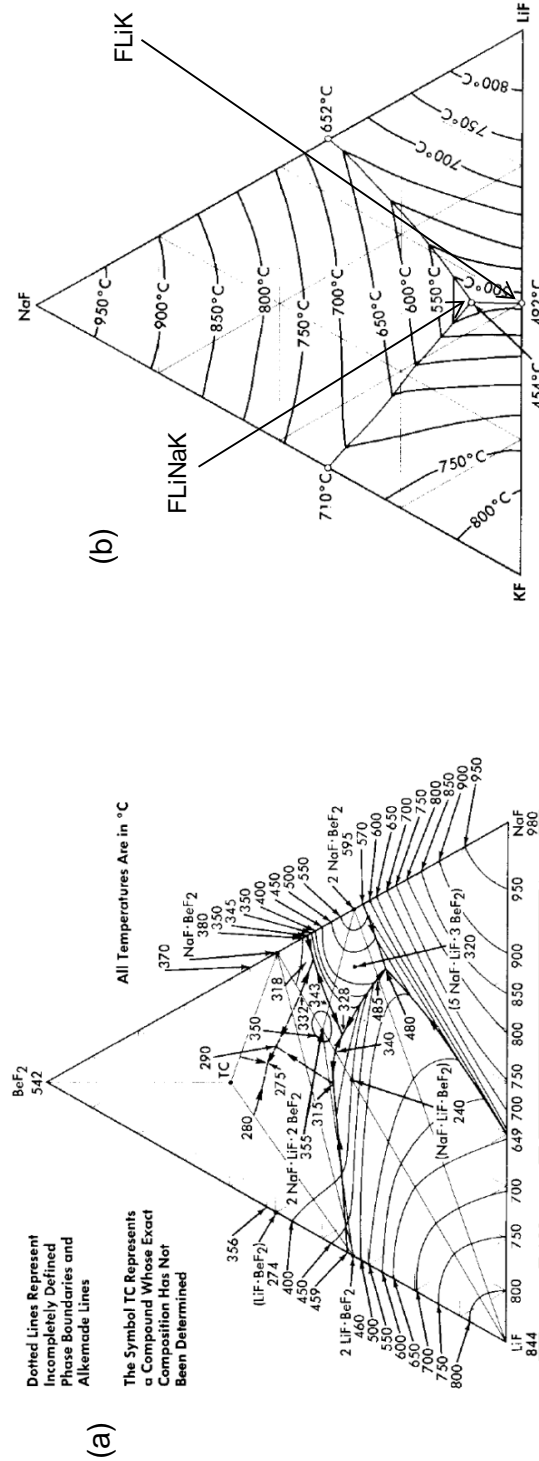


Figure 1.2. Phase diagrams of FLiBe and FLiNaK. (a) System of LiF-NaF-BeF₂, (b) System of LiF-NaF-KF.

3.3 Compatibility

When molten salt such a fluoride salt is used as a coolant media, we should consider compatibility of structural material with it. Figure 1.3 schematically demonstrates a relationship among the materials in the system. In addition to that, the blanket system will be operated under harsh condition of high temperature over 500°C and partially in neutron irradiation condition. Life span over 20-30 years will be required for the practical system in fusion reactors. The firm allowed penetration rate, ie. reduction rate in thickness by corrosion, have to be decided. However, it has not been decided yet. Because the practical deign of the system has not been completed, it is difficult to decide it at the present stage. Even then, the criterion, penetration rate p , by R.W. Revie and H.H. Uhlig would provide us a useful guideline [28]:

(A). $p < 0.15$ mm/year — Metals in this category have good corrosion resistance to the extent that they are suitable for critical parts, for example, valve seats, pump shafts and impellers, springs.

(B). $p = 0.15$ to 1.5 mm/year — Metals in this group are satisfactory if a

higher rate of corrosion can be tolerated, for example, for tanks, piping, valve bodies, and bolt heads.

(C). $p > 1.5$ mm/year — Usually not satisfactory.

Thus, the structural material have to be maintained at $p = 0.15$ at least.

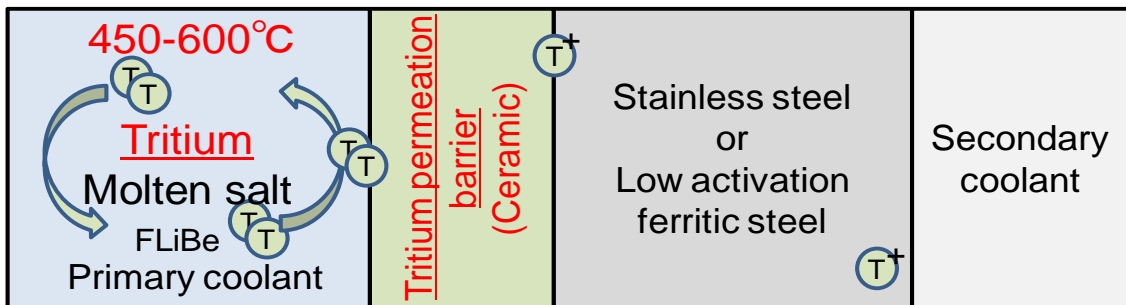


Figure 1. 3. Relationship among materials at heat exchanger in molten salt blanket system.

In FLiBe blanket, following reactions proceed by 14MeV neutron radiation:



The generated TF and F are quite corrosive. To use steel structural material such low active ferritic steel, stabilization of F and transformation from T⁺ to T₂ are required by redox control. Fortunately, it was found that addition of beryllium to FLiBe promotes

transformation from T^+ to T_2 as follows [29]:



This reaction avoids the corrosion by TF. Figure 1. 4 demonstrates HF behavior in HF with molten FLiBe with dipping beryllium.

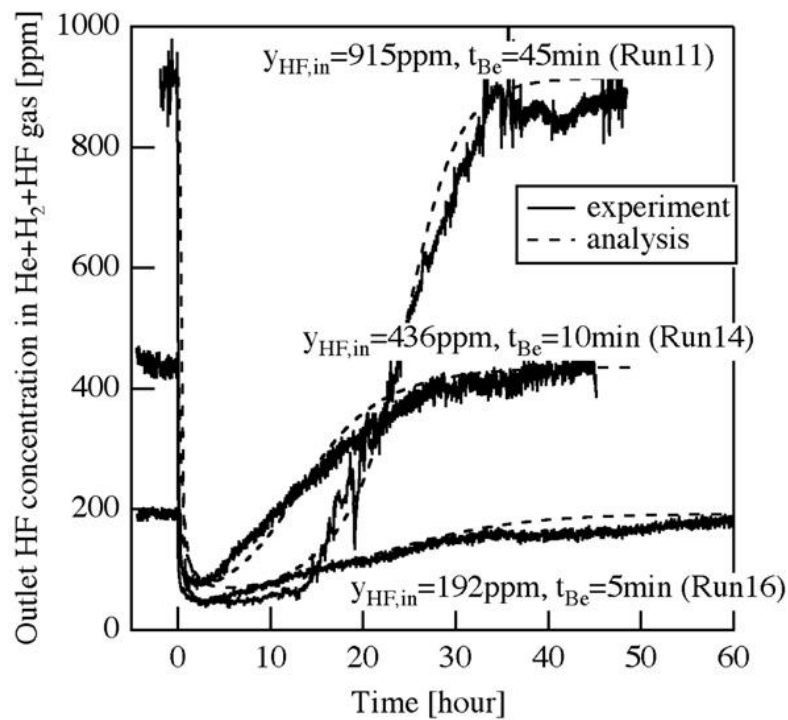


Figure 1. 4. HF behavior in molten FLiBe with dipping beryllium [30].

Since beryllium works as a neutron multiplier, this is favorable from viewpoint of nuclear design. Rate theoretical data in JUPITER-II project, obtained also demonstrated reduction of HF by beryllium addition [31].

However, issue of corrosion of steel structural material by LiF and BeF_2

are remained. Although using any kinds of metal material as a structural material, metal oxides cover its surface of structural material. And LiF and Be₂F are certain to react the oxides.

3.4 Heat transfer

Because FLiBe is high Prandtl number liquid ($Pr = 30$), to apply to cooling first wall, cooling performance should be improved in some engineering design. In Tohoku-NIFS Thermofluid loop (TNT loop), using Heat Transfer Salt (HTS: 53% KNO₃, 40% NaNO₂, 7% NaNO₃ in molar ratio) instead of fluoride salt, heat transfer of molten salt is simulated. Due to inertness of HTS against to structural material and its heat transfer property similar to FLiBe, HTS is available as a substitute salt against FLiBe. Experiments for turbulent flow by metal ball filling and improvement for cooling have done [32].

3.5 Tritium inventory

As described above, tritium is consumed in reactor itself and at same time is bred in blanket by reaction between lithium and neutron.

“Blanket system” which consists of pump, tritium recovery facility, heat exchanger and pipe line, assume the roles of first wall/blanket cooling and tritium inventory. The heat energy is used for electric power generation. This means that blanket system links incore facilities to excore facilities via the pipeline. Tritium will be accumulated over the whole system. In case of FFHR, the tritium accumulation was evaluated [33]. Figure 1. 5 demonstrates the schematism of the blanket system in FFHR2 which is the latest FFHR design. Molten salt, FLiBe, is employed as a liquid blanket. Structural material and dimensions is summarized in Table 1. 3. Material The reactor is assumed to be operating at 1GW. When the heat exchanger material is made by tungsten alloy, proportion of FLiBe flow into tritium recovery system (TRS) α is 0.2 and efficiency of TRS η is 0.85, the tritium inventory is summarized as shown in Table 1. 4.

Tritium inventory is deeply committed to its safety. The fusion reactor will use a few kilo grams of tritium. The tritium will transfer in the complicate system. Safety related with tritium also has been discussed. Through consideration of its leakage from the system to

outside and its accumulation in the system, it has been discussed what design is available for safety [34, 35].

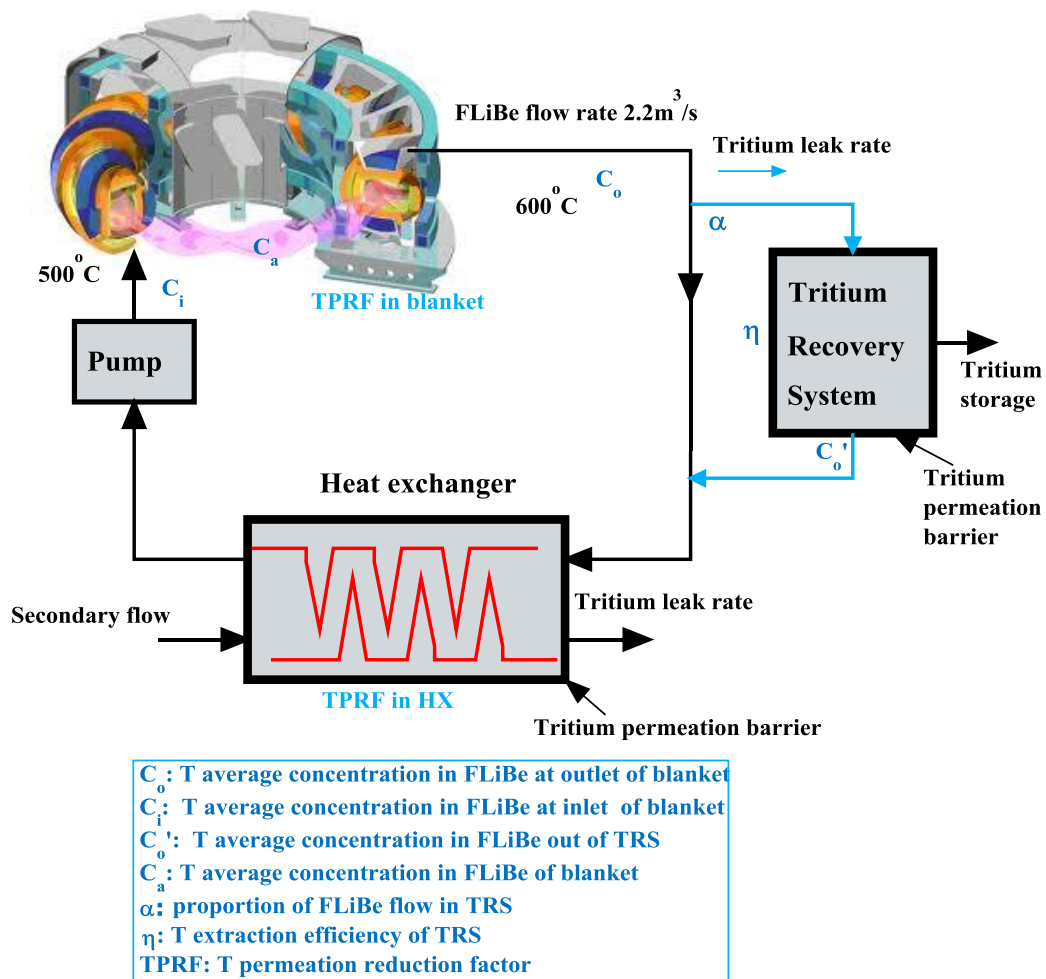


Figure 1. 5. Schematism of blanket system. This demonstrates the system in FFHR2 (the latest design of FFHR in 2011).

Table 1. 3. Structural material and dimensions for FFHR2 blanket system.

Component	Area (m ²)	Diameter (m)	Material
Blanket[36]	489	0.010	JLF-1 (low radioactive steel)
Heat exchanger [7]	700	0.001	Ta/Nb/W/Sic
Pipe from blanket to tritium recovery system	10	0.005	SS316
Pipe from tritium recovery system to heat exchanger	15	0.005	SS316
Pipe from heat exchanger to blanket	15	0.005	SS316

Table 1. 4. Tritium inventory evaluation of FLiBe for FFHR.

T recover in tritium recovery system	1.72×10 ⁶ Ci/day
T permeation into vacuum vessel	7.06×10 ⁴ Ci/day
T leak from blanket to tritium recovery system	1.15×10 ¹ Ci/day
T leak from tritium recovery system to heat exchanger	1.58×10 ¹ Ci/day
T leak from heat exchanger to blanket	1.58×10 ¹ Ci/day
T leak through secondary flow	4.13×10 ³ Ci/day

According to the evaluation, the tritium inventory in operating at 1GW is as follows: 1.44×10^6 Ci-T/day burns up in plasma. Then, 1.72×10^6 Ci/day ($9.58 \times 10^{-1}\%$) of tritium is recovered from FLiBe in the tritium recovery system. 7.06×10^4 Ci/day of tritium permeates through the blanket into the vacuum vessel, which should be extracted from the system by an isotope separation system and stored for fueling. The total tritium inventory of permeation into the auxiliary system is 4.32×10^1 Ci/day. To keep the tritium release to environment below the allowable level i.e. 10Ci/day, an effective ventilation detritiation system is needed to separate and recovery tritium from the effluent gas before release to the environment. According to ITER design [37], the impurity stream from the vacuum vessel is disposed to reduce the tritium content by a factor of $\sim 10^7$ before releasing into the atmosphere. Considering tritium disposal in the impurity stream from the vacuum vessel, tritium release in FFHR2 design also should be attained by the same level as that in ITER design. Significant amount of tritium, 4.13×10^3 Ci/day, permeates from the first loop into the secondary loop. Thus, an effective coolant purification system (CPS) should be also designed for FFHR2.

4. Purpose of the present work

In the moment, nobody is completing a “blanket system” for fusion reactor. There is too many issues to develop and complete it as described above. To attain that, all those issues should be settled step by step. The present work focuses on compatibility of steel structural material with fluoride salt. Addition of beryllium to fluoride salt as a liquid blanket can avoid corrosion of steel structural material by most corrosive hydrogen fluoride HF. However, corrosion by lithium fluoride LiF is still remained. To overcome it, some novel concept and approach are needed.

Thus, ceramic layer formation at the steel surface was tried against the corrosion in this work. First of all, candidate materials were considered based on thermodynamics. According to the thermodynamic prediction about corrosion, while almost all oxides will dissolve into fluoride salt including lithium, nitrides do not dissolve into that. For the reason, nitride layer was tried to form at the surface of steel material.

Nitrides have long history for wear-protection coating s for tools

and mechanical components, decorative coatings, electrical contacts, and diffusion barriers in electronic devices [38]. For these purposes, nitriding has been done by PVD deposition, CVD deposition, plasma nitriding, etc [39, 40, 41, 42, 43, 44, 45, 46, 47, 48, 49, 50]. Although the structural and chemical properties have been analyzed crystal in detail, those behaviors are quite intricate. Several phases of nitrides often exist at the same time and also cause spinodal decomposition. Those situations make it difficult to isolate nitrides.

When the structural for the blanket system is considered, it has to bear against harsh condition over 500°C. And it contacts flow of hot molten fluoride salt. It means that the risk of erosion must be also taken into consideration [51]. Although many kinds of coating on the surface were tried for the purpose, coating, a different material joint between metal and ceramic, is often cracked and/or causes exfoliation. Although wide area with intricate shape such a pipe line inside should be also covered, it would be also difficult to attain it.

Nitriding surface modification with gradient composition was therefore tried at the surface of steel material. Due to gradient

composition, mechanical toughness was expected with corrosion resistance. Although gaseous process, plasma assist process and process using molten salt are known as conventional nitriding processes, each process has advantage and disadvantage. Gaseous nitriding needs ammonia gas for nitriding. Disposal and release to atmosphere often cause problem about environmental load due to its toxicity. Plasma assist nitriding needs intense electric fields to generate ionized molecules of the gas around the surface to diffuse the nitrogen into the workpieces. Thus, it needs the vessel which affords enough space for the workpieces. Considering large workpieces such facilities and equipments for blanket system, this is inconvenient.

In this work, a process in molten salt was applied to modify the steel surface. Small amount of nitrogen was added into molten fluoride salt. The surface was nitrided by an electrochemical technique. Figure 1.6 demonstrates schematism of electrochemistry. The reaction, which is impossible to be caused in thermodynamic equilibrium status, can be achieved by electric power assistance in electrochemical technique. The surface modification in molten fluoride salt has several advantages:

Needless of cleaning after the treatment. Because of using fluoride salt of similar composition to liquid blanket, cleaning and replacement are not needed. This means reduction of environmental load. For example, although Tufftride is known as a nitriding using cyanic salt, the disposal can be issue after the treatment due to its toxicity. Considering disposal, similar composition to blanket itself is advantageous. From viewpoint of maintenance, possibility of nitriding in fluoride salt would be advantageous. It is possible to heel broken parts without disassembling the facilities and equipments.

As described above, the electrochemical processing was studied for nitriding of steel surface in molten fluoride salt.

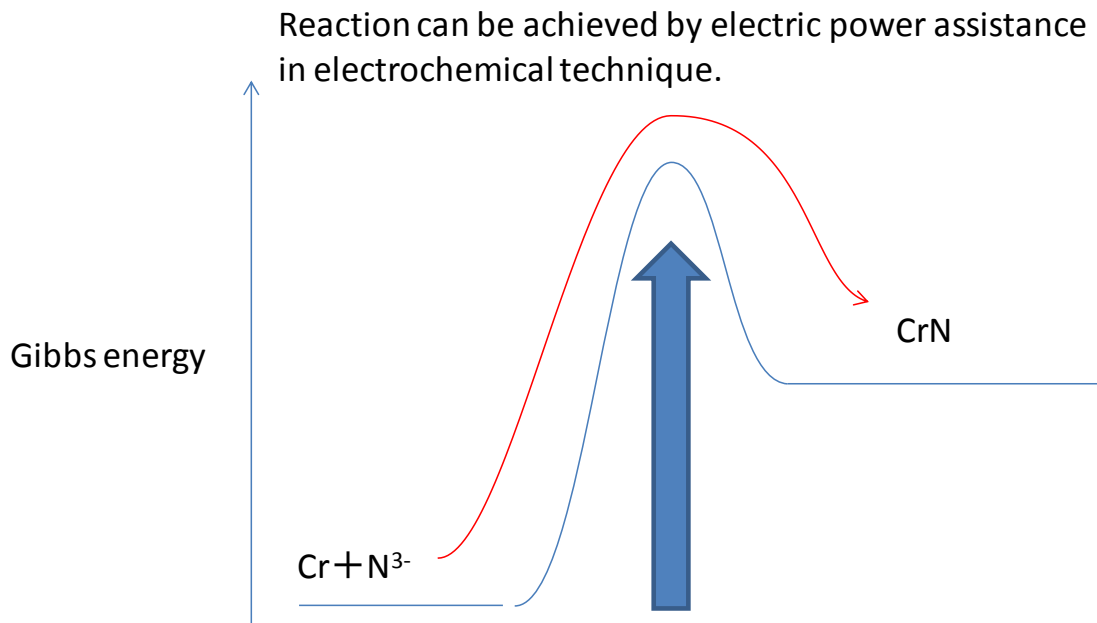


Figure 1. 6. Surface modification of structural material by electrochemical nitriding in fluoride molten salt. The reaction, which is impossible to be conducted in thermodynamic equilibrium status, can be achieved by electric power assistance in electrochemical technique.

References

- [1]The atomic energy society of Japan ed., “Nuclear power will open the next century”, 「原子力がひらく世紀(New Century Opened by Nuclear Power)」 in Japanese, 2004.
- [2] BP Statistical Review of World Energy, 2011.
- [3] OECD NEA & IAEA, Uranium 2009: Resources, Production and Demand ("Red Book").

- [4] C. Marchetti, “Primary Energy Substitution Models: On the Interaction Between Energy and Society”, *Technological Forecasting and Social Change*, 10(1977)345.
- [5] The society of molten-salt technology ed., *Metal & Technology*, “Fundamentals of Molten salt and Thermal technology”, 「溶融塩・熱技術の基礎」 in Japanese, *AGNE*, 8(1993).
- [6] K. Uo, “The Helical Heliotron field for plasma confinement”, *Plasma Phys.*, 13(1971) 243.
- [7] M. Tanase, K. Mohri, H. Hashizume, S. Tanaka, Y. Ueda, 「トリチウム製造技術 (Tritium production technology)」in Japanese, *J. Plasma and Fusion Research*, 70 (1994) 32.
- [8] Energy Research Advisory board, *Accelerator Production of Tritium(APT)*, DOE/S-0074(1990).
- [9] G.P. Lawrence, “High Power Linear Accelerators for Tritium Production and Transmutation of Nuclear Waste”, L.A-UR-90-3315(1990).
- [10] Y. Asaoka, K. Mohri, H. Hashizume, S. Tanaka, Y. Ueda, “Roles and Requirements of the Blanket System of Fusion Power Reactors”, *J. Plasma Fusion Res.*, 79 (2003) 652.
- [11] Y. Asaoka, K. Okano, T. Yoshida, K. Tomabechi, “Requirements of tritium breeding ratio for early fusion power reactors”, *Fusion Sci. Technol.*, 30 (1996)853.
- [12] Y. Asaoka, K. Okano, T. Yoshida, R. Hiwatari, K. Tokimatsu, “Maximum implementation capacity of fusion power reactors”, *Fusion Sci. Technol.*, 39 (2001)518.

- [13] Y. Asaoka, S. Konishi, S. Nishio, R. Hiwatari, K. Okano, T. Yoshida, K. Tomabechi, "Commissioning of a DT Fusion Reactor without External Supply of Tritium", Proc. Of 18th IAEA fusion Energy Conference, Sorrento, Italy (2000)PDP-08.
- [14] M. Nishikawa, E. Tachibana, K. Watanabe, T. Narikawa, S.Toda, "Quick replacement of the fusion core parts in a cassette compact toroid reactor", Fusion Eng. Des., 5(1988)401.
- [15] H. Hashizume, Y. Usui, S. Kitajima, Y.Hida, A.Sagara, "Numerical analysis of MHD flow in remountable first wall", Fusion Eng. Des., 61(2002)251.
- [16] M.A. Abdou, The APEX Team, "Exploring novel high power density concepts for attractive fusion systems", Fusion Eng. Des., 45(1999)145.
- [17] S. Konishi, S. Nishio, K. Tobita, The DEMO design team, "DEMO plant design beyond ITER", Fusion Eng. Des., 63(2002)11.
- [18] S. Itoh, S. Ito, H. Hashizume and S. Kitajima, " Study on mechanical jointing of high temperature superconductors", Int. J. Appl. Elemag. Mech., 14(2001)85.
- [19] H. Hashizume, K. Kitagoh, S. Kitajima, A. Sagara," Cost Assessment of Fusion Reactor with External Conductor Systems", Fusion Sci. Technol., 44(2003)284.
- [20] The Japanese Society of Mechanical Engineers ed., 「伝熱工学資料 第4版 (JSME Data Book: Heat Transfer 4th Edition) 」, in Japanese, Tokyo, Maruzen, (1986).
- [21] A. Sugano et al.,「溶融塩炉開発の現状と将来 (Current Status and Future plan in Development of Molten Salt Reactor)」in Japanese, Journal of the Atomic Energy Society of Japan, 16(1974)249.

- [22] T. Terai, S. Fukada, Y. Hatano, Y. Oya, 「溶融塩 Flibe システムの研究 (Studies on Molten-Salt FLiBe Systems)」 in Japanese , J. Plasma Fusion Res., 85 (2009) 251.
- [23] ANL/FPP-84-1, Blanket Comparison and Selection Study Final Report, (1984).
- [24] A. Sagara, O. Motojima, K. Watanabe, S. Imagawa, H. Yamanishi, O. Mitarai, T. Satow, H. Tikaraishi, FFHR Group, “Blanket and divertor design for force free helical reactor (FFHR)”, Fusion Eng. Des., 29 (1995)51.
- [25] M.A. Abdou et al., “On the exploration of innovative concepts for fusion chamber technology”, Fusion Eng. Des., 54(2001)181.
- [26] S. Tanaka et al., “Status of fusion technology activities in Japan”, Fusion Sci. Technol., 39 No.2.2(2000)298.
- [27] Lane, James A. Chapter 12 “Chemical Aspects of Molten Fluoride Salt Reactor Fuels” in “Fluid Fuel Reactors”, MA: Addison-Wesley Pub., 1958.
- [28] R.W. Revie, H.H. Uhlig, “Corrosion and Corrosion Control - An Introduction to Corrosion Science and Engineering”, 4th edition, Hoboken New Jersey, John Wiley (2008).
- [29] P. Calderoni, P. Sharpe, H. Nishimura, T. Terai, “Control of molten salt corrosion of fusion structural materials by metallic beryllium”, J. Nucl. Mater., 386-388(2009) 1102.
- [30] S. Fukada, M.F. Simpson, R.A. Anderl, J.P. Sharpe, K. Katayama, G.R. Smolik, Y. Oya, T. Terai, K. Okuno, M. Hara, D.A. Petti, S. Tanaka, D.-K. Sze, A. Sagara, “Reaction rate of beryllium with fluorine ion for Flibe redox control”, J.Nucl. Mater., 367-370(2007)1190.

- [31] David A. Petti, G.R. Smolik, Michael F. Simpson, John P. Sharpe, R.A. Anderl, S. Fukada, Y. Hatano, M. Hara, Y. Oya, T. Terai, D.-K. Sze, S. Tanaka, “JUPITER-II molten salt Flibe research: An update on tritium, mobilization and redox chemistry experiments”, *Fusion Eng. Des.*, 81(2006)1439.
- [32] S. Toda, S. Chiba, K. Yuki, M. Omae, A. Sagara, “Experimental research on molten salt thermofluid technology using a high-temperature molten salt loop applied for a fusion reactor Flibe blanket”, *Fusion Eng. Des.*, 63-64(2002)405.
- [33] Y. Song, A. Sagara, T. Muroga, Q. Huang, M. Ni, Y. Wu, submitted to *J. Plasma Fusion Res.*
- [34] M. Enoda, K. Okuno, 「核融合燃料プロセス系の安全解析(Safety Analysis of Fusion Fuel Processing System)」 in Japanese, *J. Plasma and Fusion Res.*, 73(1997)786.
- [35] T. Homma, H. Noguchi, 「環境流出放射線物質による被曝評価(Dose Assessment for Radioactive Materials Released into the Environments)」 in Japanese, *J. Plasma and Fusion Res.*, 74(1998)707.
- [36] A. Sagara, O. Mitarai, T. Tanaka, S. Imagawa, Y. Kozaki, M. Kobayashia, T. Morisaki, T. Watanabe, K. Takahata, H. Tamura, N. Yanagi, K. Nishimura, H. Chikaraishi, S. Yamada, S. Fukada, S. Masuzaki, A. Shishkin, Y. Igitkhanov, T. Goto, Y. Ogawa, T. Muroga, T. Mito, O. Motojima, FFHR design group, “Optimization activities on design studies of LHD-type reactor FFHR”, *Fusion Eng. Des.*, 83(2008)1690.
- [37] H. Yoshida, O. Kveton, J. Koonce, D. Holland, R. Haange, “Status of the ITER Tritium Plant design”, *Fusion Eng. Des.*, 39-40(1998)875.
- [38] H. Hultman, “Thermal stability of nitride thin films”, *Vacuum*

57(200)1.

[39] H. Holleck, "Binäre und Ternäre Carbide und Nitridsysteme der Übergangsmetalle", Berlin: Gebrüder Borntraeger, (1994).

[40] T. Yamamoto, S. Kikkawa, M. Takahashi, Y. Miyamoto, F. Kanamaru, "High pressure synthesis of B1-type solid solutions $Nb_{1-x}M_xN$ (M=Ga, Ti)", *Physica C*, 185-189(1995)2719.

[41] P. Duwez, F. Odell, "Phase Relationships in the Binary Systems of Nitrides and Carbides of Zirconium, Columbium, Titanium, and Vanadium", *J. Electrochem. Soc.*, 97(1950)299.

[42] H. Nowotny, F. Benesovsky, E. Rundy, "Hochschmelzende Systeme mit Hafniumkarbid und -nitrid", *Monatsh. Chem.*, 91(1960)348.

[43] R. Kieffer, H. Nowotny, P. Ettmayer, G. Dufek, "New Investigations Concerning Miscibility of Transition-Metal Nitrides and Carbides", *Metall*, 7(1972)701.

[44] U. Wahlström, L. Hultman, J.-E. Sundgren, F. Adibi, I. Petrov, J.E. Greene, "Crystal growth and microstructure of polycrystalline $Ti_{1-x}Al_xN$ alloy films deposited by ultra-high-vacuum dual-target magnetron sputtering", 235(1993)62.

[45] F. Adibi, I. Petrov, L. Hultman, U. Wahlström, T. Shimizu, D. McIntyre, J. E. Greene, and J. - E. Sundgren, "Defect structure and phase transitions in epitaxial metastable cubic $Ti_{0.5}Al_{0.5}N$ alloys grown on MgO(001) by ultra - high - vacuum magnetron sputter deposition", *J. Appl. Phys.* 69(1991)6437.

[46] O. Knotek, A. Barimani, "On spinodal decomposition in magnetron-sputtered (Ti,Zr) nitride and carbide thin films", 174(1991)51.

- [47] R.A. Andrievski, I.A. Anisimova, V.P. Anisimov, "Structure and microhardness of TiN compositional and alloyed films", 205(1991)171.
- [48] W. Lengauer, J. Bauer, A. Guillou, D. Ansel, J.-P. Bars, M. Bohn, E. Etchessahar, J. Debuigne, P. Ettmayer, "WDS-EPMA nitrogen profile determination in TiN/Ti diffusion couples using homotypic standard materials", *Mikrochimica acta*, 107(1992)303.
- [49] H. Michel, T. Czerwiec, M. Gantois, D. Ablitzer, A. Ricard, "Progress in the analysis of the mechanisms of ion nitriding", *Surf. Coat. Technol.*, 72(1995)103.
- [50] R. Grün, H.J. Günther, "Plasma nitriding in industry—problems, new solutions and limits", *Mater. Sci. Eng. A* 140(1991)435.
- [51] B.J. Merrill, M. Sawan, C.P.C. Wong, R.E. Nygren, L.C. Cadwallader, S. Malang, S. D.-K. Sze, "Safety assessment of two advanced ferritic steel molten salt blanket design concepts", *Fusion Eng. Des.*, 72(2004)277.

Chapter 2 Thermodynamic prediction

1. Introduction

As described in Chapter 1, corrosion of steel structural materials by HF or TF can be restrained by reduction by beryllium. However, lithium fluoride corrodes structural materials. It remains as another issue for compatibility with using molten fluoride salt. Coating or surface modification by ceramics which has compatibility with LiF on the surface of steel structural materials is available against corrosion. In this chapter, reactions of several materials in molten fluoride salt were predicted based on an equilibrium theory. Because Lithium fluoride is most active, compatibility of candidate materials with it was considered. Considering each reaction, difference between Gibbs energy between

before and after the reaction was calculated. Compatibility was considered from the results.

In research and development for liquid blanket system, from view point of restraint of hydrogen permeation, many research and development about oxide coating have been discussed. First, oxides thus were considered. Next, because nitrides are known anti-corrosive materials, nitrides were considered.

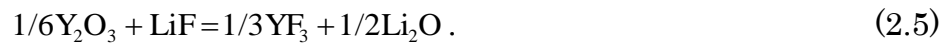
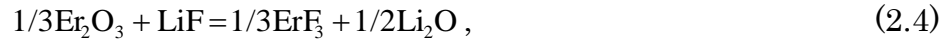
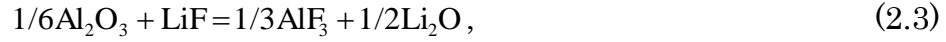
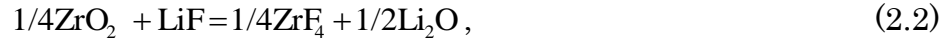
2. Compatibility with lithium fluoride

When a reaction is predicted based on equilibrium theory, Gibbs energy G for formation before the reaction is compared with that after the reaction. Difference of the Gibbs energy consists of difference of enthalpy H and entropy S and temperature T .

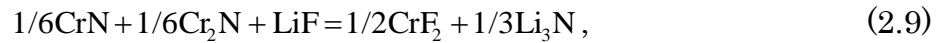
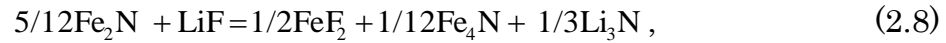
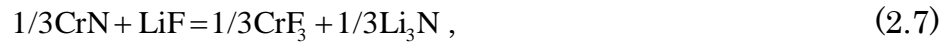
$$\Delta G = \Delta H - T\Delta S \quad (2.1)$$

Thermodynamics data such Gibbs energy, enthalpy and entropy were summarize in data base such a JANAF thermochemical tables [1, 2, 3, 4, 5, 6, 7]. In the present work, MALT [8] was used for calculation for the thermodynamics. The considered reactions follow:

Reaction between oxide and LiF:



Reaction between nitride and LiF:



Here, in these equations, left side indicates the system before reaction and right side indicates that after reaction. When difference of Gibbs energy about a ceramics material is positive ($\Delta G > 0$), the equilibrium will be shifted to left side. That means that it will has compatibility with LiF. On the contrary to that, when difference of Gibbs energy about a ceramics material is negative ($\Delta G < 0$), the equilibrium will be shifted to

right side. It is predicted that it will dissolve into molten salt including LiF.

3. Results of thermodynamics evaluation

Figure 2. 1 demonstrates difference between Gibbs energy between before and after reaction ΔG in lithium fluoride. This figure known as Ellingham diagram shows formation trend between materials and dependence of thermal stability on temperature [9, 10, 11] and provides us a clue to presume compatibility of materials with molten fluoride salt. The Gibbs energy was normalized by LiF. In this figure, temperature dependence of the reaction also indicates from 750 to 1000 K. The material whose plots are in upper half area ($\Delta G > 0$) has compatibility with LiF. That means the material would be stable in molten fluoride salt with LiF. On the contrary to the material whose plots are in lower half ($\Delta G < 0$) will dissolve into molten fluoride salt with LiF.

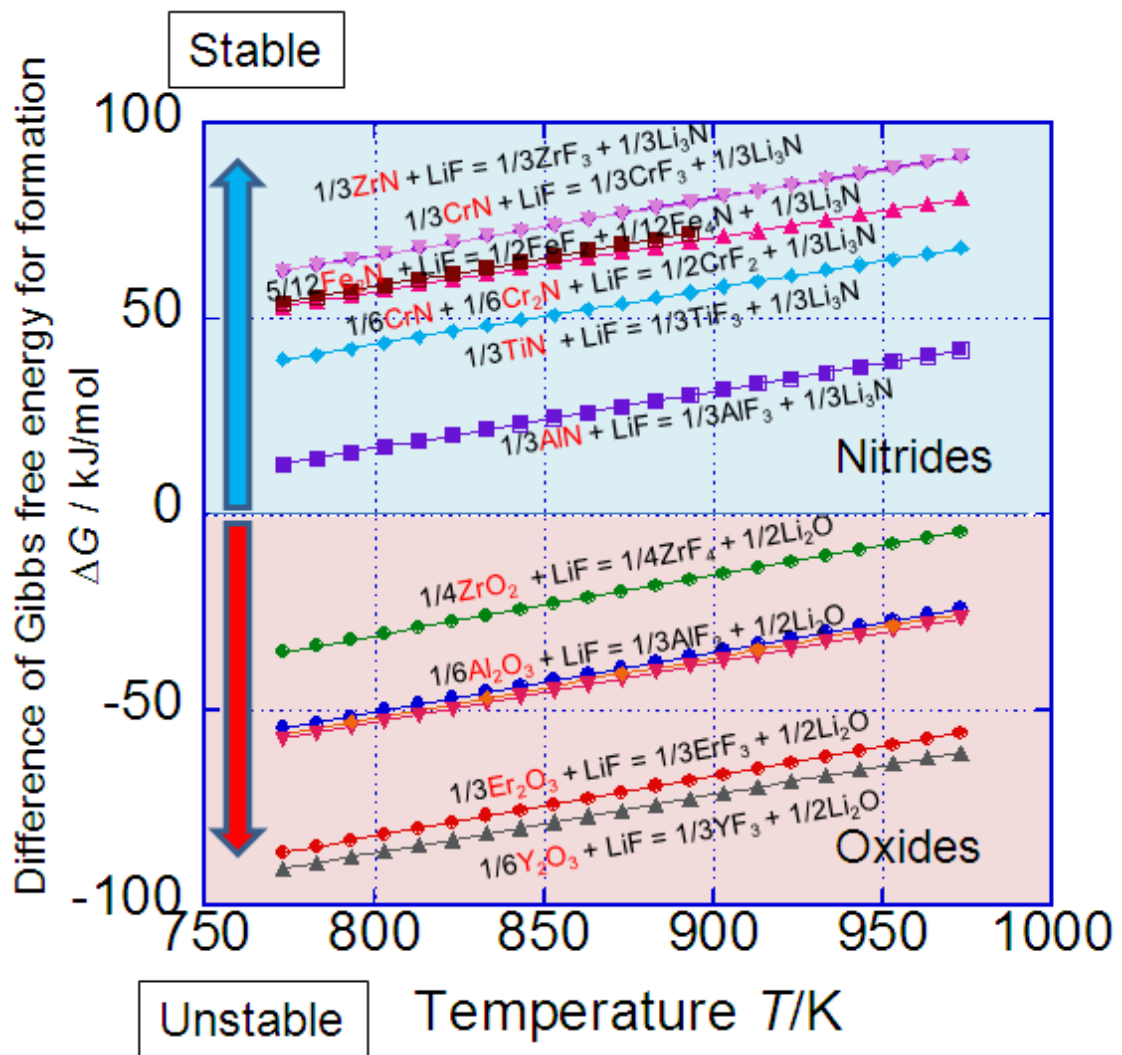


Figure 2. 1. Ellingham diagram of nitrides and oxides. It demonstrates temperature dependence of Gibbs energy difference between metal nitride or metal oxide and its fluoride. The material whose plots are in upper half area ($\Delta G > 0$) has compatibility with LiF. That means the material would be stable in molten fluoride salt with LiF. On the contrary to the material whose plots are in lower half ($\Delta G < 0$) will dissolve into molten fluoride salt with LiF.

From the results, it is predicted that nitrides have compatibility with lithium fluoride. That means that nitrides can be accredited as

candidate materials. On the other hand, oxides will dissolve into molten fluoride with lithium. Anti-corrosion by oxide coating on the surface of structural material will be impossible. To confirm those thermodynamic predictions, corrosion test using specimens made by oxides or nitrides will be needed. Using specimen with coating or surface medication on structural material will be also needed. For that, technique for coating or surface modification should be established. These predictions on compatibility with molten fluoride salt were verified using bulk specimens as a preliminary experiment. Appendix describes results about immersion test of Er_2O_3 , Y_2O_3 , Al_2O_3 and AlN in molten fluoride salt FLiNaK .

References

- [1] Wagman, D. D. Evans, W. H., Parker, V. B., Schumm, R. H., Halow, I., Bailey, S. M., Churney, K. L., Nuttall, R. L.; The NBS tables of chemical thermodynamic properties, selected values for inorganic and C1 and C2 organic substances in SI units; J. Phys. Chem. Ref. Data, Vol. 2, Supplement No. 2, 1982.
- [2] D.R. Stull, H. Prophet, 2nd ed., 1971, NSRDS-NBS-37.
- [3] M.W. Chase Jr., J.L. Curnutt, A. T.Hu, H. Prophet, A.N. Syverud, L.C.

Walker, "JANAF Thermochemical Tables, 1974 Supplement", J. Phys. Chem. Ref. Data 3 (1974)311.

[4] M. W. Chase, Jr., J.L. Curnutt, H. Prophet, R.A. McDonald, A.N. Syverud, "JANAF thermochemical tables, 1975 supplement", J. Phys. Chem. Ref. Data 4 (1975)1.

[5] M. W. Chase, Jr., J.L. Curnutt, R. A. McDonald, A. N. Syverud, "JANAF thermochemical tables, 1978 supplement", J. Phys. Chem. Ref. Data 7(1978) 793.

[6] M. W. Chase, Jr., J.R. Curnutt, J. R. Downey Jr., R.A. McDonald, A.N. Syverud, E. A. Valenzuela, "JANAF Thermochemical Tables, 1982 Supplement", J. Phys. Chem. Ref. Data 11(1982)695.

[7] M. W. Chase, Jr., C. A. Davies, J. R. Downey, Jr., D. J. Frurip, R.A. McDonald, A. N. Syverud, "JANAF Thermochemical Tables, 1985 Supplement", J. Phys. Chem. Ref. Data 14 (1985) Supplement No. 1.

[8] Materials-oriented Little Thermodynamic Database for PC (MALT), 科学技術社(Kagaku Gijutsu-Sha) .

[9] F.D. Richardson, Physical Chemistry of Melts in Metallurgy, Vol.2. Acad .Press, (1974).

[10] D.R. Gaskell, "Introduction to Metallurgical Thermodynamics", McGraw-Hill, (1973).

[11] D.R. Gaskell, "Introduction to the Thermodynamics of Materials, 3rd Edition", Taylor& Francis, (1995).

Chapter 3 Electrochemical nitriding

1. Introduction

Molten salt is a promising coolant material for self-cooled liquid blanket systems for heliotron fusion reactors of large helical device (LHD) type [1]. It has attractive safety advantages: low tritium solubility, inertness against air, inertness against water, low pressure operation, and low magnetohydrodynamic (MHD) resistance.

Because the most realistic thermonuclear fusion reaction is the deuterium-tritium reaction (D-T reaction), both deuterium and tritium as the fuel are actually necessary in the nuclear reaction in a fusion reactor whose construction is planned. Tritium is generated from a nuclear reaction between lithium and neutrons. The neutrons are supplied from the D-T reaction in the fusion reactor. A cooling system employing salt and including

lithium can also work as a tritium breeder. Hence, due to its inherent safety and high thermal efficiency in operation at temperatures above 773K, LiF-BeF₂ (FLiBe, LiF66.6mol%-BeF₂33.3mol%) has been discussed as a promising candidate for tritium breeding. LiF-NaF-KF (FLiNaK, LiF46.5mol%-NaF11.5mol%-KF42mol%) possesses chemical characteristics similar to those of FLiBe. Since it is permitted in laboratory experiments due to beryllium-free, FLiNaK can be used as a kind of material for simulation in the transportation of heat and movement of the material within the plant [2,3,4]. FLiNaK could also be an alternative to the liquid blanket for cooling and tritium breeding.

Development of a tritium penetration barrier, a tritium recovery system, and a heat exchanger were crucial steps in designing the blanket system. In the heat exchanger, tritium must be inhibited from permeating to the secondary coolant loop. At the same time, degradation of the heat transfer efficiency of the heat exchanger must be prevented.

We previously reported the chemical stability of nitride and metal oxide (AlN, Y₂O₃, Er₂O₃, and Al₂O₃) in FLiNaK [5,6]. It was demonstrated that AlN is promising as a tritium barrier material because it is more

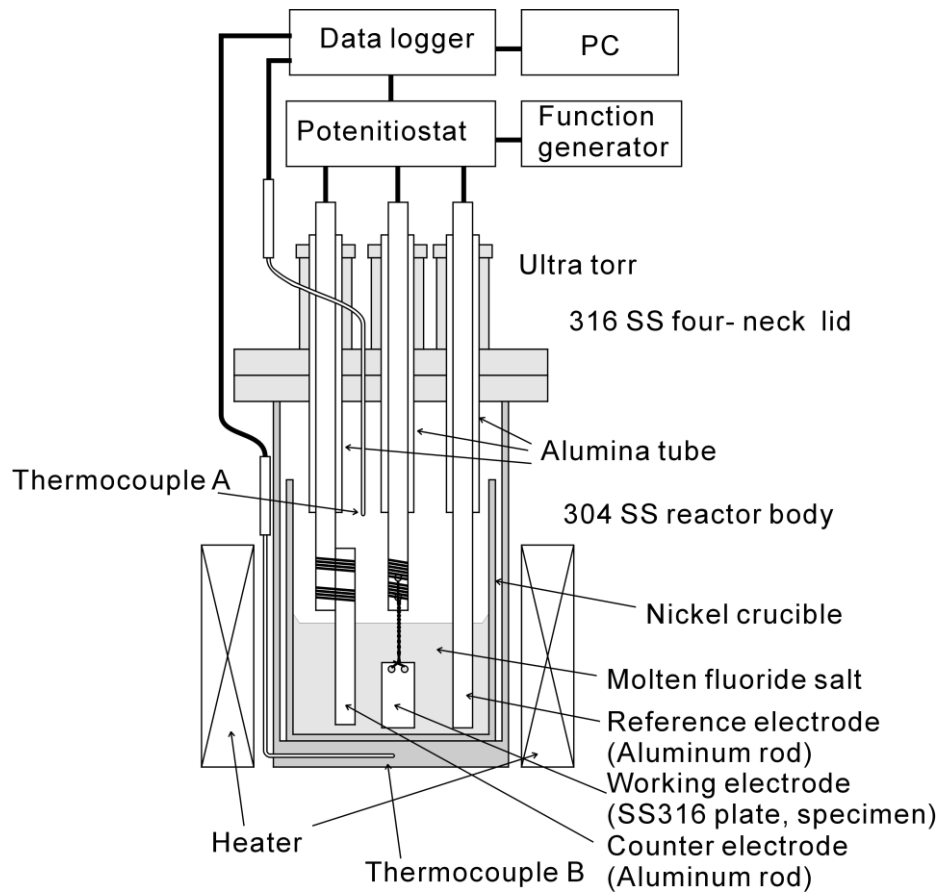
compatible with FLiNaK than the other candidates. In the next stage, the formation of a nitride layer on the surface of structural materials such as stainless steel and low activation steel is required for developing the system components. The present study seeks to develop the nitriding process for the structural material. Considering the nitriding treatment of such a large component, molten salt bath processing, such as Tafftride of Dufferrit GmbH, might be a more advantageous technique than other vapor-phase nitride processing, gas-phase nitriding treatments, ion nitriding, radical nitriding, etc. Nitride processing in a fluoride salt similar to the salt used for the blanket system is advantageous in cleaning up after processing. From the maintenance viewpoint, being able to repair a damaged nitride layer while the system is running might be advantageous [7].

Nitriding treatment of austenitic steel in molten fluoride salt containing lithium nitride Li_3N was therefore tried in this work. This is, as far as we know, the first experiment involving a nitride layer in molten fluoride salt.

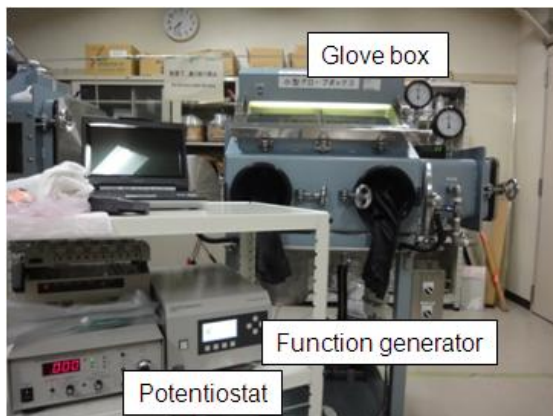
2. Experimental

When experiment using molten fluoride is considered, it needs dry and hot environment over 500°C. Ordinary commercial available glass experimental setups can not be used for the experiment. Under those situations, original experimental setups, in which temperature and moisture can be controlled, had to be designed and assembled for this work. Figure 3. 1 illustrates the experiment setup. The electrochemical reactor, which was designed for the present study, consists of a 304 SS container body and a 316 SS four-neck lid (Keiichirou Yasuji, Inc., Kobe).

(a)



(b)



(c)

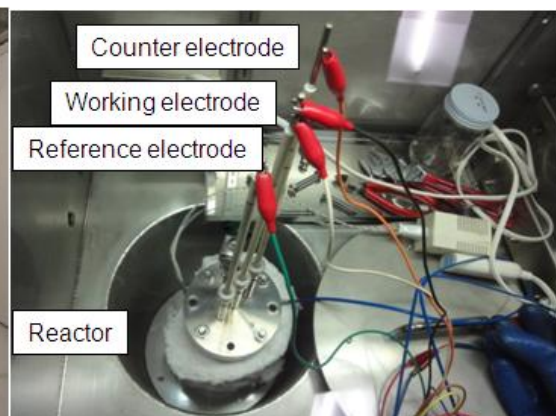


Figure 3. 1. Experiment setup for electrochemical measurement and treatment. The cell was filled with Ar gas at 1 atm. The measurement and treatment were done at 873 K. (a) Schematism for the experiment setup. (b) Overview of the experiment setup. The reactor vessel is installed in the grove box. (c) Inside view of the grove box.

The fluoride salt used in this study is a binary eutectic mixture of LiF-KF. It was prepared by combining LiF (Kanto chemical) and KF (Kishida Chemical) reagent-grade chemicals without purification. In the following, the eutectic salt consisting of 50mol% LiF and 50mol% KF is denoted as FLiK. Its melting point is 763K [8, 9]. For the nitrogen source, we referred to examples of Li₃N being added to chloride salt [10, 11]. Li₃N was added to FLiK with a mixture ratio of 49mol% LiF, 49mol% KF and 2.0mol% Li₃N. Rods of 99.99% pure aluminum (Nilaco) were employed as counter and reference electrodes [12,13,14]. The potential $-E$ was determined by the equilibrium reaction of lithium in a lithium-aluminum alloy. At this point, the coupling of lithium and lithium ion is in equilibrium:



A plate of austenitic stainless steel containing chromium and nickel, 316 SS (Nilaco), was employed as a working electrode and specimen for the nitriding treatment. The initial composition of 316 SS is given in Table 3. 1. A plate of 5mm × 10mm × 1mm was firmly bound to a pure nickel rod with nickel wire. These electrodes were inserted into an alumina tube (TYK, ALM) that was

sealed by a silicon gasket (ThreeBond, TB1211) for electronic insulation between the electrodes and the electrochemical reactor. Powdery LiF, KF, and Li₃N were put into the pure nickel crucible, and it was packed into the electrochemical reactor. The electrodes were inserted into tubes (necks) from the reactor lid and tightly fastened by ultra-torr connectors (Swagelok). The fourth neck was used for a safety valve. To avoid infiltration of ambient moisture come from the atmosphere, all procedures used to prepare the experiment setup were conducted in a glove box filled with dry argon gas.

Table 3. 1 Composition of 316 stainless steel specimen and treated specimen

Elements atomic ratio (%)	Fe	Cr	Ni	Mn	Mo	Si	C	O	N
*Composition from inspection certificate	Balance (68.56)	18.06	9.57	0.99	1.18	1.36	0.27	NS	NS
**Initial surface composition	81.25	10.88	4.18	1.21	1.28	ND	1.20	ND	ND
***Surface composition after treatment	44.36	23.07	12.07	ND	0.46	ND	0.72	13.09	6.23

*Corresponding values from wt%. **,*** These value were obtained from XPS analysis after 52 min argon ion sputtering. It approximately corresponds to 200nm etching.

Two thermocouples were used for measurement of temperature. As seen in Fig. 1, the one, thermocouple A, was inserted into the reactor through the four-neck lid. The measuring end was placed at the position where the specimen was hanged before and after the electrochemical treatment. The other, thermocouple B, was inserted into the bottom plate of the reactor and also used for proportional-integral-derivative (PID) control temperature controlling. Figure 3. 2 presents time-temperature curves for the electrochemical treatment. Curve (a) shows temperature at the position above the crucible where the ends of the electrodes were hanged before and after the treatment. Curve (b) shows temperature of the bottom of the reactor. The temperature of the molten salt in the crucible would change approximately along curve (b). The electrochemical reactor was heated from room temperature to 873K. After reaching this temperature, the electrode assemblies were brought down to immerse the electrode ends into the molten salt. Although the temperature of the working electrode, i.e., the specimen, could not be measured directly, it would change as shown on curve (c). The specimen would be heated from α to β along curve (a). When the electrodes were brought down after the reactor temperature reaching 873K, the

temperature of the specimen would be heated from β to γ . It was kept at 873K during the treatment for 100minutes from γ to δ along curve (b). When the electrodes were brought up after the treatment, the specimen would be cooled from δ to ε . And it would be cooled from ε to ζ along curve (a).

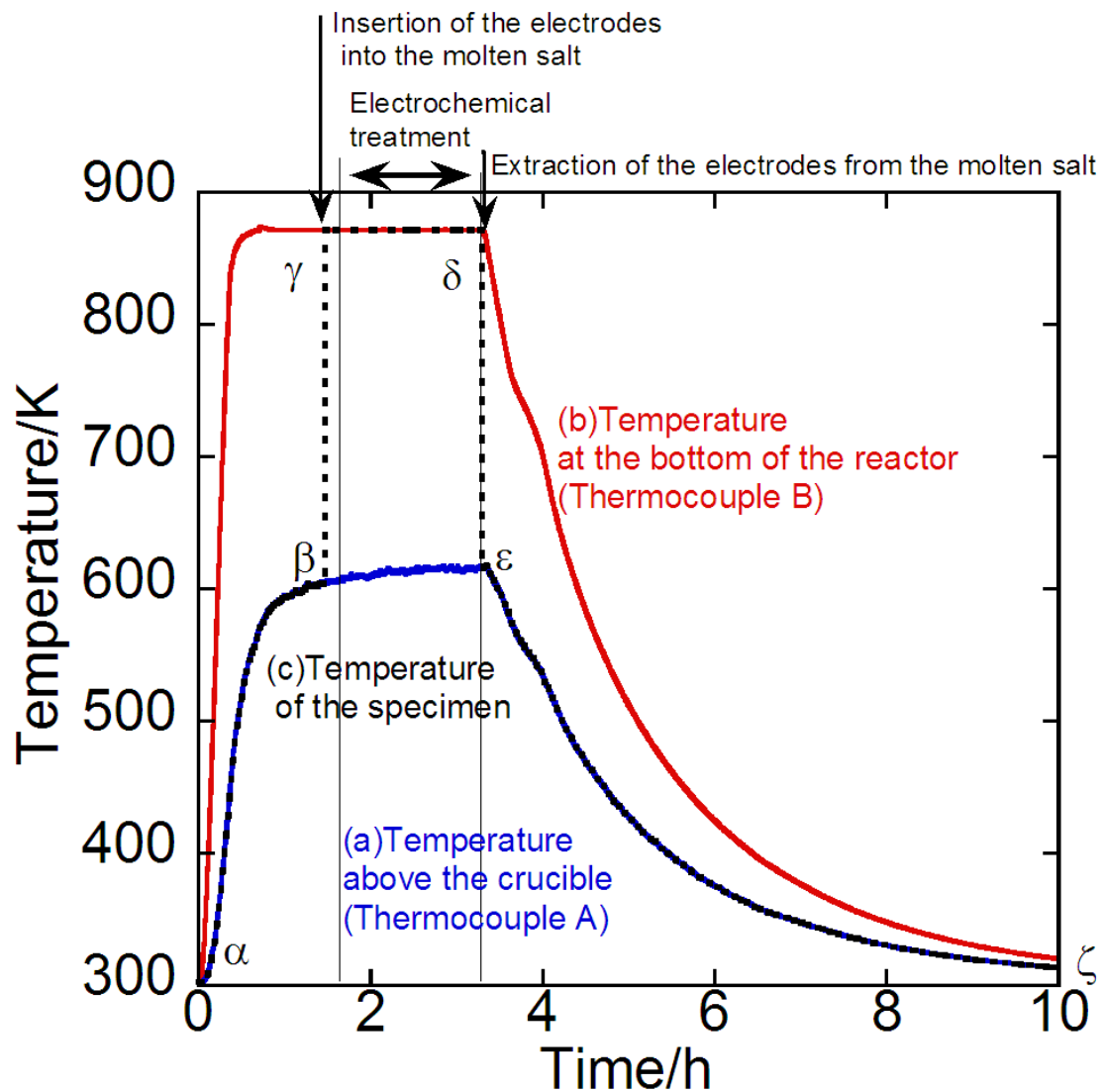


Figure 3. 2. Time-temperature curves for the electrochemical treatment. (a)Temperature above the crucible measured by thermocouple A. (b)Temperature at the bottom of the reactor measured by thermocouple B. (c)Temperature of the specimen assessed from (a) and (b).

The top ends of the electrode assemblies were connected via cables to a potentiostat and a function generator (Hokuto Denko, HA-151A and HB-305). Both electrochemical measurement and electrolysis treatment were conducted using the experiment setup. Potentiostatic electrolysis was conducted as an electrochemical treatment for nitriding. The potential was determined considering the cyclic voltammogram obtained prior to the treatment.

The specimen was characterized before and after the treatment. The surface structure was observed by scanning electron microscopy (SEM, JEOL JSM-5600). The cut specimen was embedded into resin after being treated. The cross-section, which was prepared by polishing, was analyzed by an electron probe micro-analyzer (EPMA, JEOL JXA-8500F and JXA-8100). Depth variations in the chemical composition and valence state were analyzed by X-ray photoelectron spectroscopy (XPS, Phi ESCA 1800). The crystal structure was characterized by X-ray diffraction (XRD, Rigaku RINT-2200/VTK).

3. Results and Discussion

3.1 Electrochemical behavior

Figure 3. 3 presents typical cyclic voltammograms obtained when a 316 SS electrode was immersed into molten FLiK. Figure 3. 3(a) presents a cyclic voltammogram of Li₃N-free FLiK. Current hardly flowed when scanning between 0.5V vs. Li/Li⁺ and 1.20V vs. Li/Li⁺. Over 1.2V vs. Li/Li⁺, cathodic and anodic currents of 0.01mA.cm⁻² were observed at 1.41V vs. Li/Li⁺ and 1.24V vs. Li/Li⁺, respectively. When the FLiK does not contain Li₃N, 316 SS is comparatively stable in electrochemical reactions below 1.2V vs. Li/Li⁺. This suggests that FLiK is electrochemically inactive within this potential range. In contrast, as seen in Fig. 3 (b), significant anodic current was observed in the cyclic voltammogram of FLiK containing 2.0mol% Li₃N. Adding Li₃N to FLiK drastically changes the electrochemistry. The current began to rise gradually at 0.25V vs. Li/Li⁺. In the potential range of 0.50V vs. Li/Li⁺ to 1.06V vs. Li/Li⁺, the current for forward scanning exceeded that for return scanning. The current corresponds to the oxidation to nitrogen atoms of the adsorbed nitride ions on the working electrode. The nitrogen atoms become a nitrogen source for nitride formation in the 316 SS specimen. This

difference in pathways in the cyclic voltammogram for this potential range suggests the possibility of an irreversible reaction on the electrode. The potentiostatic electrolysis for the nitriding treatment was therefore conducted at 1.00V vs. Li/Li⁺.

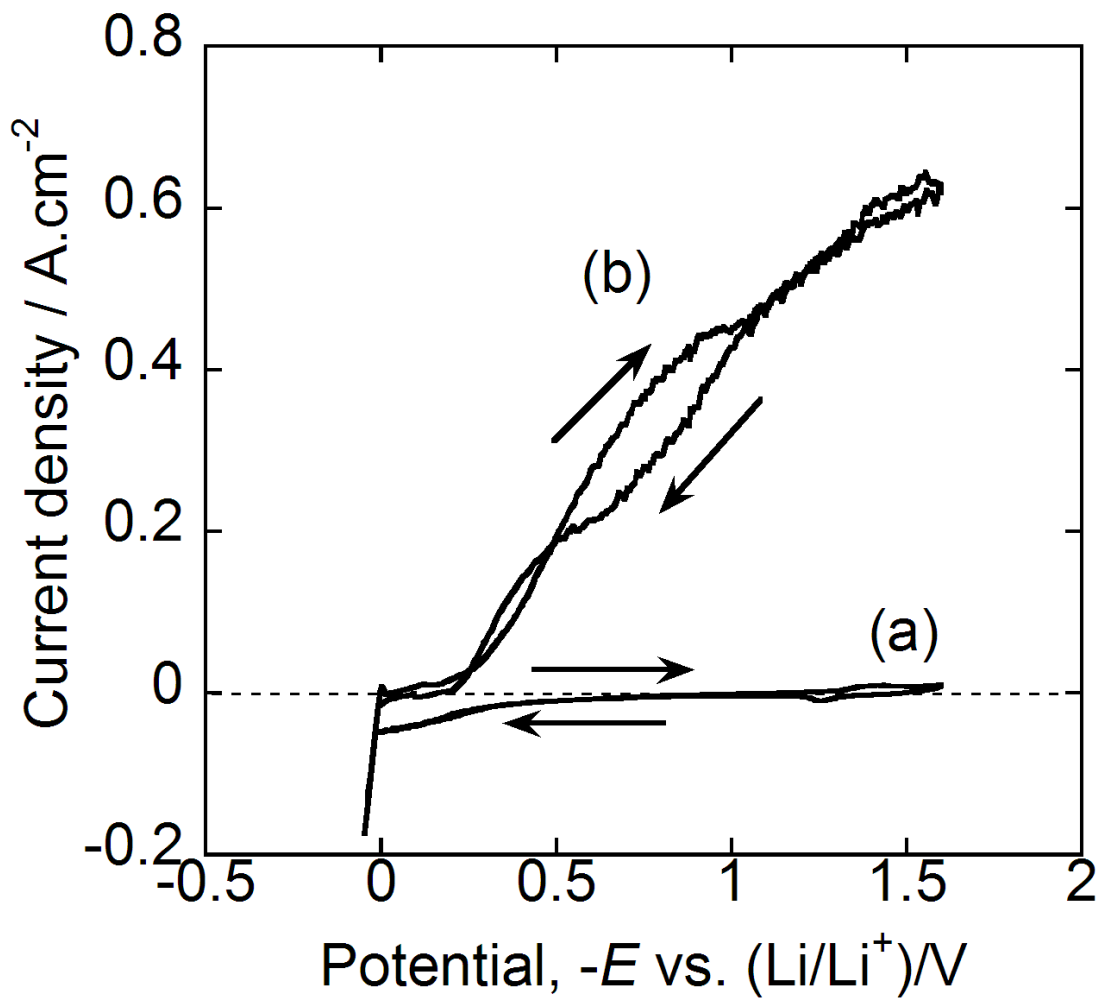


Figure 3. 3. Cyclic voltammogram of for 316 SS electrode in fluoride eutectic salt FLiK. (a) Li₃N free FLiK. (b) FLiK containing 2.0mol% Li₃N.

3.2 Surface structure

Figure 3. 4 presents typical SEM images of the specimen surface before and after electrical nitriding treatment. Figure 3. 4 (a) illustrates the initial surface of the specimen obtained prior to the nitriding treatment. It is composed of smooth grains of about 10 μ m in width packed in a lath structure. In contrast, as seen in Fig. 4 (b), the smooth surface of the grains changed drastically to a rough structure after the treatment for 100min. A rugged structure like wrinkles 1 to 2 μ m in width was formed on the surface of the grains after nitriding. These grains also were packed in a lath structure. Figure 3. 4 (c) illustrates the surface of the specimen treated for 241min. The wrinkle structure was lost. And the surface got more rugged. Several cracks were observed on the surface clearly. This implies that long treatment could cause the surface layer formed by the treatment to peel off. Considering practical applications, optimized treatment time should be determined carefully.

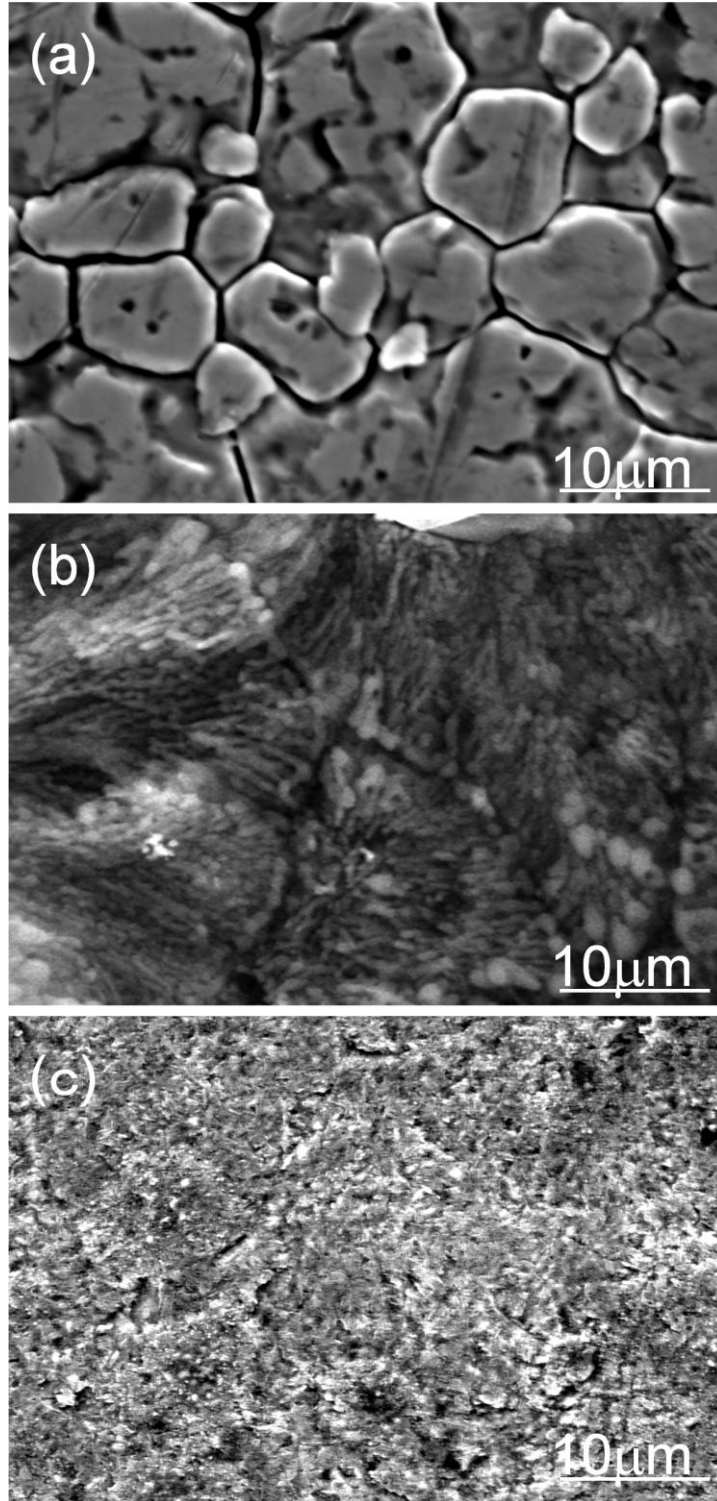


Figure 3. 4. SEM images. (a) Initial surface of 316 SS specimen. (b) Surface of the specimen treated for 100min in FLiK containing 2mol% of Li_3N at 873 K. (c) Surface of the specimen treated for 241min in FLiK containing 2mol% of Li_3N at 873 K.

3.3 Cross-section

Figure 3. 5 presents images of a cross-section of the treated specimen obtained by EPMA. The dark area indicates the resin layer; gray and colored areas indicate the specimen cross-section. Figure 3. 5 (a), the compositional image, reveals that a layer 35 μm in width exists which is apparently different from the base material 316 SS. When it was more minutely examined, several cracks that reached from the surface to a depth of 5 μm were found. Another interface seems to exist there. Figures 3. 4 (b), (c), and (d) present elemental mapping images obtained by EPMA which correspond to the distribution of iron (b), chromium (c), and nitrogen (d). As seen in Fig. 5 (b), there were four steps of iron concentration. In order of increasing depth: a surface and lowest-concentration layer of 2 μm width (green layer facing the resin), a second layer from there to a depth of 22 μm (green and yellow layer), a third layer from there to a depth of 35 μm (yellow and orange layer), and finally a bulk layer (red layer). As seen in Fig. 5(c), the chromium concentration also had four steps. The concentration trend, however, differs from that of iron. Chromium concentration was the highest in the 2 μm -wide

surface layer (red layer). In the second layer, from there to a depth of 22 μm (blue and green layer), the concentration decreased. In the third layer, from there to a depth of 35 μm (green and yellow layer), the chromium concentration increased. The next layer is the bulk layer (the yellow layer). As seen in Fig. 5 (d), the nitrogen concentration trend was more complicated. There are five concentration steps. The layer (2 μm -wide) where nitrogen concentration is the highest existed at the surface (red layer). This concentration trend seems to correspond to that of chromium. In the second layer, from there to a depth of 5 μm (yellow and green layer), the nitrogen concentration decreased. This layer corresponds to the cracked layer confirmed in Fig. 5 (a). The endpoint of the crack reached the boundary between the second and third layers. In the third layer, from there to a depth of 22 μm (yellow and red layer), the concentration again increased. In the next layer, from there to a depth of 35 μm , the concentration decreased. The final layer (blue and black layer) was the bulk layer. This result indicates that nitrogen reached from the surface to a depth of 35 μm . Figure 3. 5 (e) presents line profiles corresponding to the areas between each two lines on the mapping images. The profiles indicate that the iron concentration was

lower in the layer from the surface to a depth of 35 μ m than in the base layer. In contrast, chromium and nitrogen were concentrated near the surface. The chromium concentration seems to go up and down along with nitrogen near the surface. It is also clear from this figure that the chromium concentration decreased from there to a depth of 35 μ m. Upon reaching the bulk layer at a depth of 35 μ m, it increased again. When compared with the bulk layer, the concentrations of both iron and chrome in the nitrogen diffusion layer decreased by about 8%. Nitrogen reached a depth of 35 μ m from the surface. The penetration depth seems to correspond to the concentration trend for iron and chromium.

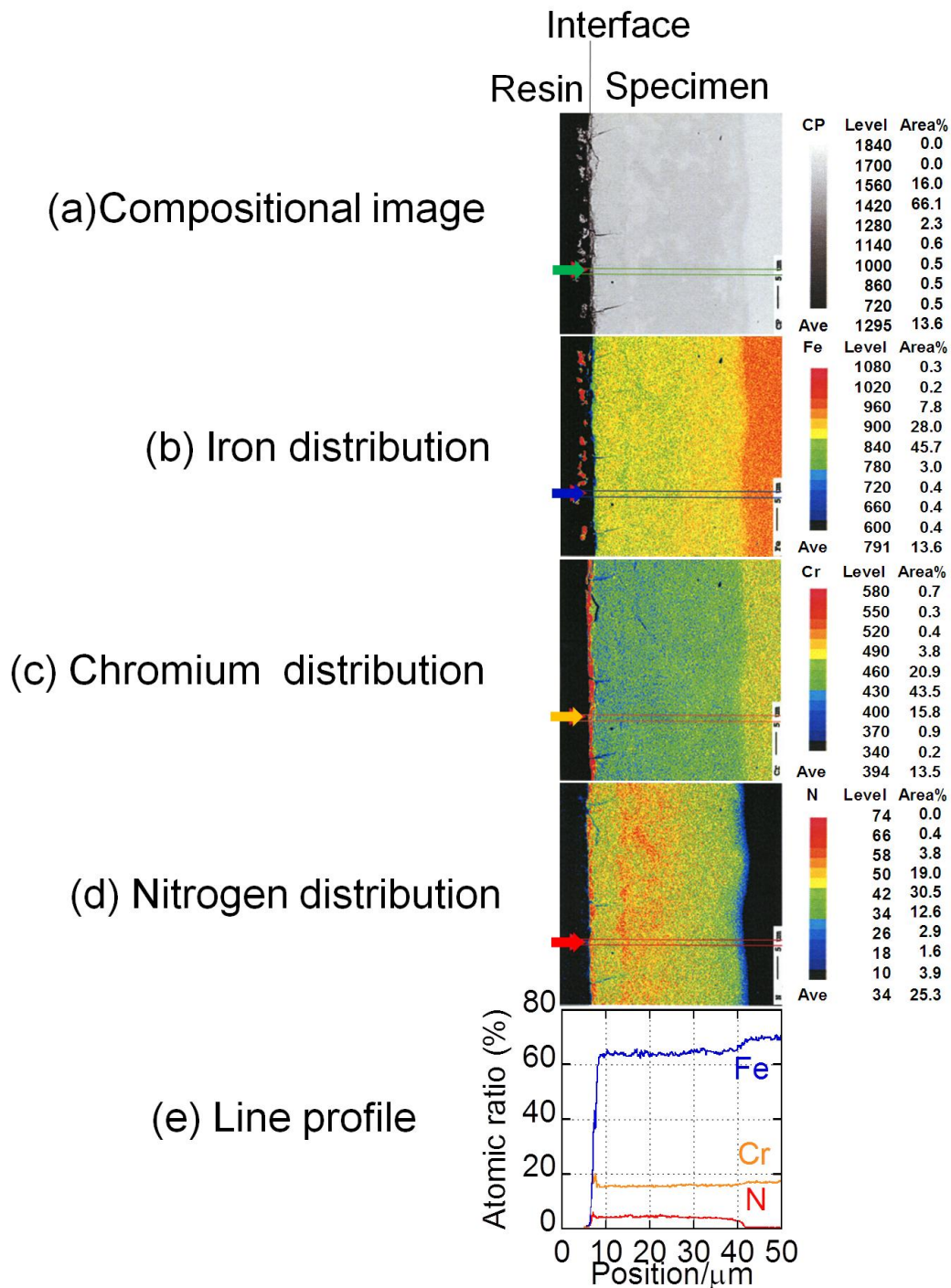
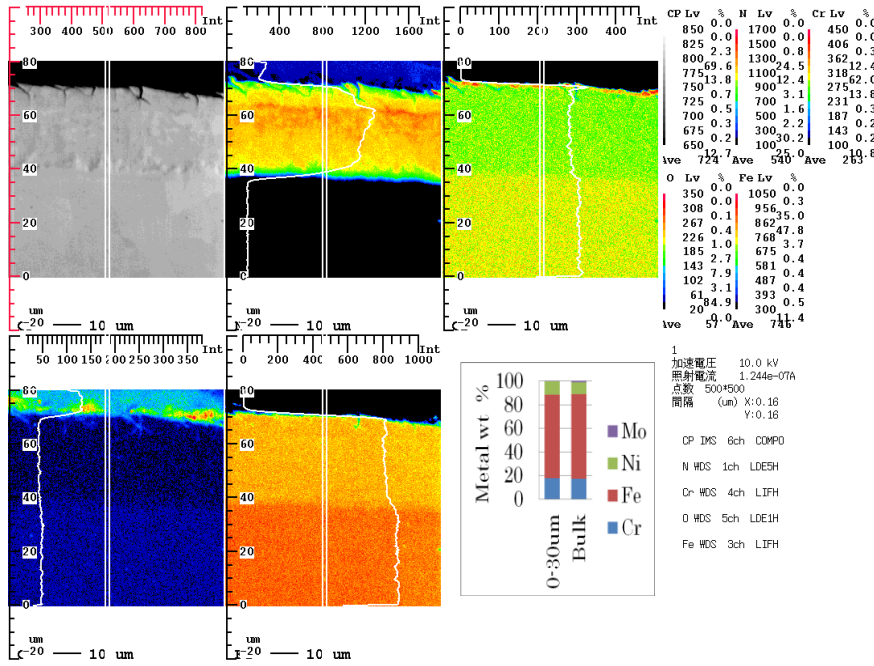


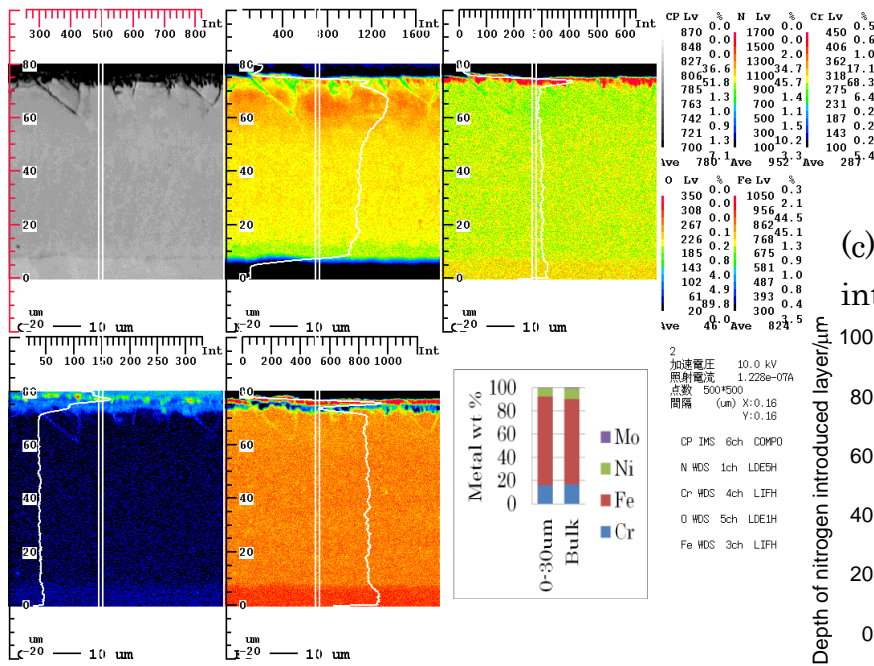
Figure 3. 5. Compositional analysis of cross-section of the specimen treated in FLiK including 2mol% of Li_3N for 100min. (a) Compositional image by FE-SEM. (b)-(d) Elemental mapping images by EPMA. (b) Iron distribution. (c) Iron distribution and nitrogen distribution. (e) Line profiles from EPMA. These profiles correspond to each band between lines on the mapping images.

Oxygen distribution was also examined in wider area using EPMA. Figure 3. 6 presents distribution of oxygen, nitrogen, chromium and iron. According to EPMA analysis as shown in fig. 6, concentration of oxygen decreased in nitrogen introduced layer. Figure 3. 6(a) shows the cross section of the specimen obtained by 100 min treatment; Figure 3. 6(b) shows that by 241 min treatment. This means that nitriding is dominant reaction rather than oxidation. And, metal ratio in the nitrogen diffusion layer was almost same as that in bulk. Figure 3. 6(c) demonstrates a relationship between treatment time and depth of nitrogen introduced layer. It shows that nitrogen was introduced in proportion to treatment time. The nitrogen distribution has plateau shape. This clearly shows that it is different from Gaussian distribution with broaden tail which is often found in atomic diffusion process and that this nitrogen introduction process is different from usual diffusion process. As described later in section 3.5, it is accompanied with drastic change of crystal structure.

(a) Cross-section of specimen treated for 100 min



(b) Cross-section of specimen treated for 240 min



(c) Depth of nitrogen introduced layer

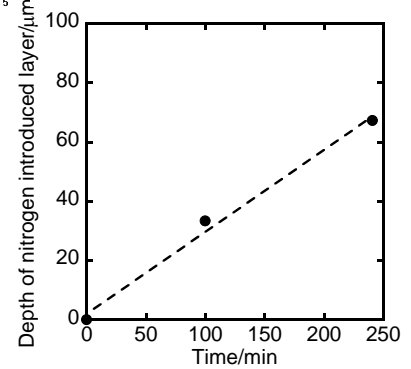


Figure 3. 6 Compositional analysis of cross-section of the specimen treated in FLiK. Element mapping was conducted by EPMA and metal weight ratio was evaluated by EDX. (a) Cross-section of specimen treated for 100 min. (b) Cross-section of specimen for 240 min. (c) Relationship between treatment time and depth of nitrogen introduced layer.

3.4 XPS analysis

Figure 3. 7 presents a composition depth profile obtained by XPS. Figure 3. 7 (a) indicates the atomic ratio of the initial specimen surface before treatment. Table 3. 1 compares the results from the XPS analysis with those listed on the inspection certificate from the manufacturer. This suggests that the iron concentration was higher and the chromium and nickel concentrations were lower near the surface. Figure 3. 7 (b) indicates the atomic ratio of the treated specimen, and also reveals that the treatment drastically changed the surface composition. The iron concentration decreased and the chromium concentration increased, and nitrogen was clearly introduced into the specimen. This result is consistent with the result from EPMA.

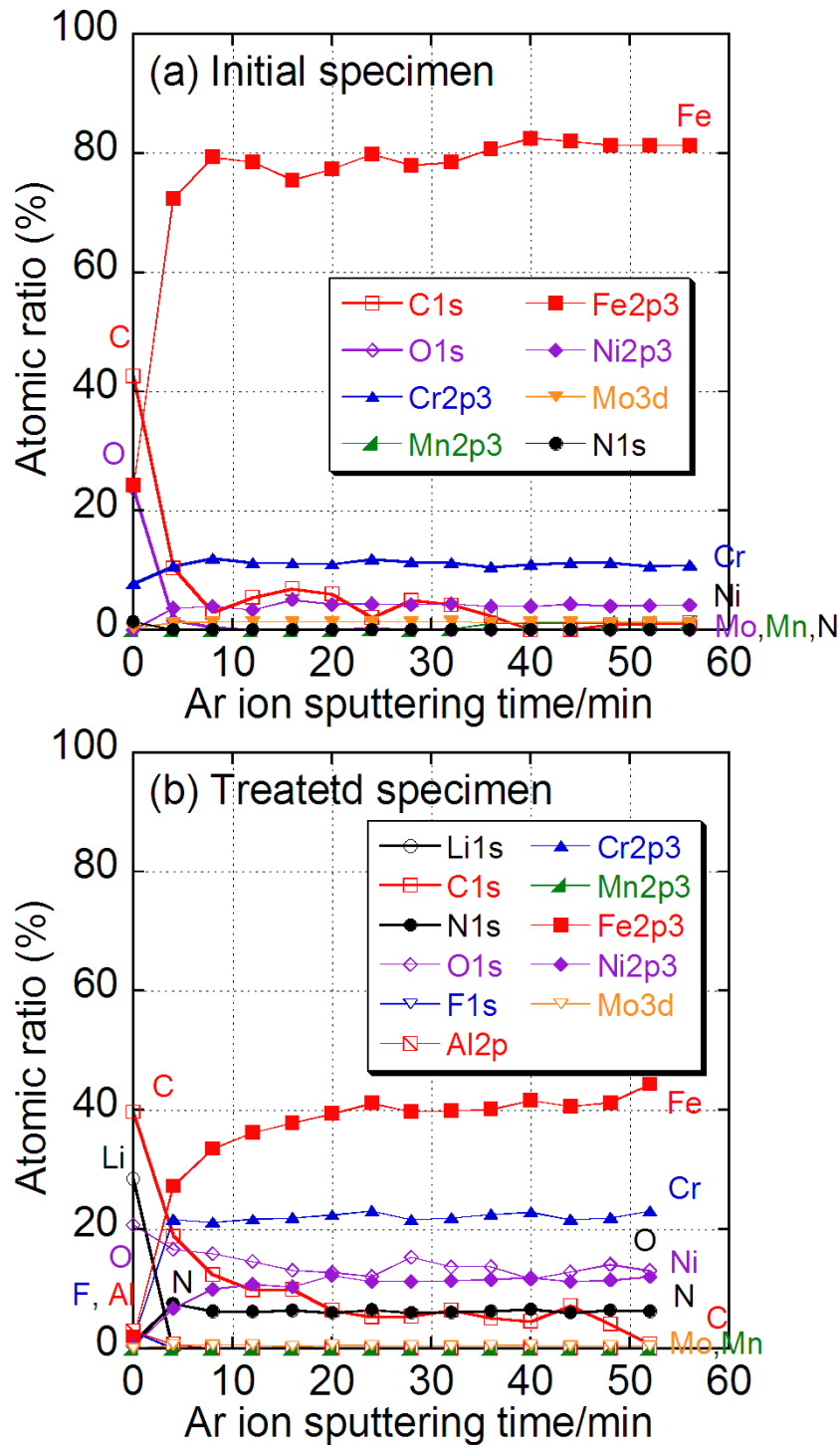


Figure 3. 7. Compositional depth variation obtained by XPS. The atomic ratio was evaluated from XPS spectra measured by 4min Ar ion sputtering. The etching rate is about 4nm/min.; 50min sputtering corresponds to about 200nm. (a) Initial specimen. (b) Specimen after treatment for 100min in

FLiK containing Li_3N .

Figure 3. 8 presents XPS spectra: (a) iron 2p, (b) chromium 2p, (c) nickel 2p, and (d) nitrogen 1s peaks. To discuss oxidation state from chemical shift, the spectra from the initial specimen can be compared with those taken after the treatment [15]. As seen in Fig. 8 (a), the $2p_{1/2}$ peak and $2p_{3/2}$ peak of iron were detected at 719.78eV and at 706.66eV [16]. The strength of these peaks was reduced after the treatment. However, their width and position were retained. As seen in Fig. 8 (b), the peaks of $2p_{1/2}$ and $2p_{3/2}$ for chromium were detected at 583.12eV and at 573.95eV [17,18]. In this case, although the peak height was lower after the treatment, the width broadened and the area expanded. This means that the treatment changed the chemical state of the chromium into a higher valence state by nitriding. As seen in Fig. 8 (c), the $2p_{3/2}$ peak of nickel increased. In this case, the peak position and width were retained. This result represents an increase in nickel concentration. Finally, as seen in Fig. 8 (d), the 1s peak of nitrogen was detected. This peak was detected after the treatment but not before. This means that the treatment introduced nitrogen into the base material 316 SS. Considering the detection of the 1s peak of nitrogen and the broadening of the chromium 2p peak, these results suggest that chromium

nitride formed at the surface. The atomic ratio would also have changed due to nitride formation.

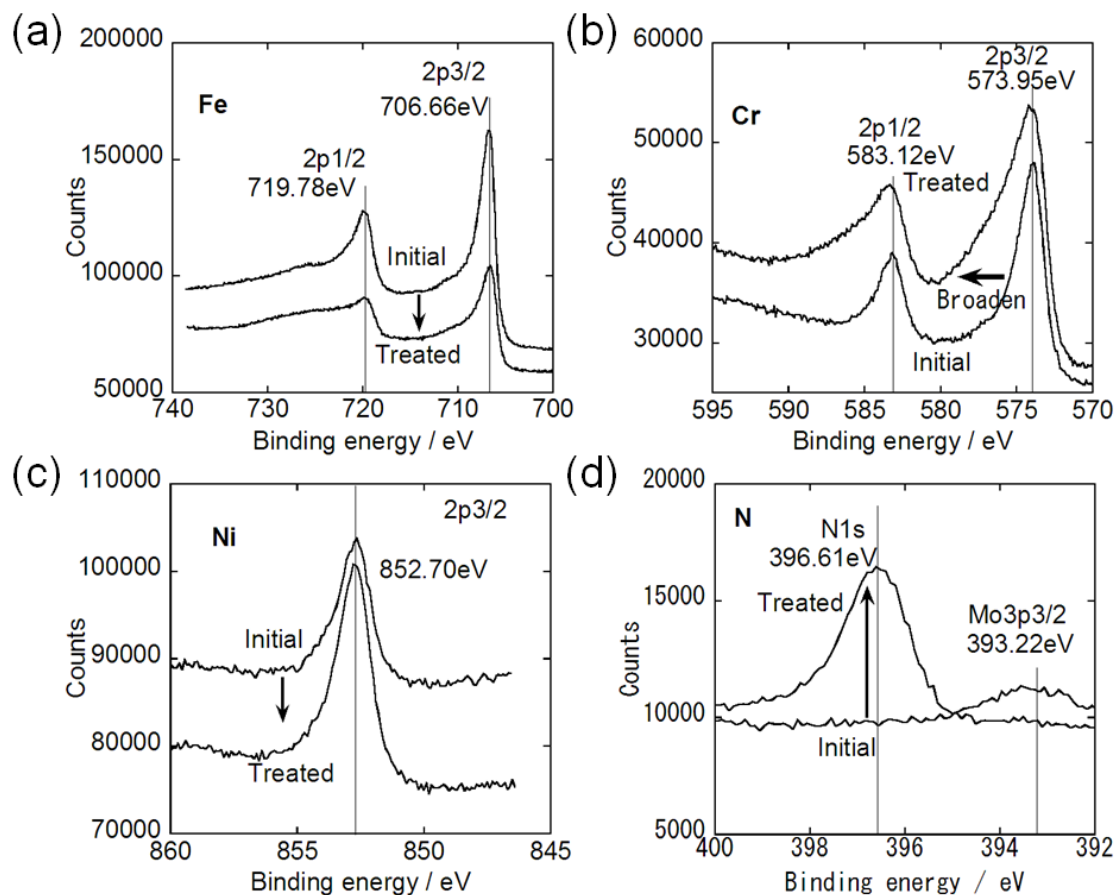


Figure 3. 8. XPS spectra of the specimen before and after electrochemical treatment for 100min in FLiK containing Li_3N . (a) Fe2p. (b) Cr2p. (c) Ni2p. (d) N1s. These spectra were obtained after 52min Ar ion sputtering, which corresponds to about 200nm etching from the surface.

Figure 3. 9 presents separation views of the chromium 2p peaks. These are separations of the spectra presented in Fig. 8(b). As seen in Fig. 9 (a), three peaks can be separated within the 2p_{3/2} peak. The peaks at

573.95eV correspond to the metallic state. The other peaks at 575.04eV and 577.00eV indicate that chromium ions are in the trivalent state. These peaks correspond to oxide and hydroxide. Also, as seen in Fig. 9 (b), four peaks can be separated within the $2p_{3/2}$ peak. The peak at 573.95eV corresponds to the metallic state. The peaks at 574.95eV and 577.17eV indicate that the chromium ions are trivalent. These peaks correspond to nitride and oxide. The peak rose significantly at 574.95eV. Considering rise in concentration of nitrogen and chromium at the surface seen in Fig. 5, it would be reasonable for chromium nitride to form. The peak at 579.13eV indicates higher valence corresponding to oxide.

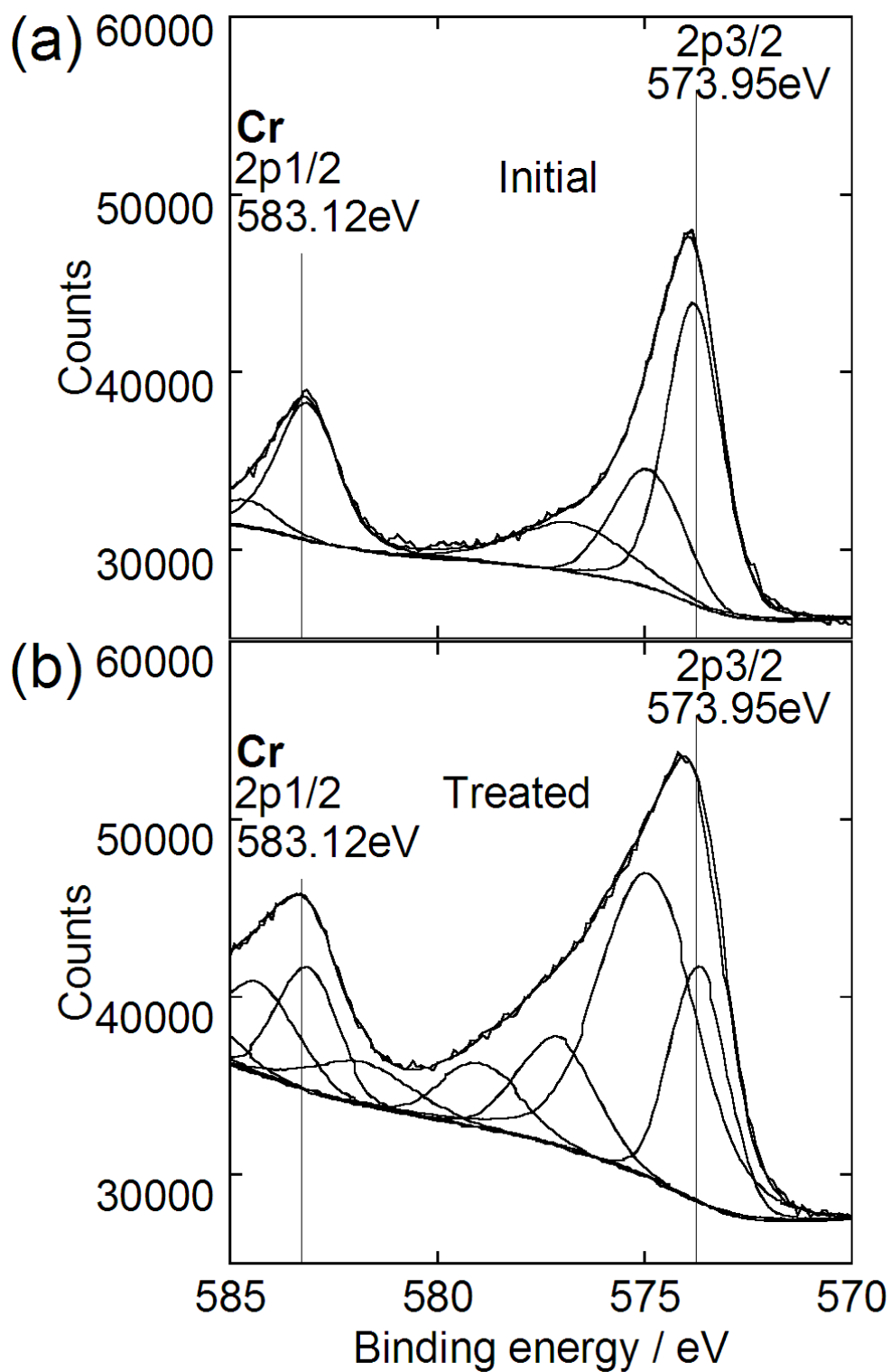


Figure 3. 9. Separation of chromium 2p peaks in XPS. These spectra were separated from those in Fig. 6. (a) Initial specimen. (b) Treated specimen.

3.5 XRD analysis

Figure 3. 10 presents XRD patterns of the 316 SS specimen. As seen in Fig. 10 (a), the pattern of the initial specimen closely resembles that of austenitic steel. No diffraction peaks of nitrides were detected in the pattern. Figure 3. 10(b) presents the pattern of 316 SS treated applied 1.0V vs. Li/Li⁺ in FLiK without Li₃N for 100minutes. Although the specimen underwent the same heating and cooling process as the process which the specimen treated in FLiK including Li₃N underwent, the XRD pattern was identical with the initial pattern. This means that the heating and cooling process does not affect on the crystal structure of the specimen in the treatment. Phase transition of iron does not cause through the heating and cooling process. However, as seen in Fig. 10 (c), the treatment drastically changed the diffraction pattern. Several peaks that had not existed in the initial pattern appeared in the pattern obtained after treatment. Several diffraction patterns were superimposed on the initial diffraction pattern. According to pattern matching based on JCPDS and literature, one of those diffraction patterns was that of chromium nitride CrN [19]. Another one seemed to be

the pattern of ferritic iron or that of iron nitride $\alpha\text{-Fe}_{x(x>8)}\text{N}$ [20]. Recalling the investigation of the cross-section, i.e., the EPMA mapping images in Figs. 5 and 6, a 35 μm -thick nitrogen diffusion layer was formed for 100 min treatment. A 65 μm -thick nitrogen diffusion layer also was formed for 240 min treatment. This means that the pattern corresponds to $\alpha\text{-Fe}_{x(x>8)}\text{N}$. Nitrogen atoms would be dispersed between metal atoms as a solid solution. These results are also consistent with the result of XPS seen in Figs. 7 and 8. As described above, chromium nitriding seems to compete with iron nitriding, and more chromium nitride than iron nitride tends to form. Since there are several kinds of iron nitride, it would be complicated to discuss their formation in stainless steel. Figure 3. 10(d) presents the pattern of 316 SS treated for 240min. In this pattern, peaks from $\alpha\text{-Fe}_{x(x>8)}\text{N}$ are mainly indicated. Nitrogen introduction seems to promote the phase change from face-center cubic (fcc) structure to body-centered tetragonal (bct) structure

$\alpha\text{-Fe}_{16}\text{N}_2$ possesses 3.0 μ B of magnetic momentum and 240emu/g of saturated magnetization. It is expected as a novel rare earth less magnetism material [21]. The nitrogen introduced stainless steel might possess magnetic property bear comparison with their $\alpha\text{-Fe}_{16}\text{N}_2$.

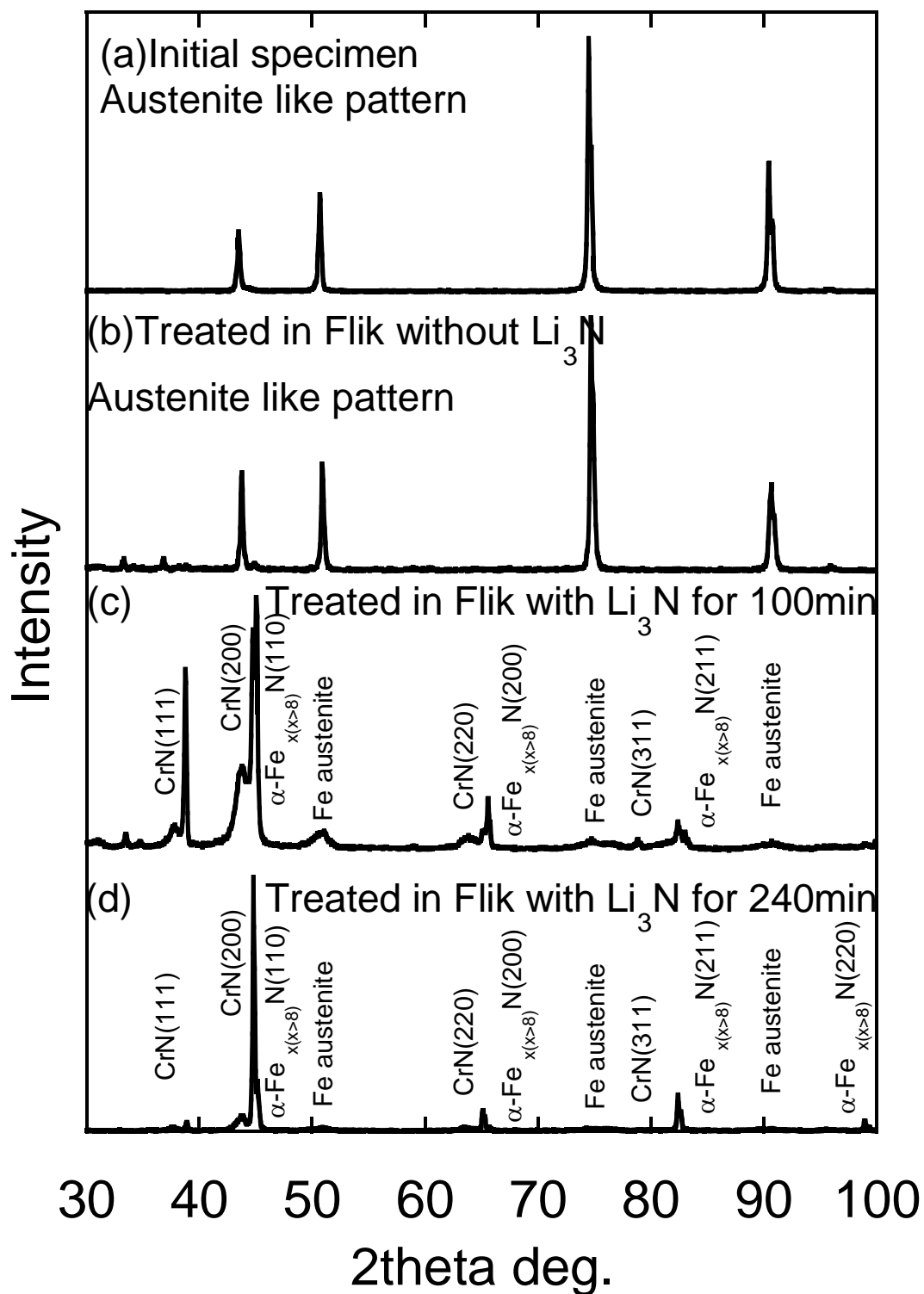


Figure 3. 10. X-ray diffraction patterns. (a) Initial 316 SS specimen. (b) 316 SS specimen applied 1.0V vs. Li/Li^+ without Li_3N for 100min. (c) Specimen after electrochemical treatment for 100min in FLiK containing Li_3N . (d) Specimen after electrochemical treatment for 240min in FLiK containing

Li_3N .

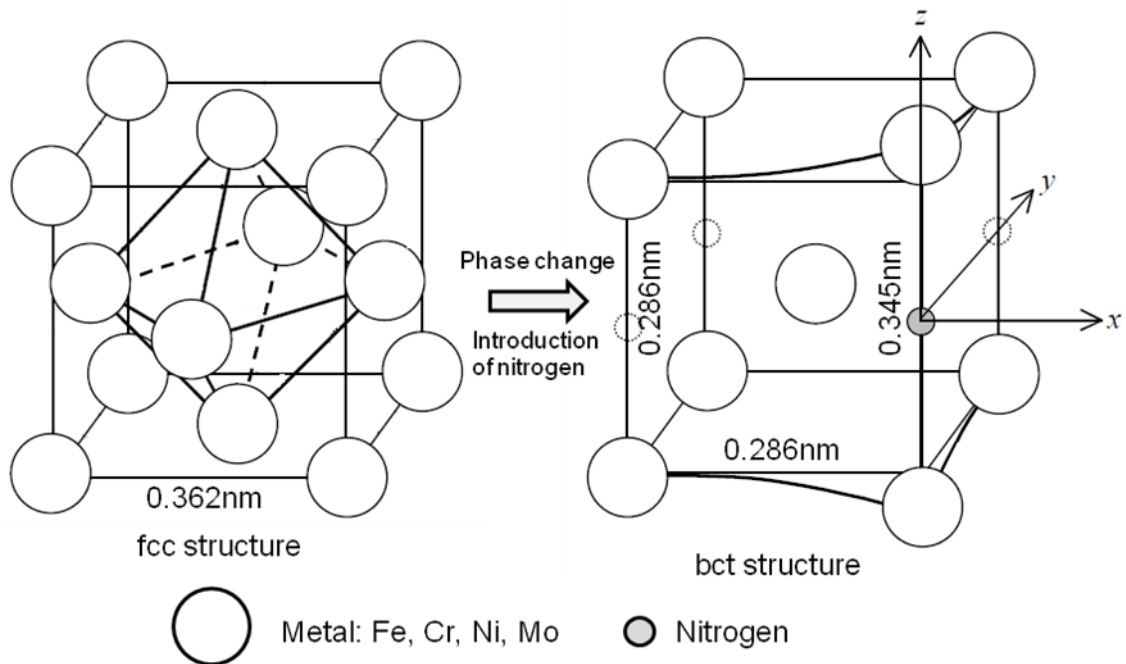


Figure 3. 11. Phase change from face-center cubic (fcc) structure to body-centered tetragonal (bct) structure in nitrogen introduction.

References

- [1] A. Sagara, S. Imagawa, O. Mitarai, T. Dolan, T. Tanaka, Y. Kubota, K. Yamazaki, K.Y. Watanabe, N. Mizuguchi, T. Muroga, N. Noda, O. Kaneko, H. Yamada, N. Ohya, T. Uda, A. Komori, S. Sudo and O. Motojima, "Improved structure and long-life blanket concepts for heliotron reactors", Nucl. Fusion 45 (2005) 258.
- [2] M. Kondo, T. Nagasaka, A. Sagara, N. Noda, T. Muroga, M. Nagura, A. Suzuki, T. Terai, J. Nucl. Mater., "Metallurgical study on corrosion of austenitic steels in molten salt $\text{LiF}\text{-BeF}_2$ (Flibe)", 386–388 (2009) 685.
- [3] M. Kondo, T. Nagasaka, T. Muroga, A. Sagara, N. Noda, Q. Xu, D. Ninomiya, N. Masaru, A. Suzuki, T. Terai, "High Performance Corrosion Resistance of Nickel-Based Alloys in Molten Salt Flibe", Fusion Technol.

56(2009)190.

[4] M. Kondo, T. Nagasaka, Q. Xu, T. Muroga, A. Sagara, N. Noda, D. Ninomiya, M. Nagura, A. Suzuki, T. Terai, N. Fujii, "Corrosion characteristics of reduced activation ferritic steel, JLF-1 (8.92Cr-2W) in molten salts Flibe and Flinak", Fusion Eng. Des. 84 (2009)1081.

[5] T. Watanabe, M. Kondo, T. Nagasaka, A. Sagara, Book of Abstracts for APFA 2009 and APPTC 2009, "Chemical stability and thermal conductive property of tritium permeation barrier materials for molten salt system", (2009)140.

[6] T. Watanabe, M. Kondo, T. Nagasaka, A. Sagara, "Corrosion characteristic of AlN, Y₂O₃, Er₂O₃ and Al₂O₃ in Flinak for molten salt blanket system", J. Plasma and Fusion Res. series 9(2010)342.

[7] Z. Yao, A. Suzuki, T. Muroga, T. Nagasaka, "Structural stability and self-healing capability of Er₂O₃ in situ coating on V-4Cr-4Ti in liquid lithium", Fusion Eng. Des. 81(2006) 2887.

[8] R. E. Thoma, (Ed.), "PHASE DIAGRAMS OF NUCLEAR REACTOR MATERIALS", ORNL-2548 Chemistry - General TID-4500 (15th ed.)

[9] A. G. Bergman, E.P. Dergunov, "Fusion Diagram of LiF-KF-NaF", C.R. Acad. Sci., U.R.S.S., 31(1941)754.

[10] T. Goto, Y. Ito, "Electrochemical reduction of nitrogen gas in a molten chloride system", Electrochimica Acta 43(1998)3379.

[11] H. Tsujimura, T. Goto, Y. Ito, "Electrochemical surface nitriding of pure iron by molten salt electrochemical process", J. Alloy and Compd., 376(2004)246.

[12] K. Amezawa, Y. Ito, Y. Tomii, J. Electrochem. Soc., "The Single-Electrode Peltier Heats of Li-Al Alloy Electrodes in LiCl-KCl Eutectic System",

141(1994)3096.

[13] C.J. Wen, B. A. Boukamp, R. A. Huggins, W. Weppner, "Thermodynamic and Mass Transport Properties of "LiAl", J. Electrochem. Soc. 126(1979)2258.

[14] R.A. Sharma and R.N. Seefurth, "Thermodynamic Properties of the Lithium-Silicon System", J. Electrochem Soc. 123 (1976) 1763.

[15] J. Chastain, in R.C. King, Jr. (Ed.), Handbook of X-ray Photoelectron Spectroscopy, Physical Electronics, Inc., 1995.

[16] I. Olefjord, L. Wegrelius, "Surface analysis of passive state", Corrs. Sci.,31(1990)89.

[17] I. Milošev, H.H. Strehblow, B. Navinšek, "Comparison of TiN, ZrN and CrN hard nitride coatings: Electrochemical and thermal oxidation", Thin Solid Films 303(1997)246.

[18] S.B. Sant, K.S. Gill, "Growth and characterization of cathodic arc evaporated CrN, (TiAl)N and (TiZr)N films", Sur. Coat. Technol., 68-69(1994)152.

[19] Powder Diffraction File from the Joint Committee for Powder Diffraction Standards (PDF JCPDS) #11-0065.

[20] P. Prieto, J. F. Marco, J. M. Sanz, "Synthesis and characterization of iron nitrides. An XRD, Mössbauer, RBS and XPS characterization", Surf Interface Anal., 40(2008)781.

[21] T. K. Kim and M. Takahashi, "New Magnetic Material Having Ultrahigh Magnetic Moment", Appl. Phys. Lett. 20 (1972) 492.

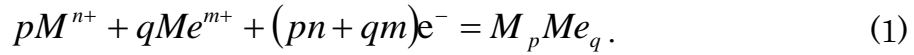
Chapter 4 Thermodynamic consideration

1. Thermodynamic consideration

The reaction at electrode surface is assisted by power source such a potentiostat. This means non-equilibrium process. Cyclic voltammogram also includes non-equilibrium process. In fact, the reaction rate for theoretic treatment is required for consideration of reaction. However, when scan rate is enough slow, the reaction can be pseudo-equilibrium reaction. The reaction was predicted from combination of Gibbs free energy from thermodynamics and standard potential from electrochemistry. It is based on an equilibrium assumption.

2. Equilibrium electrochemical synthesis

Equilibrium electrochemical synthesis (EES) diagram will give us a practical prospect about deposition of elements and compounds on the surface of the specimen at a constant temperature [1, 2]. It is constructed by calculation of the deposition potentials. Considering formation of compound in a binary system from components, M and Me ,



Deposition potential $E^{synthesis}$ is given as follows:

$$E_{M_pMe_q}^{synthesis} = E_{Me}^{inert} + \frac{-\Delta G_{M_pMe_q}^{\circ} + pnF(E_M^{inert} - E_{Me}^{inert})}{(pn + qm)F}, \quad (2)$$

where p and q are the stoichiometric coefficients of M and Me ; m and n are the charge of ions of the components M and Me ; E^{inert} is the equilibrium deposition potential of the given element on the inert electrode; ΔG° is standard free energy of formation; and F is Faraday constant. Comparison of deposition potential allows us to guess what kind of compound will be formed on the surface of the specimen at a constant temperature. For convenience, considering M is chromium or iron; Me is nitrogen, variable x is defined as follows:

$$E_{Me}^{inert} = E_N^{inert} \equiv 0, \quad (3)$$

$$x \equiv E_N^{inert} - E_M^{inert} . \quad (4)$$

Then, x is potential applied to the working electrode. Considering reactive specimen surface with N^{3-} , Eq. (2) can be simplified as follows:

$$E_{nitride}^{synthesis} = \frac{\Delta G_{T,nitride}^{\circ}}{3qF} , \quad (5)$$

where the standard free energy of formation on nitride at a temperature T , ΔG° is defined using standard enthalpy H° and standard entropy S° as follows:

$$\Delta G_{T,nitride}^{\circ} = \Delta H_{T,nitride}^{\circ} - T\Delta S_{T,nitride}^{\circ} . \quad (6)$$

The difference of standard entropy ΔS° can be obtained from standard entropy S . For example, in case of Cr_2N formation at 873K,

$$\Delta S_{873,Cr_2N}^{\circ} = S_{873,Cr_2N}^{\circ} - 2S_{873,Cr}^{\circ} + \frac{1}{2}S_{873,N_2}^{\circ} . \quad (7)$$

The deposition potentials $E^{synthesis}$ can be calculated using Eq.(6). Here, CrN , Cr_2N , Fe_2N and Fe_4N were considered as nitrides. Unfortunately, we do not have thermodynamic data of $\alpha-Fe_{x(x>8)}N$. The deposition potentials at 873K are summarized in Table 4. 1. Figure 4. 1 demonstrates the relationship between deposition potentials and potential of working electrode in $Fe-Cr-N^{3-}$ system on the 316SS nitriding at 873K. The nitride or metal will be deposited on the surface

of the specimen in order of decreasing deposition potential at each x. Figure 4. 1 give us the following conclusion: Cr_2N will be formed on the fresh surface of the working electrode (specimen) when x is over -0.1995V vs. N/N^{3-} . After the surface has been covered by Cr_2N , CrN will be formed over -0.1802V vs. N/N^{3-} . Next, after nitridding almost all chromium near the surface of the working electrode, Fe_2N will be formed via formation of Fe_4N . Indeed, formation of these nitrides will compete with diffusion of nitrogen in iron crystals.

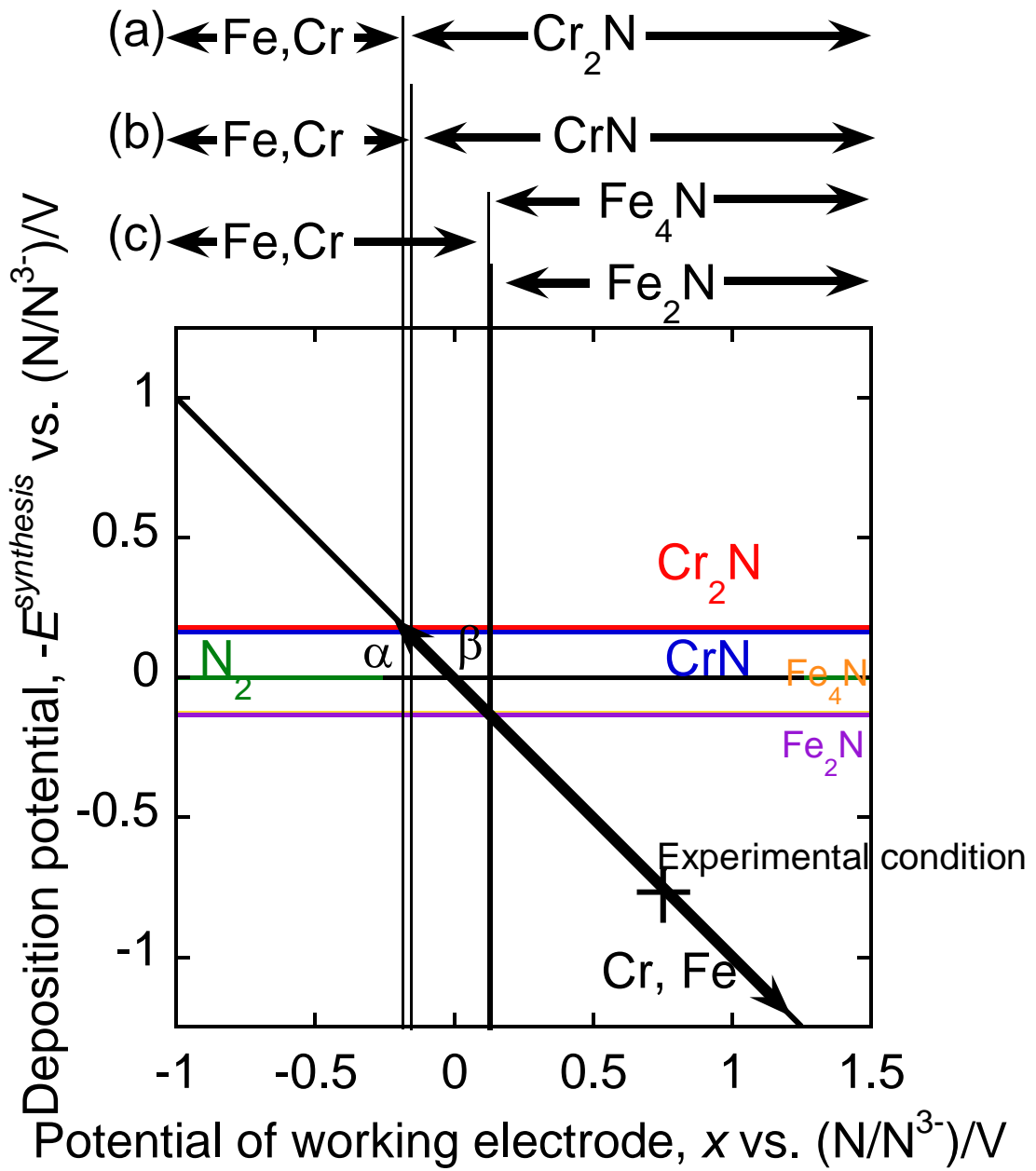


Figure 4. 1. Deposition potential of nitrides in Fe-Cr-N³⁻ system on the nitrating of 316 SS. Nitride will be formed in order of (a)Cr₂N, (b)CrN, (c)Fe₄N and Fe₂N.

Table 4. 1 Deposition potential of nitrides on 316 stainless steel specimen

	System	Compound	Deposition potential at 873K [vs. (N/N ³⁻)/V]
(a)	$2\text{Cr} + \text{N}^{3-} = \text{Cr}_2\text{N} + 3\text{e}^-$	Cr ₂ N	-0.1995
(b)	$\text{Cr} + \text{N}^{3-} = \text{CrN} + 3\text{e}^-$	CrN	-0.1802
(c)	$4\text{Fe} + \text{N}^{3-} = \text{Fe}_4\text{N} + 3\text{e}^-$	Fe ₄ N	0.1272
(d)	$2\text{Fe} + \text{N}^{3-} = \text{Fe}_2\text{N} + 3\text{e}^-$	Fe ₂ N	0.1329
(e)	Deposition of metal (working electrode)	Fe, Cr	<i>x</i>
(f)	Formation of N ₂ from N ³⁻	N ₂	0

Eq.(7) provides $\Delta G_{\text{nitride}}$ at different temperatures. And the deposition potentials from Eq.(6) allows us EES diagram to be constructed. Figure 4. 2 demonstrates EES diagrams described in the temperature range from 773K to 973K. In each temperate condition, Cr₂N will be initially formed. Next, CrN will be formed after the surface of the working electrode has been covered by Cr₂N. And Finally, Fe₂N will be formed. During the electrolysis process, the initial condition for formation of Cr₂N will transfer to that for formation of Fe₂N via that for formation of CrN.

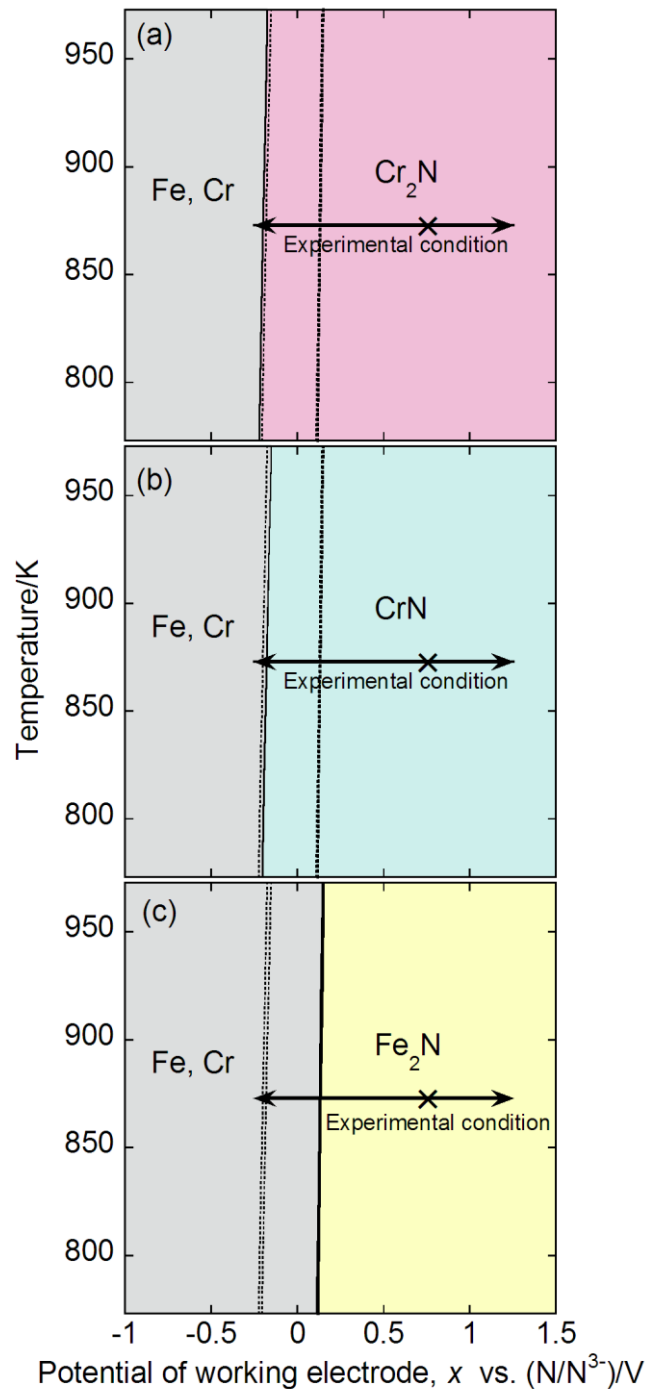


Figure 4. 2. Equilibrium electrochemical synthesis (EES) diagram on nitriding of 316SS. (a) Cr_2N will initially be formed. (b) CrN will be formed after Cr_2N formation. (c) Fe_2N will be formed when almost all chromium is nitrided near surface. Diagram (a) will be gradually transformed to diagram (c) via diagram (b) during the electrolysis process.

When $pN^{3-} = -\log[N^{3-}]$ is defined as a nitride-ion concentration index, given that P_{N_2} is the partial nitrogen pressure, R is the gas constant and F is Faraday constant, the Nernst equations related with nitrogen can be obtained as follows.

$$(a) \quad \frac{1}{2}N_2 + 3e^- = N^{3-}$$

$$E_{N_2/N^{3-}} = E_{N_2/N^{3-}}^{\circ} + \frac{2.303RT}{3F} pN^{3-} + \frac{2.303RT}{6F} \log P_{N_2}. \quad (8)$$

Considering $pN^{3-} = 1.67$ and $P_{N_2} = 1 \text{ atm}$ from the experimental condition, Eq.(9) provides relationship between the potential of working electrode $-x$ [V vs. N/N^{3-}] used the EES diagrams and the potential $-E$ [V vs. Li/Li^+] described in the experiment:

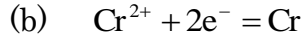
$$-E = x + 0.25. \quad (9)$$

The double-headed arrows in Figs 1 and 2 correspond to the experimental condition.

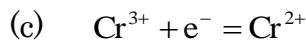
Although it is qualitative discussion partly, it is also able to examine the possibility of nitride formation under the terms and conditions of the temperature T , the potential of electrode $-E$ and the concentration $[M]$. Using $pN^{3-} = -\log[N^{3-}]$, a relationship between

electrode potential and nitride ion concentration, i.e. a potential-pN³⁻ diagram, may be drawn using standard potentials and thermodynamic data. Here, the concentration [M] is defined as an ionic fraction. CrN and Cr₂N can be assumed as chromium nitrides; Fe₂N and Fe₄N can be assumed as iron nitrides. In this case also, unfortunately, we do not have thermodynamic data for a solid solution of iron nitride such as α-Fe_{x(x>8)}N, so the diagram in this work does not include its formation. Given that *R* is the gas constant and *F* is Faraday constant, the Nernst equations related with nitride formation can be obtained as follows.

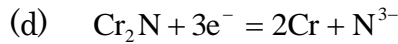
Reactions for chromium:



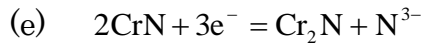
$$E_{\text{Cr}^{2+}/\text{Cr}} = E_{\text{Cr}^{2+}/\text{Cr}}^{\circ} + \frac{2.303RT}{2F} \log[\text{Cr}^{2+}], \quad (10)$$



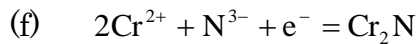
$$E_{\text{Cr}^{3+}/\text{Cr}^{2+}} = E_{\text{Cr}^{3+}/\text{Cr}^{2+}}^{\circ} + \frac{2.303RT}{F} \log \frac{[\text{Cr}^{3+}]}{[\text{Cr}^{2+}]}, \quad (11)$$



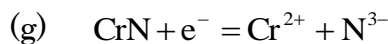
$$E_{\text{Cr}_2\text{N}/\text{Cr},\text{N}^{3-}} = E_{\text{Cr}_2\text{N}/\text{Cr},\text{N}^{3-}}^{\circ} + \frac{2.303RT}{3F} \text{pN}^{3-}, \quad (12)$$



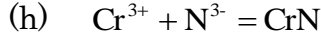
$$E_{\text{CrN}/\text{Cr}_2\text{N},\text{N}^{3-}} = E_{\text{CrN}/\text{Cr}_2\text{N},\text{N}^{3-}}^{\circ} + \frac{2.303RT}{3F} \text{pN}^{3-}, \quad (13)$$



$$E_{\text{Cr}^{2+},\text{N}^{3-}/\text{Cr}_2\text{N}} = E_{\text{Cr}^{2+},\text{N}^{3-}/\text{Cr}_2\text{N}}^{\circ} + \frac{2 \times 2.303RT}{F} \log[\text{Cr}^{2+}] - \frac{2.303RT}{F} \text{pN}^{3-}, \quad (14)$$

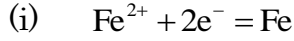


$$E_{\text{CrN/Cr}^{2+},\text{N}^{3-}} = E_{\text{CrN/Cr}^{2+},\text{N}^{3-}}^{\circ} - \frac{2.303RT}{F} \log[\text{Cr}^{2+}] + \frac{2.303RT}{F} \text{pN}^{3-}, \quad (15)$$

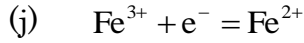


$$K_{\text{SP}} = [\text{Cr}^{3+}][\text{N}^{3-}]. \quad (16)$$

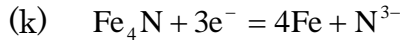
Reactions for iron:



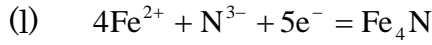
$$E_{\text{Fe}^{2+}/\text{Fe}} = E_{\text{Fe}^{2+}/\text{Fe}}^{\circ} + \frac{2.303RT}{2F} \log[\text{Fe}^{2+}], \quad (17)$$



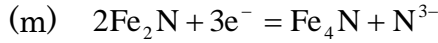
$$E_{\text{Fe}^{3+}/\text{Fe}^{2+}} = E_{\text{Fe}^{3+}/\text{Fe}^{2+}}^{\circ} + \frac{2.303RT}{F} \log \frac{[\text{Fe}^{3+}]}{[\text{Fe}^{2+}]}, \quad (18)$$



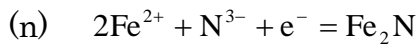
$$E_{\text{Fe}_4\text{N}/\text{Fe},\text{N}^{3-}} = E_{\text{Fe}_4\text{N}/\text{Fe},\text{N}^{3-}}^{\circ} + \frac{2.303RT}{3F} \text{pN}^{3-}, \quad (19)$$



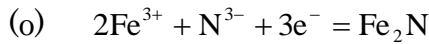
$$E_{\text{Fe}^{2+},\text{N}^{3-}/\text{Fe}_4\text{N}} = E_{\text{Fe}^{2+},\text{N}^{3-}/\text{Fe}_4\text{N}}^{\circ} - \frac{2.303RT}{5F} \text{pN}^{3-} + \frac{4 \times 2.303RT}{5F} \log[\text{Fe}^{2+}], \quad (20)$$



$$E_{\text{Fe}_2\text{N}/\text{Fe}_4\text{N},\text{N}^{3-}} = E_{\text{Fe}_2\text{N}/\text{Fe}_4\text{N},\text{N}^{3-}}^{\circ} + \frac{2.303RT}{3F} \text{pN}^{3-}, \quad (21)$$



$$E_{\text{Fe}^{2+},\text{N}^{3-}/\text{Fe}_2\text{N}} = E_{\text{Fe}^{2+},\text{N}^{3-}/\text{Fe}_2\text{N}}^{\circ} - \frac{2.303RT}{F} \text{pN}^{3-} + \frac{2 \times 2.303RT}{F} \log[\text{Fe}^{2+}], \quad (22)$$



$$E_{\text{Fe}^{3+},\text{N}^{3-}/\text{Fe}_2\text{N}} = E_{\text{Fe}^{3+},\text{N}^{3-}/\text{Fe}_2\text{N}}^{\circ} - \frac{2.303RT}{F} \text{pN}^{3-} + \frac{2 \times 2.303RT}{3 \times F} \log[\text{Fe}^{3+}]. \quad (23)$$

Because reports for measurements of standard potentials in fluoric molten salt are quite few, potentials of chromium and iron measured for FLiNaK at 1023K were employed in this estimation [3,4]. The standard potential for nitride ions was presumed from the arising position at

0.25V vs. Li/Li⁺ in the cyclic voltammogram. These potentials were referred to the potential of the Li/Li⁺ couple. Here, since the standard potentials of reactions (d), (e), (f), (g), (k), and (l) were unknown, these potentials were estimated using thermodynamic data summarized in Table 4. 2 [5, 6, 7, 8, 9, 10, 11]. For instance, the standard potential of Cr₂N/Cr, N³⁻ was estimated as indicated below. The standard chemical potential μ° is $3FE^\circ$. When the standard chemical potential μ° of Cr₂N is defined by $\Delta G_{873}^\circ(\text{Cr}_2\text{N})$, $E_{\text{CrN/Cr}_2\text{N},\text{N}^{3-}}^\circ$ can be given as

$$E_{\text{Cr}_2\text{N/Cr},\text{N}^{3-}}^\circ = \frac{\mu_{\text{Cr}_2\text{N}}^\circ - \mu_{\text{N}^{3-}}^\circ}{3F}. \quad (24)$$

Using thermodynamic data, the potential is -0.0463V vs. Li/Li⁺. The other unknown standard potentials were determined using a method similar to this estimation. These potentials are listed in Table 4. 3. Figure 4. 3 presents a potential-pN³⁻ diagram drawn using the standard potentials. For drawing the figure, 5×10^{-6} was chosen as the concentration of metal ions such as [Cr²⁺], [Cr³⁺], [Fe²⁺] and [Fe³⁺]; 1atm was used for the partial nitrogen pressure.

Table 4. 2. Thermodynamic data at 873K.

Substance	Standard free energy	Standard enthalpy	Standard entropy	
	ΔG_{873}° kJ/mol	ΔH_{873}° kJ/mol	S_{873}° J/K.mol	ΔS_{873}° kJ/K.mol
N ₂	0	0	233.742	-
Cr	0	0	52.388	-
CrN	-52.163	-120.132	91.402	-0.077857
Cr ₂ N	-57.772	-122.365	147.660	-0.07399
Fe	0	0	60.407	-
Fe ₂ N	38.475	-4.985	182.903	-0.049782
Fe ₄ N	36.819	-8.673	306.389	-0.05211

Table 4. 3. Standard potential E° / V referred to the Li⁺/Li couple.

Nitrogen	E° vs. (Li/Li ⁺)/V	Iron	E° vs. (Li/Li ⁺)/V
(a) N ₂ /N ³⁻	0.152	(i) Fe ²⁺ /Fe	1.62
Chromium	E° vs. (Li/Li ⁺)/V	Fe ³⁺ /Fe	1.79*
(b) Cr ²⁺ /Cr	1.01	(j) Fe ³⁺ /Fe ²⁺	1.93
(c) Cr ³⁺ /Cr ²⁺	1.45	(k) Fe ₄ N/Fe, N ³⁻	0.279*
(d) Cr ₂ N/Cr, N ³⁻	-0.0463*	(l) Fe ²⁺ , N ³⁻ /Fe ₄ N	2.44*
(e) CrN/Cr ₂ N, N ³⁻	-0.0101*	(m) Fe ₂ N/Fe ₄ N, N ³⁻	0.291*
(f) Cr ²⁺ , N ³⁻ /Cr ₂ N	4.18*	(n) Fe ²⁺ , N ³⁻ /Fe ₂ N	5.66*
(g) CrN/Cr ²⁺ , N ³⁻	-2.11*	(o) Fe ³⁺ , N ³⁻ /Fe ₂ N	3.17*

* Estimated using thermodynamic data in Table 4. 2.

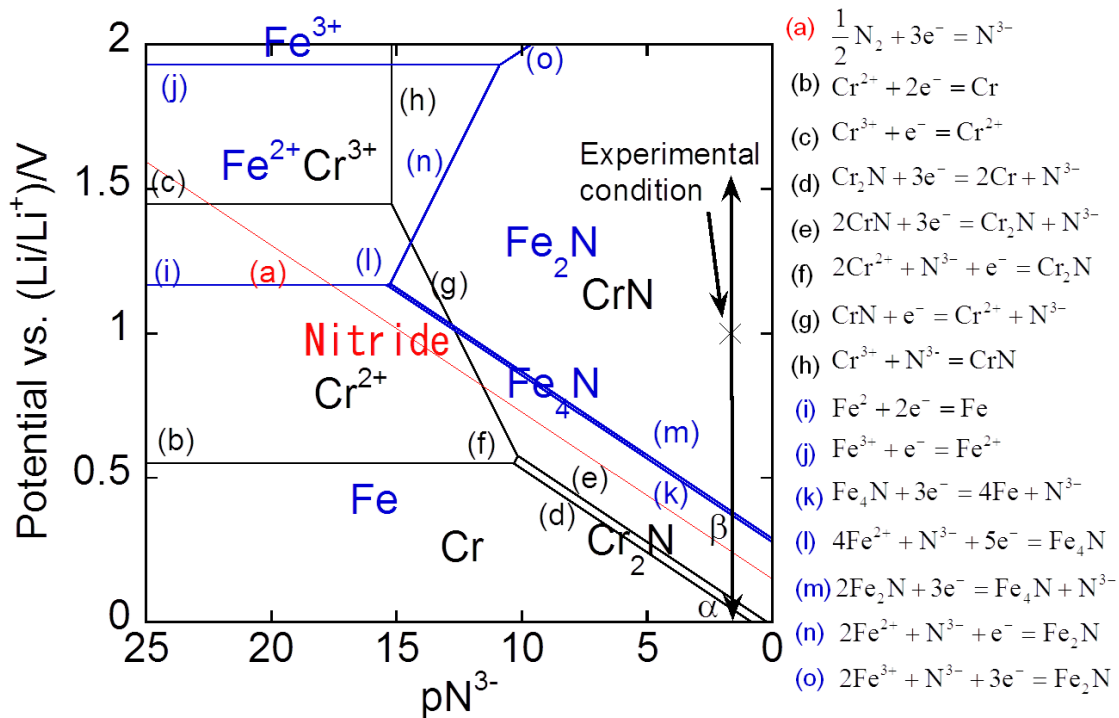


Figure 4. 3. Potential- pN^{3-} diagram of chromium nitride and iron nitride in fluoride eutectic salt.

In Fig. 4.3, the diagrams for three substances, nitrogen, chromium, and iron, are superposed. The red line indicates the potential for redox of nitrogen. The black lines indicate the boundaries of the chromium compounds. The area of Cr_2N is surrounded by lines (e), (f), and (d); the area of CrN is surrounded by lines (e), (g), and (h). It is understood that the area of Cr_2N is significantly narrower than that of CrN . The blue lines indicate the areas of iron compounds. The area of Fe_4N is surrounded by lines (k), (l), and (m); the area of Fe_2N is surrounded by

lines (m), (n), and (o). In this case, the area of Fe_4N is significantly narrower than that of Fe_2N . The formation tendency of the compounds can be understood from the figure. The double-headed arrow and cross indicate the experiment conditions. In the present work, the nitrogen concentration was 0.02, which corresponds to $p\text{N}^{3-} = 1.67$. The cyclic voltammogram was measured along the double-headed arrow. The intersection points of the double-headed arrow, line (d) and line (k), α and β , correspond to α and β in Figs. 1 and 2. The cross corresponds to the conditions of the nitriding electrolysis treatment. The arrow and cross are placed in the area of chromium nitride CrN and iron nitride Fe_2N , an area surrounded by lines (d), (f), (g), and (l). The arrow crosses over the red line, i.e., the nitrogen redox line. The treatment condition was placed at the upper-potential point of the electrode, above the red line. This implies that the potential and nitrogen concentration for nitride formation were chosen in the experiments. Lines (d) and (e), indicating chromium nitride formation, are under lines (k) and (m), for iron nitride formation. This means that chromium nitrides form before iron nitrides form.

This can also be explained using the change in standard Gibbs energy. Table 4. 4 indicates the changes in the standard Gibbs free energy of the reactions between nitrides. These changes were estimated using the thermodynamic data in Table 4. 2. All of the changes in the reaction formula in the table are negative. Each chemical reaction will proceed to the right. This suggests that, comparing the nitriding reactions of chromium and iron, chromium nitrides are apt to form from iron nitrides. Additionally, CrN will form, considering the reaction between Cr₂N and CrN. These are almost consistent with the results in our experiments.

Table 4. 4. Change in standard Gibbs free energy at 873K

Reaction		Change in free energy $\Delta G[\text{J/K.mol}]^*$
Chromium nitride and iron nitride	$\frac{1}{2}\text{Fe}_2\text{N} + \frac{1}{2}\text{Cr} = \text{Fe} + \frac{1}{2}\text{CrN}$	-47.5
	$\frac{1}{2}\text{Fe}_2\text{N} + \text{Cr} = \text{Fe} + \frac{1}{2}\text{Cr}_2\text{N}$	-50.3
	$\frac{1}{4}\text{Fe}_4\text{N} + \frac{1}{4}\text{Cr} = \text{Fe} + \frac{1}{4}\text{CrN}$	-22.3
	$\frac{1}{4}\text{Fe}_4\text{N} + \frac{1}{2}\text{Cr} = \text{Fe} + \frac{1}{4}\text{Cr}_2\text{N}$	-23.6
Chromium nitrides	$\frac{1}{2}\text{Cr}_2\text{N} + \frac{1}{4}\text{N}_2 = \text{CrN}$	-25.5

* Estimated using thermodynamic data in Table 4. 1.

However, the diagram only shows the equilibrium state at each potential; the real reaction is different from this. In fact, not only was chromium nitride selectively formed, but nitrogen was also deeply diffused into the bulk at low concentration. A structural change from austenitic structure to ferritic structure was then observed, and this would create a solid solution. This relates to the fact that the boundary line in the diagram between Cr_2N and Cr, i.e. line (d), is below the boundary line between Fe_4N and N, i.e. line (k). In the nitriding treatment, Cr_2N would be formed first at the surface. CrN would form because many more nitrogen atoms had been supplied at the surface. Fe_4N might be formed after CrN formed. More specifically, iron nitride might be formed if the treatment was carried out at a higher potential. However, even in such a treatment condition, nitrogen atoms would still easily diffuse into the bulk iron and make a solid solution. Iron forms several nitride compounds, depending on the atomic ratio and temperature [12]. According to iron nitriding in molten chloride salt [13], an $\text{Fe}_2\text{N}_{1-x}$ layer with a concentration gradient and a homogeneous Fe_4N

layer were formed. It may have also included a solid-solution layer. Because stainless steel consists of several kinds of different metals, it is natural that the nitriding of stainless steel exhibits complicated behavior.

The diagram has additional implications. If a dilute nitrogen concentration of pN^{3-} of 15 or more is assumed, the behavior might change drastically. This corresponds to experiment conditions above line (i) in the diagram. The stainless steel would melt into the molten salt if processing were conducted at a potential over 1.16V vs. Li/Li⁺. Both chromium and iron would change from metal to bivalent or trivalent ions. Due to this transition, it would be difficult to maintain the structure as the base material. In contrast, if a nitrogen concentration of $pN^{3-}=14$ and potential of 1.16V vs. Li/Li⁺ is assumed, iron nitride might form selectively. In this case, the nitride will form slowly, and the yield will be small.

Indeed, besides formation of Cr₂N or CrN, nitrogen atoms dissolve in iron crystal as $\alpha\text{-Fe}_{x(x>8)}\text{N}$ and diffuse. Nonequilibrium process is included. The temperature and processing time are sure to influence the

result. It would be necessary to optimize the treatment conditions considering the desired structure.

3. Conclusions

Nitriding of stainless steel (316 SS) was investigated in molten eutectic fluoride salt containing lithium nitride, $\text{LiF49mol\%-KF49mol\%-Li}_3\text{N2.0mol\%}$, at 873K. A cyclic voltammogram suggested that an irreversible nitriding reaction occurs between 0.50V vs. Li/Li^+ and 1.06V vs. Li/Li^+ at 873K.

Formation of chromium nitride CrN and iron nitride $\alpha\text{-Fe}_{x(x>8)}\text{N}$ was confirmed. After potentiostatic treatment at 1.0V vs. Li/Li^+ for 100 min, the specimen was characterized by SEM, XPS, EPMA and XRD. SEM observation revealed that the initially smooth surface changed into a rugged structure covered by a wrinkle structure about 1 to 2 μm in width after electrolysis. XPS analysis revealed that chromium nitride (CrN) was selectively formed at the surface layer. According to the EPMA analysis, the treatment promoted nitrogen diffusion from the surface to a depth of 35 micrometers. CrN was formed from the surface

to a depth of two micrometers. It was determined that iron nitride $\alpha\text{-Fe}_{x(x>8)}\text{N}$ was formed from there to a depth of 35 micrometers as an inside diffusion layer, but neither Fe_2N nor Fe_4N was detected. Formation of CrN and $\alpha\text{-Fe}_{x(x>8)}\text{N}$ was also confirmed by XRD measurement and XPS analysis. The formation of chromium nitride and iron nitride was discussed in terms of thermodynamics, EES diagram and pN^3 -potential diagram.

References

- [1] V.I. Shapoval, G. Kaptay, S. Deviatkin, in: N. Masuko, T. Osaka, Y. Ito (Ed.), *Electrochemical Technology: Innovation and New Developments*, Kodansha Ltd. and Gordon and Breach Science Publishers S.A., 1996, Ch.18.
- [2] G. Kaptay, E. Berecz, in: T.M. Letcher(Ed.), “Chemical Thermodynamics - A 'Chemistry for the 21st Century' monograph”, Blackwell Science, 1999, Ch. 11.
- [3] J. A. Plambeck and A. J. Bard (Ed.), “Encyclopedia of Electrochemistry of the Elements”, vol. 10, Marcel Dekker, NY, 1976, Ch. 13.
- [4] G. Mellors, S. Senderoff, in :“Electrode Reactions in the Electrolysis of Fused Salts” in *Applications of fundamental thermodynamics to metallurgical processes*, G. Fitterer, Ed., 1967.
- [5] Wagman, D. D. Evans, W. H., Parker, V. B., Schumm, R. H., Halow, I.,

Bailey, S. M., Churney, K. L., Nuttall, R. L.; The NBS tables of chemical thermodynamic properties, selected values for inorganic and C1 and C2 organic substances in SI units; J. Phys. Chem. Ref. Data, Vol. 2, Supplement No. 2, 1982.

[6] D.R. Stull, H. Prophet, 2nd ed., 1971, NSRDS-NBS-37.

[7] M.W. Chase Jr., J.L. Curnutt, A. T.Hu, H. Prophet, A.N. Syverud, L.C. Walker, "JANAF Thermochemical Tables, 1974 Supplement", J. Phys. Chem. Ref. Data 3 (1974)311.

[8] M. W. Chase, Jr., J.L. Curnutt, H. Prophet, R.A. McDonald, A.N. Syverud, "JANAF thermochemical tables, 1975 supplement", J. Phys. Chem. Ref. Data 4 (1975)1.

[9] M. W. Chase, Jr., J.L. Curnutt, R. A. McDonald, A. N. Syverud, "JANAF thermochemical tables, 1978 supplement", J. Phys. Chem. Ref. Data 7(1978) 793.

[10] M. W. Chase, Jr., J.R. Curnutt, J. R. Downey Jr., R.A. McDonald, A.N. Syverud, E. A. Valenzuela, "JANAF Thermochemical Tables, 1982 Supplement", J. Phys. Chem. Ref. Data 11(1982)695.

[11] M. W. Chase, Jr., C. A. Davies, J. R. Downey, Jr., D. J. Frurip, R.A. McDonald, A. N. Syverud, "JANAF Thermochemical Tables, 1985 Supplement", J. Phys. Chem. Ref. Data 14 (1985) Supplement No. 1.

[12] T. Liapina, A. Leineweber, E. J. Mittemeijer, "Phase transformations in iron-nitride compound layers upon low-temperature annealing: Diffusion kinetics of nitrogen in ϵ - and γ '-iron nitrides", Metall. Mater. Trans. A, 37A(2006)319.

[13] T. Goto, R. Obata, Y. Ito, "Electrochemical formation of iron nitride film in a molten LiCl-KCl-Li₃N system", Electrochimica Acta 45(2000)3367.

Chapter 5 Conclusions

The results described in the previous chapters are summarized as follows:

First, several kinds of oxides and nitrides were thermodynamically considered for compatibility with fluoride molten salts. The thermodynamic consideration predicted that oxides dissolve into molten fluoride salt and that nitride have compatibility with molten fluoride salt. And prior to development of the surface modification process, compatibilities of oxides and nitrides in FLiNaK at 600°C were examined in immersion test over 1000 hours using bulk test specimens such Er_2O_3 , Y_2O_3 , Al_2O_3 and AlN. The results also demonstrated that nitride, AlN, indicated excellent compatibility with molten fluoride salt, FLiNaK.

Secondly, coating processes were considered. To form robust graded compositional nitride layers using compositional elements from the structural material, an electrochemical process was proposed. In the process, the surface of structural material is electrochemically treated in molten fluoride salt including Li_3N as a nitrogen source.

Thirdly, because the experiments using molten fluoride salt have to be conducted in dry environment at high temperature over 500°C , an original experimental setup, which consists of a stainless steel reactor, a nickel crucible, thermocouples, heaters and electrodes, was designed and assembled for the experiments in a dry Ar gas filled glove box. Data was recorded by a data logger connected with the potentiostat.

Fourthly, cyclic voltammograms about 316 stainless steel immersed into a binary eutectic mixture of LiF-KF (FLiK) including Li_3N were measured using the experimental setup. From the results, the nitriding condition was decided.

Fifthly, surface of 316 stainless steel was treated in a binary eutectic mixture of LiF-KF (FLiK) including Li_3N in a potentiostatic condition. The treatment was conducted at 1.0V with respect to lithium

redox potential as the standard potential, ie, 1.0V vs. Li/Li⁺. For the treatment for 100 and 240 minutes, nitrogen was introduced into a depth of 35 and 65 μ m from the surface, respectively. These specimens were analyzed using analytical methods such as X-ray diffraction (XRD), electron probe micro analyzer (EPMA), electron energy dispersive X-ray spectrometry (EDX), X-ray photoelectron spectroscopy (XPS), and scanning electromicroscopy (SEM). According to the results, it was revealed that chromium nitride CrN was formed as a main nitride. The initial face-center cubic (fcc) structure transformed to the body-centered tetragonal (bct) structure. The transformation suggests that α -Fe_{n(n>8)}N was also formed. Although oxygen impurities were expected to be introduced to the nitride layer, in fact, oxygen was not introduced into the layer. This means that nitrogen was mainly introduced in the layer through the treatment.

Finally, considering the experimental conditions such as temperature, nitrogen concentration and specimen composition, nitride formation was theoretically analyzed based on combination of thermodynamics and electrochemistry. CrN, Cr₂N, Fe₂N and Fe₄N were

considered from composition of 316 stainless steel. Potential-nitride formation diagram and potential-nitrogen ion concentration diagram were drawn. From discussions on formation of these nitrides based on these conditions, it was theoretically derived that CrN is most stable. This theoretical consideration was well in agreement with the experimental result.

In conclusion, these results demonstrate availability of this nitriding method and will allow a guideline for optimization of this nitriding process in molten fluoride salt.

Appendix Corrosion characteristic of AlN, Y₂O₃, Er₂O₃ and Al₂O₃ in FLiNaK for molten salt blanket system

1. Introduction

As described in Chapter 1, force Free Helical type Reactor (FFHR) with self-cooled liquid blanket system has been designed [1]. Molten salt is known as a promising self cooling tritium breeder for the system for fusion reactor because of the attractive advantages on safety aspects: low tritium solubility, low reactivity with air and water, low pressure operation, and low MHD resistance. LiF·BeF₂ (FLiBe) is planned to be employed as tritium breeder and coolant of the blanket due to inherent safety and high thermal efficiency operated above 500°C [2].

46.5LiF-11.5NaF-42KF (mol%) called as FLiNaK possesses similar characteristics to FLiBe. It would mean potentiality to be used as a simulant for the heat and mass transfer investigation. FLiNaK would be also one of alternative candidates of the coolant and tritium breeder of the blankets [33]. For the blanket system, the corrosion of the structural materials and the development of tritium barrier, anti-corrosion barrier, tritium recovery system and heat exchanger are key issues. Especially in the heat exchanger, the permeation of tritium to secondary coolant loop must be inhibited by the tritium barrier [4]. And deterioration of heat transfer efficiency of the heat exchanger by the barrier must be prevented concurrently.

Corrosion of several candidate structural materials in FLiNaK has been studied for the blanket. It was found that the corrosion of reduced activation ferritic steel, JLF-1(Fe-8.92Cr-2W) is caused by the impurity as H₂O, O₂ and HF dissolved in the molten salts [5]. In the corrosion of austenitic steel, Ni rich corrosion resistant layer was formed after certain time for the corrosion via Cr dissolution [6]. And the corrosion resistance of Ni based alloy was demonstrated [7]. The corrosion could be controlled by the impurity control.

Ceramic coating to prevent tritium permeability has also been studied because of the low hydrogen diffusivity and the low hydrogen surface recombination constants [8,9]. Ceramics such AlN, Y₂O₃, Er₂O₃ and Al₂O₃ are promising as candidate materials for tritium barrier. But the stability in molten salt is not made clear so far. To develop liquid blanket system using molten salts, we hence have to optimize the heat and mass transfer property between FLiNaK and the metal specimen coated with the barrier material. In the present study, the corrosion resistance of those ceramics in FLiNaK was studied by static immersion test.

This work conducted to confirm compatibility of nitride with molten fluoride salt with lithium fluoride.

2. Experimental

2.1 Specimen preparation

The bulk specimens were prepared as follows: after AlN powder including polyvinyl butyral as a binder was shaped to a tablet by compression at 500 tons, it was calcined at 1850 °C for 4 hours. After Er(NO₃)₃·5H₂O was calcined at 1000 °C for 5 hours, it was ground. The obtained powder was shaped to a tablet by compression at 60 kg/cm² and calcined at 1700 °C for 2 hours. Y₂O₃ powder was

shaped to a tablet at 60 kg/cm² and calcined at 1650 °C for 5 hours. Al₂O₃ power including polyvinyl alcohol as a binder was shaped to a tablet by hand press machine at 80 °C. It was calcined at 400 °C for 3hours, 800 °C for 3 hours and finally 1600 °C for 5 hours step by step. These specimens were cut to adjust into the size of 10 mm × 15 mm × 5.0 mm. Initial composition of the specimens was analyzed by X-Ray Fluorescence Spectroscopy (XRF). Table A. 1 shows initial composition of the specimens.

Table A. 1 Composition of specimens (at%)

AlN	Al 49.63	Y 0.47	Si 0.16	Mg 0.08	S 0.01	Ca 0.01	O 0.00	N 49.63		
Er ₂ O ₃	Er 37.91	Zr 1.24	Pb 0.15	Y 0.09	Al 0.17	Si 0.11	P 0.07	O 60.25		
Y ₂ O ₃	Y 39.61	Fe 0.02	Si 0.06	Al 0.03	Mg 0.04	O 60.22				
Al ₂ O ₃	Al 39.68	Ce 0.09	Si 0.07	S 0.03	Mg 0.04	Cl 0.03	Sr 0.02	K 0.01	Ca 0.02	O 60.01

2.2 Test condition

The FLiNaK used in the present immersion tests was purified by electrolytic refining method, and had initial impurity as shown. The FLiNaK contained lower metal impurity and moisture than that in the previous study [5].

Figure A. 1 shows a capsule for immersion test made from stainless steel 316L (SS316L). The specimens were putted in SS316L crucibles filled with

FLiNaK [7] and packed in dry Ar atmosphere. The capsule was heated at 600°C [4]. After 230 hour and 1010 hour immersion, the specimens were extracted from the capsules.

The specimens were rinsed in pure water for 4 days at room temperature to remove FLiNaK from the specimens. After drying the specimens, the weight was measured using micro-balance with 0.1mg in accuracy, and compared to that before the immersion test. X-ray diffraction (XRD) patterns were measured before and after the immersion test. The surface was observed by scanning electron microscopy (SEM). Chemical analysis at the specimen surface was carried out by X-ray photoelectron spectroscopy (XPS). The surface was etched by Ar ion beam and analyzed by XPS. Chemical composition of FLiNaK was also analyzed by inductively coupled plasma mass spectrometry (ICPMS) and Karl Fischer titration.

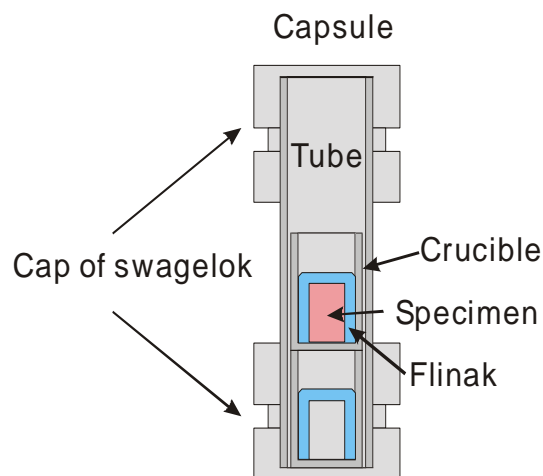


Figure A.1 Capsule for immersion test. It consists of SS316 tube and Swagelok.

3. Results

3.1 Surface observation

Figure A. 2 shows the photos of specimens before and after the immersion test. The initial AlN specimen was gray. Although it got slightly light gray after the immersion test, no shape change was significantly observed. In case of Er₂O₃, the specimen was pink before immersion test and the color has been kept through the immersion test. It, however, got fragile after immersion test and chipped off especially at the corners. Y₂O₃ specimens were white before immersion test. It broke and got blackish after the test. Al₂O₃ specimens were white before immersion test. After the test, the specimens colored to gray.

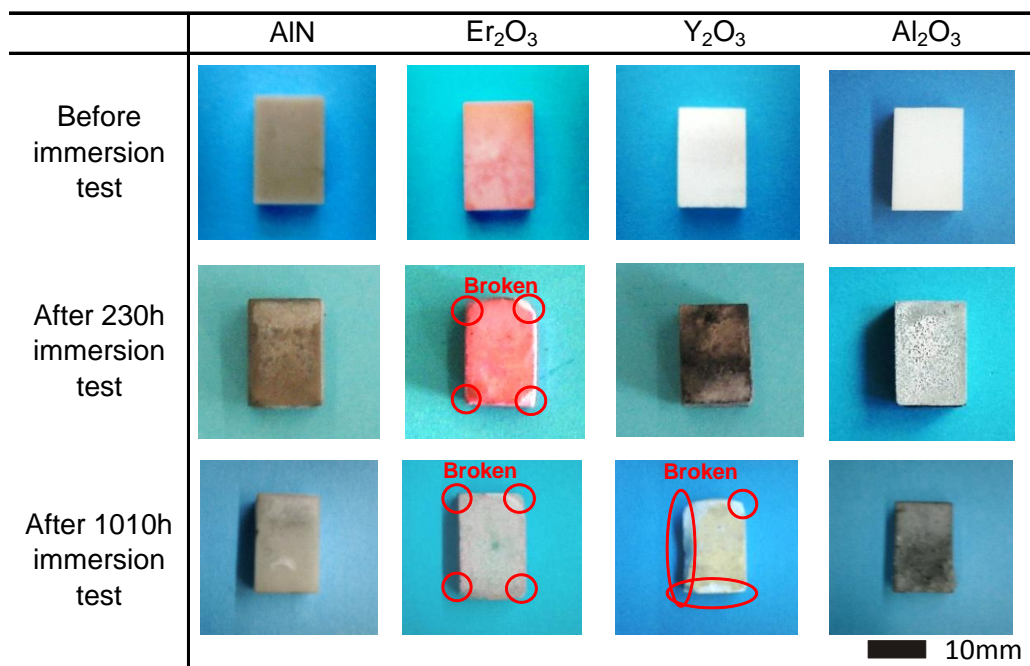


Figure A.2 Photos of specimens before and after immersion test.

Figure A. 3 shows SEM images for specimen surface before and after the immersion tests and relationship between Ar ion etching time and atomic ratio obtained from XPS measurement. The Ar ion etching time is corresponding to the depth from surface. The Ar ion etching rate corresponds 3 nm/sec of that for SiO₂. The actual Ar ion etching rate for the tested ceramics could be close to this value. The AlN specimen had rough structure at the surface before the immersion test. After the test, the surface became smooth. The initial Er₂O₃ surface consisted of round shape grains before the immersion test. After the immersion test, the grains lost roundness, got rough, and formed porous structure. The initial Y₂O₃ consisted of rough grains. The image also shows the cross sections of large grains over several micrometers. After the immersion test, the larger part of the surface area became more porous than that before the immersion test. Initial Al₂O₃ consisted of grains like gathering pine cones. After immersion test, the structure was lost and changed to be rough structure.

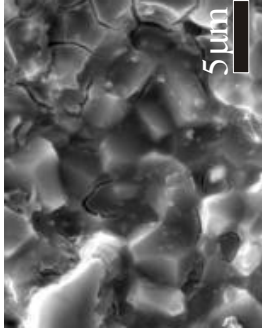
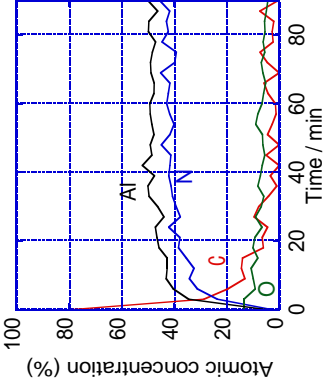
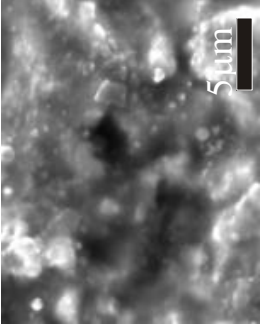
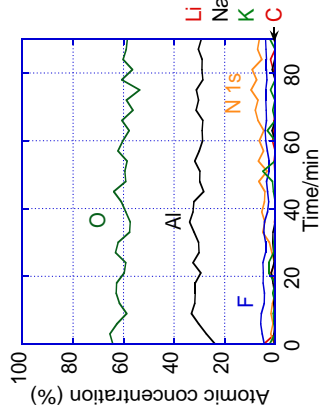
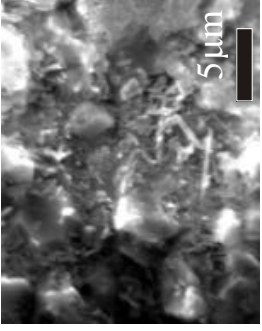
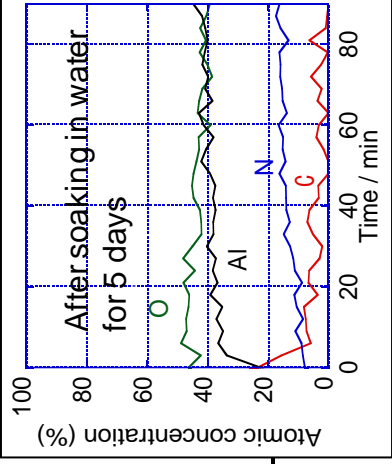
(a)	Before corrosion test	After 230-hour	After 1010-hour
AlN	 	 	 

Figure A.3(a) Surface images of AlN specimen by SEM and surface element analysis by XPS before and after immersion test in Flinak at 600°C for 230 and 1010 hours. In the figures demonstrating atomic concentration, the time axis corresponds to depth etched by Ar ion beam. The inset demonstrates surface analysis after soaking in water for 5 days at room temperature.

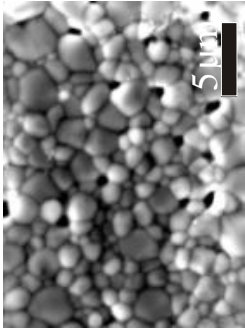
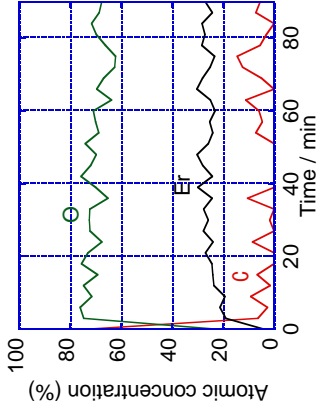
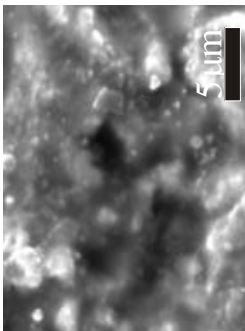
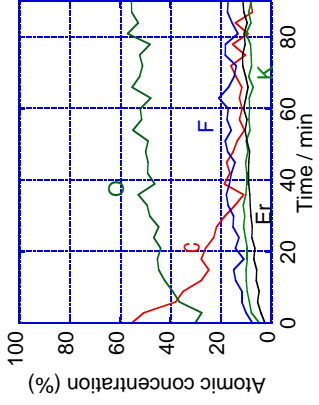
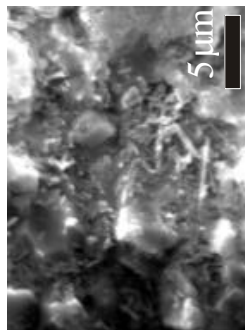
(b)	Before corrosion test	After 230-hour	After 1010-hour
Er_2O_3	 	 	

Figure A.3(b). Surface images of Er_2O_3 specimen by SEM and surface element analysis by XPS before and after immersion test in Flinak at 600°C for 230 and 1010 hours. In the figures demonstrating atomic concentration, the time axis corresponds to depth etched by Ar ion beam.

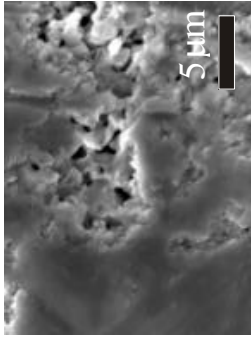
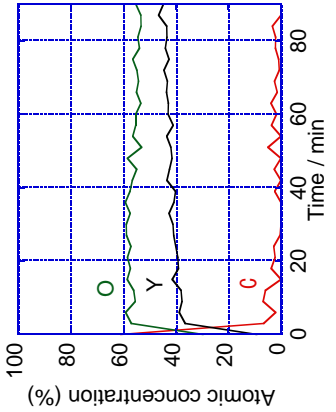
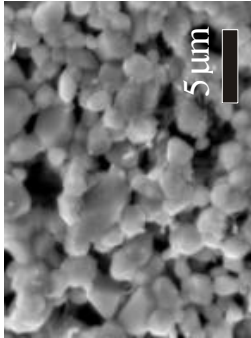
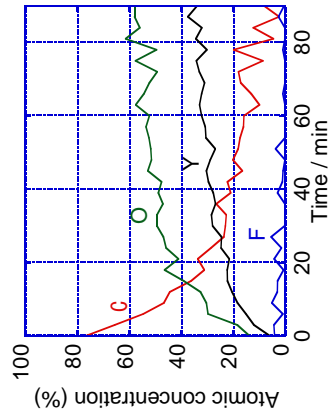
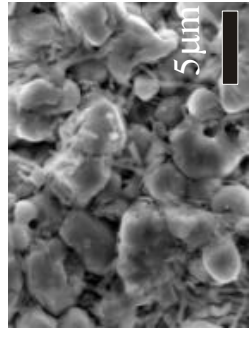
(c)	Before corrosion test	After 230-hour	After 1010-hour
Y_2O_3	 	 	

Figure A.3(c). Surface images of Y_2O_3 specimen by SEM and surface element analysis by XPS before and after immersion test in Flinak at 600°C for 230 and 1010 hours. In the figures demonstrating atomic concentration, the time axis corresponds to depth etched by Ar ion beam.

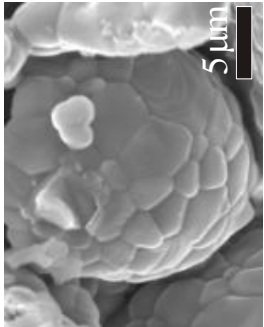
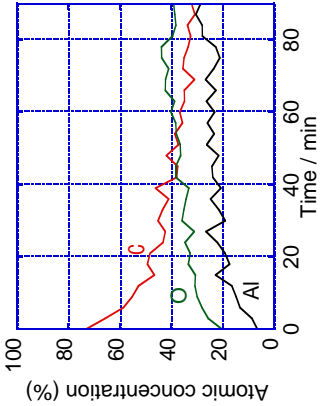
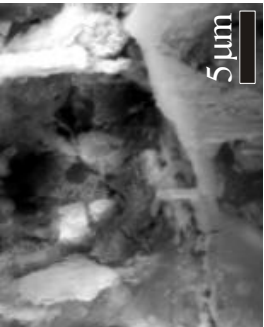
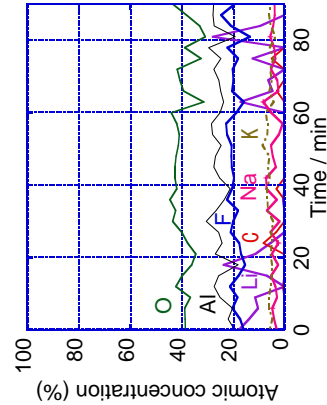
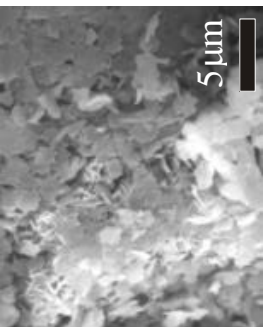
(d)	Before corrosion test	After 230-hour	After 1010-hour
Al_2O_3	 	 	

Figure A.3.(d). Surface images of specimen by SEM and surface element analysis by XPS before and after immersion test in Flinak at 600°C for 230 and 1010 hours. Al_2O_3 . In the figures demonstrating atomic concentration, the time axis corresponds to depth etched by Ar ion beam.

From the results of XPS measurement before and after the immersion test, fluorine was detected at the surface of all the specimens as a common tendency. Potassium was detected in AlN and Er₂O₃ specimens after immersion test. It is noted that substitution from nitrogen to oxygen near surface was clarified about the AlN specimen after the immersion test. In the Al₂O₃ specimens after immersion test, fluorine, lithium, sodium and potassium were detected. Those were due to the deposition of the corrosion products and FLiNaK remaining in the pore structure.

XRD measurement was carried out to investigate the affected depth due to corrosion reaction. The patterns from the specimens were compared with those from Joint Committee for Powder Diffraction Standards (JCPDS) by International Centre for Diffraction Data (ICDD). Comparison shows that the specimen's patterns are crystallographically equivalent ones from JCPDS. When the patterns before and after the immersion test were imposed, significant difference between the patterns was not recognized. This means that substance near surface

dissolved into FLiNaK and that the corrosion reaction does not reach over tens of micrometer depth.

3.2 Weight change of specimens

Table A. 2 shows weight change per unit area before and after the immersion test. The weight loss in AlN specimen was small. The losses in the Er₂O₃ specimens and the Y₂O₃ specimen after 1010 hour immersion test were large and their specimens were broken. The weight loss includes loss of fragments due to breaking during the immersion test and water rinse. On the other hand, the Y₂O₃ specimen after 230 hour immersion test and the Al₂O₃ specimens gained in weight. These specimens possess porous structure. The gain of the weight is possibly due to the FLiNaK and water permeated into the pores of those specimens.

Table A. 2 Weight Change for immersion test (unit: g/m²).

Time	230 hours	1010 hours
AlN	-0.233	-0.0928
Al ₂ O ₃	+981	+74.0
Y ₂ O ₃	+195	-58.9 (broken)
Er ₂ O ₃	-446 (broken)	-8.21 (slightly broken)

3.3 Chemical analysis

The chemical composition of FLiNaK after the immersion test was compared with the initial that of FLiNaK in Table A. 3. While the FLiNaK used for AlN 230 hour immersion test contains Al at 61 wppm, those used for Er₂O₃, Y₂O₃ and Al₂O₃ immersion tests contain Er at 1.47×10^4 wppm, Y at 3.30×10^3 wppm and Al at 930 wppm, respectively. In 1010-hour immersion test, similar tendency was also observed. These results mean that Er₂O₃, Y₂O₃ and Al₂O₃ dissolved into FLiNaK and that the corrosion is not negligible on Er₂O₃, Y₂O₃ and Al₂O₃.

Table A. 3. Impurity composition in FLiNaK before and after immersion test.

Element	Initial FLiNaK [wppm]	FLiNaK after AlN immersion test [wppm]		FLiNaK after Er ₂ O ₃ immersion test [wppm]		FLiNaK after Y ₂ O ₃ immersion test [wppm]		FLiNaK after Al ₂ O ₃ immersion test [wppm]	
		230h	1010h	230h	1010h	230h	1010h	230h	1010h
Fe	52	16	19	11	13	4.1	14	120	120
Cr	2.6	39	58	34	33	13	42	150	150
Ni	39	8.3	-	3.5	-	1.3	-	<1	-
Mn	0.07	27	-	28	-	21	-	-	-
Er	<0.01	-	-	1.47×10^4	240	-	-	-	-
Y	<0.01	-	-	-	-	0.33×10^4	110	-	-
Al	7.4	61	27	-	-	-	-	930	950
Na	5.8×10^4	5.98×10^4	-	6.11×10^4	-	6.11×10^4	-	5.89×10^4	-
K	35.6×10^4	36.2×10^4	-	37.3×10^4	-	37.5×10^4	-	36.1×10^4	-
Li	6.90×10^4	7.17×10^4	-	7.30×10^4	-	7.63×10^4	-	7.81×10^4	-
HF	42.6	<10	-	<10	-	<10	-	<10	-
H ₂ O	10	15.8	58.4	63.8	48.1	13.4	63.4	77.5	51.7

Figure A. 4 shows relationship between impurity concentration in FLiNaK and testing time on immersion test. It shows no increase of the impurity concentration with testing time after 230 hours although these results contain the breaking of specimens placed in the FLiNaK.

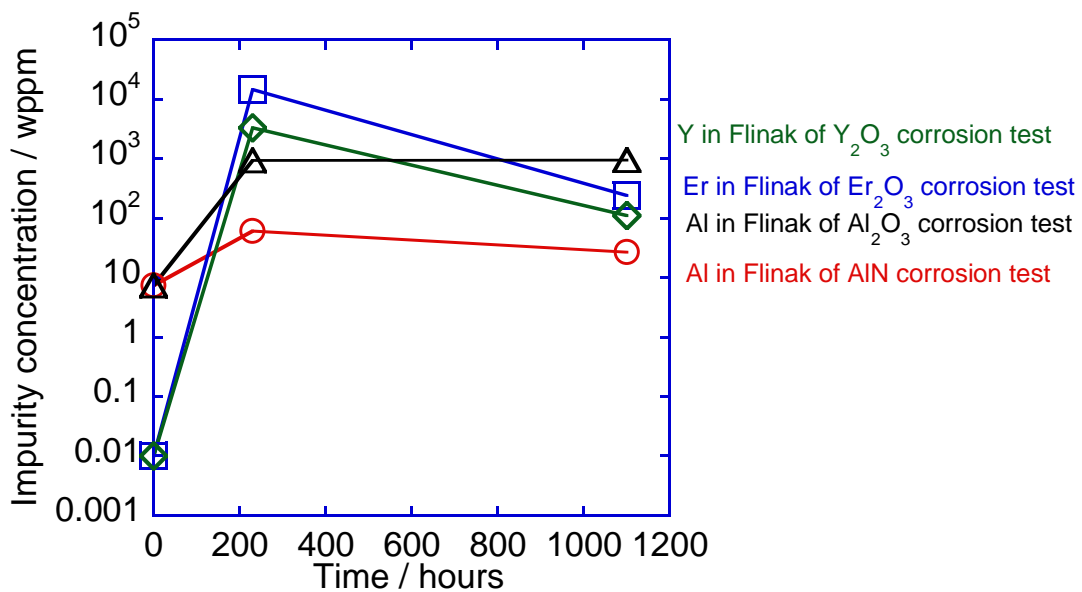


Figure A.4. Impurity concentrations in FLiNaK before and after immersion test.

4. Discussion

4.1 Thermodynamic stability

Table A. 4 shows standard Gibbs energy for reaction about these ceramics with LiF and KF, respectively. LiF occupies the largest part in FLiNaK used in this study. It is more stable than NaF and KF. KF was most unstable due to largest free energy for formation in the FLiNaK.

The energy values provide us the equilibrium tendency about the reactions in the condition in this study and allow us prediction of thermodynamical stability in FLiNaK. According to the reaction energy estimation, AlN could be stable in FLiNaK if it mainly reacted with LiF, which had the largest part in the FLiNaK. On the other hand, Er₂O₃, Y₂O₃ and Al₂O₃ would be unstable.

Table A. 4. Gibbs energy for reaction of ceramics material in FLiNaK at 600°C.

		Reaction	Δ G [KJ/mol]	Thermodynamic stability
AlN	Fluoridation	AlN + 3LiF = AlF ₃ +Li ₃ N	82.61	St able
		AlN + 3KF = AlF ₃ + 3K + 1/2N ₂	61.86	Stable
	Oxidation	AlN + 3H ₂ O = NH ₃ + 1/2Al ₂ O ₃ .3(H ₂ O)	-156.7at 27°C	Unstable <u>Humidity control is required</u>
		AlN + 3/4O ₂ = 1/2Al ₂ O ₃ + 1/2N ₂	-475.3	Unstable
Al ₂ O ₃		Al ₂ O ₃ +6LiF = 2AlF ₃ +3Li ₂ O	-236.3	Unstable
		Al ₂ O ₃ +6KF = 2AlF ₃ +3K ₂ O	354.3	Stable
Y ₂ O ₃	Fluoridation	Y ₂ O ₃ + 6LiF = 2YF ₃ + 3Li ₂ O	-454.0	Unstable
		Y ₂ O ₃ + 6KF = 2YF ₃ + 3K ₂ O	136.5	Stable
Er ₂ O ₃		Er ₂ O ₃ + 6LiF = 2ErF ₃ + 3Li ₂ O	-426.8	Unstable
		Er ₂ O ₃ + 6KF = 2ErF ₃ + 3K ₂ O	163.7	Stable

4.2 Solubility of oxide and nitride in FLiNaK

The immersion tests for the ceramics were carried out at 600°C for 230 hours and 1010 hours. The results of weight loss measurement in

these tests did not clearly show time dependence on the corrosion, because the weight loss was significantly affected by breaking of the specimens, particularly in the specimens of Er_2O_3 and Y_2O_3 . The specimen surface structure after the 230 hour test was similar to that for 1010 hour test. Although the repeatability of the corrosion characteristics were confirmed by the tests, significant time dependence on the corrosion was not obtained.

One possible reason is saturation of the dissolved elements within 230 hours. The corrosion might be suppressed after reaching it. The FLiNaK contained 950 wppm of Al after the immersion of Al_2O_3 for 1010 hours, which is comparable with Al amount in FLiNaK after 230 hour immersion. If the corrosion products were dissolved to FLiNaK via the fluoridation shown in Table A.4, Al amount in FLiNaK after the 1010 hour immersion test would correspond to solubility of Al in FLiNaK. Considering Al dissolving into FLiNaK via fluoridation, it would mean the solubility of fluoride, AlF_3 . It is 2.95×10^3 wppm obtained from molecular weight ratio of Al and AlF_3 .

In case of Er and Y, the concentration would similarly give us the

solubilities of ErF_3 and YF_3 , which are 321 wppm and 180 wppm, respectively.

4.3 Corrosion resistance of AlN in FLiNaK

The AlN specimens seem to possess corrosion resistance against FLiNaK compared with Er_2O_3 and Y_2O_3 . However, the AlN might be corroded, since the weight loss of the specimen was slightly detected. According to ref. [8], reaction of AlN with moisture forms $\text{Al}(\text{OH})_3$ and ammonia. Moreover, the hydroxide might change to Al_2O_3 and/or its hydrate. After the immersion test, the oxygen was detected on the surface by XPS as shown in Fig. A. 3. The surface of AlN specimen could be thinly covered with $\text{Al}(\text{OH})_3$ and/or Al_2O_3 . The oxygen rich layer could be formed in FLiNaK if there was reaction with moisture and/or oxygen in the FLiNaK. As another possibility, the oxygen rich layer might be formed when the specimens were rinsed in water after immersion test. Then, to confirm substitution from N to O at the AlN surface in water, another AlN specimen (7.0 mm \times 6.0 mm \times 3.0 mm) cut from the identical lot was soaked in water for 5 days. Before and after the water soaking,

XPS spectra were measured. The insets in Fig. A. 3 show the depth profile of atomic composition ratio measured with XPS and show the replacement from N to O.

The AlN might be corroded if the surface was preliminary oxidized or oxidized in the FLiNaK due to the reaction with dissolved oxygen in FLiNaK as shown in Fig. A. 5.

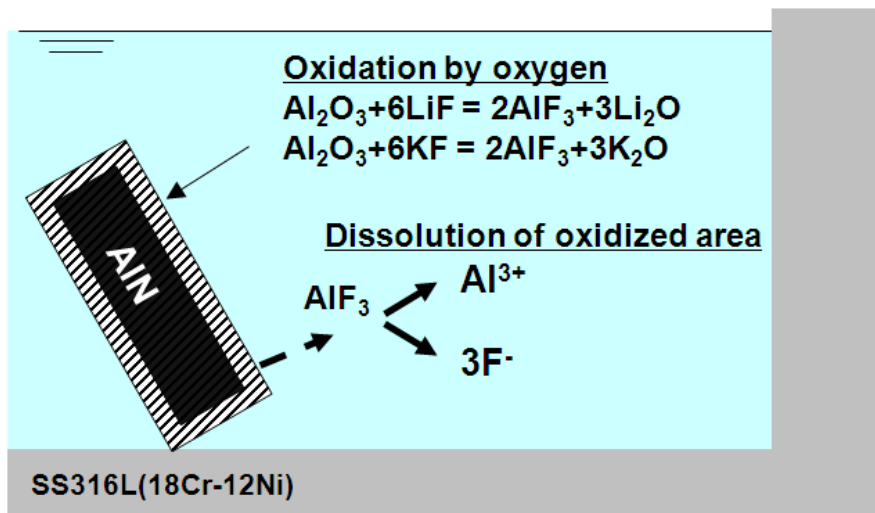
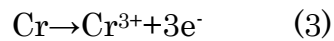
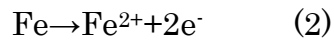
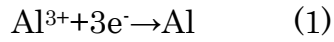


Figure A. 5. Corrosion in AlN-FLiNaK-316L steel system.

4.4 Corrosion of Al_2O_3 , Er_2O_3 and Y_2O_3 in FLiNaK

In Al_2O_3 immersion test, Fe and Cr were detected in FLiNaK after the immersion tests as shown in Table A. 3. These would be derived from SS316L crucibles. When Al was ionized and dissolved into molten

FLiNaK in the corrosion process, Fe and Cr would be oxidized as formulas (1)-(3).



Then, metal Al would be precipitated on the crucible surface. These reactions are redox reaction and would make an electrochemical circuit described as a schematism in Fig. A.6.

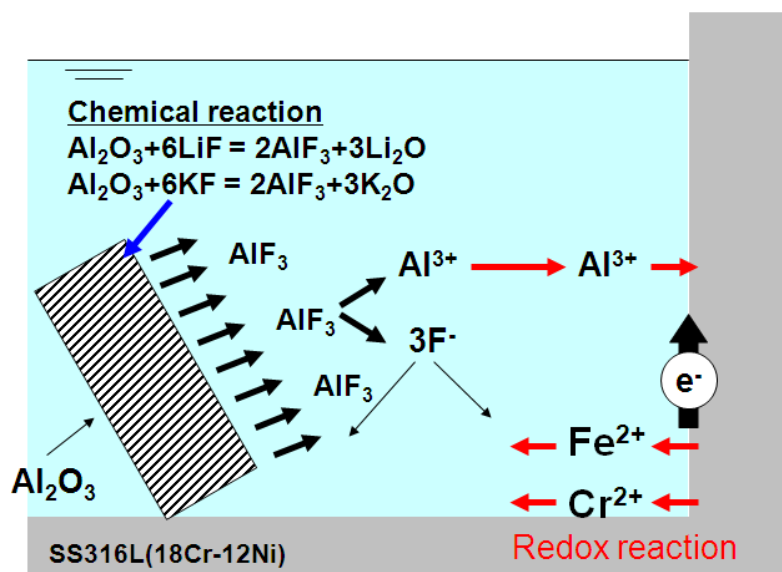


Figure A. 6 Corrosion in Al_2O_3 -FLiNaK-316L steel system.

In Er_2O_3 immersion test, Er dissolution was detected. It was found that the molar ratio of Er was low at the surface. At the same time, fluorine

was also detected on the surface as shown in Fig. A.3. The surface was corroded via the fluoridation process. Er_2O_3 specimens contained Zr as an impurity as shown in Table A. 1. Since zirconia seems to be thermodynamically unstable as shown in Table A. 4, zirconia would promote the corrosion and brittleness.

Although the corrosion of Y_2O_3 specimen was small, the fluorine was slightly detected on the surface. This suggests that the surface could be corroded via fluoridation process.

5. Conclusion

Major results are as follows:

- (1) AlN showed corrosion resistance in FLiNaK. The surface could be oxidized by the oxygen or moisture.
- (2) The corrosion of Al_2O_3 was large. The corrosion of the 316L type austenitic steel was promoted by the redox reaction caused by the dissolved Al from Al_2O_3 in FLiNaK.
- (3) The corrosion of Er_2O_3 was caused via the fluoridation process. Zr oxide dissolved in the sample of Er_2O_3 might be promoted the corrosion.

(4) The corrosion of Y_2O_3 was small, although weight loss due to the corrosion was affected by breaking of the specimens with porous structure.

(5) The corrosion intensity of the ceramic materials in FLiNaK agreed with the tendency of chemical reaction indicated by the calculation of the Gibbs reaction energy.

In conclusion, AlN might be suitable for surface coating of the structural materials for blanket system using molten salt like a FLiNaK.

References

[1] A. Sagara, S. Imagawa, O. Mitarai, T. Dolan, T. Tanaka, Y. Kubota, K. Yamazaki, K.Y. Watanabe, N. Mizuguchi, T. Muroga, N. Noda, O. Kaneko, H. Yamada, N. Ohyabu, T. Uda, A. Komori, S. Sudo, O. Motojima, "Improved structure and long-life blanket concepts for heliotron reactors", *Nuclear Fusion*, 45 (2005) 258.

[2] A. Sagara, T. Tanaka, T. Muroga, H. Hashizume, T. Kunugi, S. Fukada, A. Shimizu, "Innovative liquid breeder blanket design activities in Japan", *Fusion Technol.*, 47 (2005) 524.

[3] A.Sagara, T. Terai, S. Tanaka, H. Matsui, S. Takahasi, T. Yamamoto, S. Toda, S. Fukada, M. Nishikawa, A. Shimizu, N. Yoshida, H.

Yamanishi, T. Uda, O. Motojima, O. Mitarai, T. Kunugi, Y. Matsumoto, S.-I. Satake, Y. Wu, “Studies on FLiBe blanket designs in helical reactor FFHR”, *Fusion Technol.*, 39 (2001) 753.

[4] S. Fukada, A. Morisaki, A. Sagara, T. Terai, “Control of tritium in FFHR-2 self-cooled Flibe blanket”, *Fusion Eng. Des.*, 81 (2006) 477.

[5] M. Kondo, T. Nagasaka, Q. Xu, T. Muroga, A. Sagara, N. Noda, D. Ninomiya, M. Nagura, A. Suzuki, T. Terai, N. Fujii, “Corrosion characteristics of reduced activation ferritic steel, JLF-1 (8.92Cr–2W) in molten salts Flibe and Flinak”, *Fusion Eng. Des.*, 84 (2009) 1081.

[6] M. Kondo, T. Nagasaka, A. Sagara, N. Noda, T. Muroga, Q. Xu, M. Nagura, A. Suzuki, T. Terai, “Metallurgical study on corrosion of austenitic steels in molten salt LiF–BeF₂ (Flibe)”, *J. Nuclear Materials*, 386 (2009) 685.

[7] M. Kondo, T. Nagasaka, T. Muroga, A. Sagara, N. Noda, Q. Xu, D. Ninomiya, N. Masaru, A. Suzuki, T. Terai, “High Performance Corrosion RESISTANCE of Nickel-Based Alloys in Molten Salt Flibe”, *Fusion Technol.*, 56 (2009) 190.

[8] A Perujo, K.S Forcey, “Tritium permeation barriers for fusion technology”, *Fusion Eng. Des.*, 28 (1995) 252.

[9] K. Krnel, T. Kosmač, “Protection of AlN powder against hydrolysis using aluminum dihydrogen phosphate”, *J. Euro. Ceram. Soc.*, 21 (2001) 2075.

Publication list

- (1) T. Watanabe, M. Kondo and A. Sagara, *Nitriding of 316 stainless steel in molten fluoride salt by an electrochemical technique*, *Electrochimica Acta*, **58**, (2011) pp.681-690.
- (2) M. Kondo, T. Watanabe, T. Tanaka, D. Zhang and A. Sagara, *Nitriding Treatment of Reduced Activation Ferritic Steel as Functional Layer for Liquid Breeder Blanket*, *Plasma and Fusion Research*, **6**, (2011) pp.2405117-2405117.
- (3) T. Watanabe, M. Kondo, T. Nagasaka and A. Sagara, *Corrosion characteristic of AlN, Y₂O₃, Er₂O₃ and Al₂O₃ in Flinak for molten salt blanket system*, *Journal of Plasma and Fusion Research*, **9**, (2010) pp.342-347.